The impact of the linker in the catalytic core of the DEAD-box protein YxiN from Bacillus subtilis on substrate binding, enzymatic function and conformation

Inauguraldissertation
zur
Erlangung der Würde eines Doktors der Philosophie
vorgelegt der
Philosophisch-Naturwissenschaftlichen Fakultät
der Universität Basel

von

Regula Helena Aregger
aus
Sursee, Luzern

Basel, 2012

Genehmigt von der Philosophisch-Naturwissenschaftlichen Fakultät
auf Antrag von

Prof. Dr. Dagmar Klostermeier

Prof. Dr. Joachim Seelig

Basel, den 26.6.2012 Prof. Dr. Martin Spiess

creative commons

Namensnennung-Keine kommerzielle Nutzung-Keine Bearbeitung 2.5 Schweiz

---

Sie dürfen:

das Werk vervielfältigen, verbreiten und öffentlich zugänglich machen

Zu den folgenden Bedingungen:

Namensnennung. Sie müssen den Namen des Autors/Rechteinhabers in der von ihm festgelegten Weise nennen (wodurch aber nicht der Eindruck entstehen darf, Sie oder die Nutzung des Werkes durch Sie würden entlohnt).

Keine kommerzielle Nutzung. Dieses Werk darf nicht für kommerzielle Zwecke verwendet werden.

Keine Bearbeitung. Dieses Werk darf nicht bearbeitet oder in anderer Weise verändert werden.

- Im Falle einer Verbreitung müssen Sie anderen die Lizenzbedingungen, unter welche dieses Werk fällt, mitteilen. Am Einfachsten ist es, einen Link auf diese Seite einzubinden.
- Jede der vorgenannten Bedingungen kann aufgehoben werden, sofern Sie die Einwilligung des Rechteinhabers dazu erhalten.
- Diese Lizenz lässt die Urheberpersönlichkeitsrechte unberührt.

Quelle: http://creativecommons.org/licenses/by-nc-nd/2.5/ch/ Datum: 3.4.2009

Table of contents

1. Introduction

1.1 RNA, RNA folding and misfolding

RNA is a widespread linear biopolymer, which consists of four different types of ribonucleotides (adenine, uracile, cytosine and guanine) that are linked by phosphodiester bonds. Some viruses store their genetic information using RNA molecules in contrast to bacteria and eukaryotes that store their genetic information using DNA. Apart from storing genetic information, RNA is also used in a wide variety of tasks. Messenger RNA (mRNA) is a copy of the genes encoded in DNA and used as a template for protein synthesis, transfer RNA (tRNA) functions as an adaptor of selected amino acids to the ribosome and thus helps translate the three letter code of the genetic information into the twenty one letter code of proteins while ribosomal RNA (rRNA) forms the core of the ribosome and makes up approximately 80 % of all RNA in a cell. There are also small RNAs such as small nuclear RNA (snRNA), which directs splicing of pre-mRNA and small nucleolar RNA (snoRNA), which processes and chemically modifes rRNAs. As RNA molecules are single stranded, they can fold into many different shapes that allow some RNA molecules to have structural as well as catalytic functions. These functions include processing of tRNA[1], processing and translation of mRNA[2-3], protein translocation into the endoplasmatic reticulum (ER)[4] as well as maintenance of the ends of chromosomes[5]. All of these processes are carried out by rather complex enzymes built by proteins and structured RNAs. Similar to proteins, RNA molecules can adopt secondary and tertiary structures. To a great extent the stability of secondary structures depends on very local interactions such as base-pairing and stacking with nearby nucleotides, thus these secondary structures are extremely stable[6-8]. Starting from these stable secondary structures, specific tertiary structures can be formed. These structures are important since, although some recognition by binding proteins is based on the sequence of the RNA, most RNA recognition proteins rely on such three-dimensional elements for specific binding[9]. Unfortunately RNA does not only fold into its correct structure, but also shows a tendency for misfolding. Misfolding can be ascribed to two major problems RNA

encounters upon folding. It can be kinetically trapped in alternative conformations due to many local and global minima in the energy landscape and moreover there is a difficulty in specifying a single tertiary structure being thermodynamically favoured over competing structures[10]. Due to the fact, that the diversity of the nucleotides is very limited with four versions only, there is a high probability for an RNA strand of a significant length to end up in non-native base-pairs. These so formed secondary structures are long-lived with an RNA duplex of 10 base pairs having a dissociation half-life of about 30 minutes[11]. Therefore this non-native secondary structures can interfere with proper folding of the RNA up to time-scales that are important for RNA function[12]. RNA binding proteins can ensure proper function of the RNA by resolving these structures or by hindrance of formation of these misfolded RNAs. RNA conformations can thus temporally and spatially be controlled by RNA-dependent ATPases that might act as RNA chaperones[10]. The concept of such RNA chaperones was proposed nearly 40 years ago[13-14] and is supported by the finding, that the ribosomal subunit 5S and tRNAs kinetically trapped in alternative folds could be renatured by the action of the protein UP1, a fragment of hnRNP A1 protein[10].

1.2 DEAD-box RNA proteins

An important class of proteins that can dissolve RNA structures is the family of DExH/D proteins, which is the largest subgroup of the helicase superfamily 2[15]. Although this group of enzymes is involved in many different processes, the catalytic cores of the proteins are very similar with regard to function and possibly also mechanisms. The processes DEAD-box proteins are involved in include remodelling of RNA or protein/RNA structures[16-17], dissociating RNA/protein complexes[18], or RNA annealing[19-21] and only a few examples show unwinding activity. Specificity and differences in the function of the holoenzyme are conferred by additional N-terminal or C-terminal domains attached to the catalytic core. DEAD-box proteins share a catalytic core. Within this catalytic core ten conserved motifs that are shown in Figure 1 can be found[22].

Figure 1

Figure 1 depicts the conserved motifs found in DEAD-box proteins. Motifs I and II bind NTPs and are also known as Walker A and Walker B motif. Motif I binds phosphates of NTPs by a pocket that is formed by a loop also called P loop. Motif II on the other hand binds β and γ phosphates through a coordinated Mg^{2+}. Motifs Ia, Ib, IV and V are also involved in binding of substrates and motifs III and VI couple NTP binding and hydrolysis to conformational changes necessary for helicase activity.

Motifs I and II bind NTPs and are also known as Walker A and Walker B motif[23]. Motif I binds phosphates of NTPs by a pocket that is formed by a loop also called P loop. Motif II on the other hand binds β and γ phosphates through a coordinated Mg^{2+}[24]. Motifs Ia, Ib, IV and V are also involved in binding of substrates and motifs III and VI couple NTP binding and hydrolysis to conformational changes necessary for helicase activity[25-26]. Motif III furthermore coordinates motif I, II and VI to the γ phosphate of ATP to create a high affinity binding site for RNA[27]. Crystal structures of SF1 and SF2 helicases show two globular domains generally containing five β-strands being surrounded by five α-helices. This fold resembles the folding of the RecA ATPase[28], therefore these domains are often referred to as RecA-like domains[15]. The two RecA domains of the catalytic core are connected by a flexible linker[29]. In the absence of substrates the relative orientation of these domains is not well defined. Upon binding of RNA and/or NTPs the orientation of the two domains gets more defined, suggesting a possible mean of how cooperativity of RNA and nucleotide binding and hydrolysis is achieved[30].

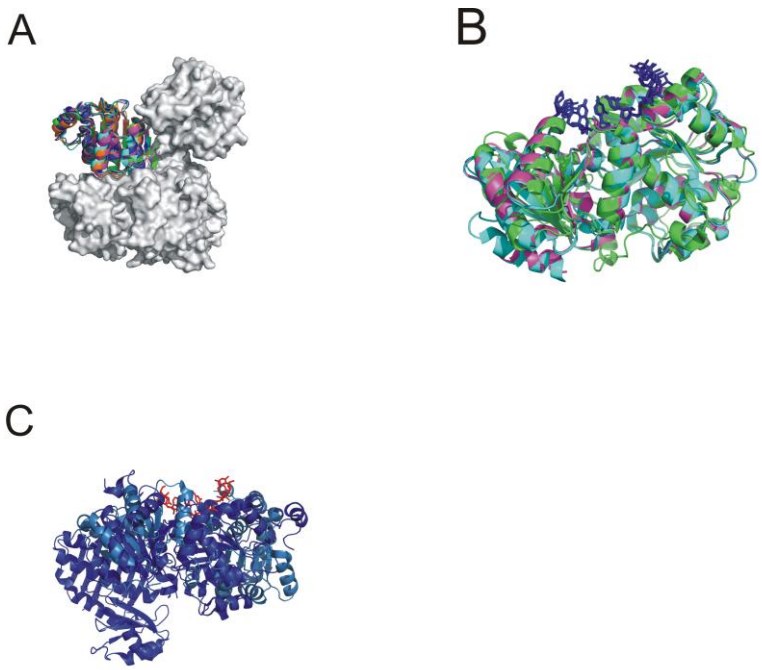

Figure 2

Figure 2: Open and closed conformations of DEAD-box proteins. Panel A is a superimposition on the N-terminal RecA domain of crystal structures of DEAD-box proteins in the absence of any ligands, the C-terminal domain is shown in surface representations. eIF4A-I (*Sachharomyces cerevisiae*, PDB-ID 1fuu) is shown in green, mjDeaD (*Methanococcus jannaschii*, PDB-ID 1hv8) is shown in magenta, Dhh1p (*Sachharomyces cerevisiae*, PDB-ID 1s2m) is shown in cyan, DeaD (*Sulfolobus tokodaii*, PDB-ID 2z0m) is shown in orange and eIF4A-III (human, PDB-ID 2hxy) in blue. Panel B shows a superimposition of DEAD-box proteins in the presence of ssRNA and ADPNP or ADP·AlF_4 respectively. The structure of Vasa in complex with RNA and ADPNP (Drosophila melanogaster, PDB-ID 2db3) in green is superimposed with the structure of eIF4A-III in complex with RNA and ADPNP (human, PDB-ID 2hyi) in magenta or in complex with RNA and ADP·AlF_4 (PDB-ID 3ex7) in cyan. Panel C is a superimposition of eIF4A-III (human, PDB-ID 2hxy) in dark blue and the structure of eIF4A-III in complex with RNA and ADPNP (human, PDB-ID 2hyi) in light blue.

Only a few DEAD-box helicases, such as the translation initiation factor eIF4A or the *Methanococcus jannaschii* DeaD protein consist of a helicase core only. The basic DEAD-box helicase functions are modulated by large N-terminal and/or C-terminal extensions. These modulations in helicase activity include conferment of substrate specificity or mediation of contacts with interacting proteins[31]. The impact of such extensions could be shown by creating a chimeric protein of the non-specific core of SrmB with the C-terminal extension of

YxiN. SrmB is an *E.coli* protein showing no RNA specificity as tRNA, rRNA and RNA homopolymers can activate ATP hydrolysis activity[32]. YxiN is a DEAD-box protein from *B.subtilis* having a strong specificity for ribosomal 23S RNA[33]. The chimera described above displayed 23S rRNA-specific activation of ATP hydrolysis, with rates corresponding to the rates observed for SrmB and similar results were found for unwinding activity *in vitro*[34]. The requirement for specificity in DEAD-box proteins is very different depending on the process the helicase is involved in. That is why many proteins such as translation initiation factors or subunits of degradation machineries show no substrate specificity, as they encounter different substrates whereas other DEAD-box proteins which are involved in ribosome biogenesis or pre-mRNA splicing could have (strong) substrate specificity[15]. Most DEAD-box proteins are non-processive enzymes. This lack of processivity can be explained by the fact that the putative substrates of the best characterised RNA helicases generally contain duplex regions below 10 basepairs. This is approximately the size of a binding site of DEAD-box proteins and can be unwound by a single step of unwinding[22], as the stepsize of DEAD-box proteins is assumed to be around 5-6 basepairs[35]. A processive activity as seen for DNA helicases is not needed and the proteins might rather act as temporary clamps preventing reassociation of RNAs and thereby allowing other RNA/RNA or RNA/protein interactions to occur. By doing so they could ensure directionality and efficiency of multistep reactions such as pre-mRNA splicing and ribosome assembly[22]. The DEAD-box protein CYT-19 from *Neurospora crassa* is able to completely separate two strands using a single ATP and the *Saccharomyces cerevisiae* proteins Mss116 and Ded1 show a similar behaviour. Strand separation is strongly dependent on ATP, which is reflected by the fact, that ADPNP does not induce this separation. Nevertheless under certain conditions considerably less than one ATP is hydrolysed per separation event[36]. ATP binding and not hydrolysis thus seems to enhance the strand separation activity by stabilising or inducing a protein conformation that promotes strand separation[36]. The process of unwinding has been described by three models known as the inchworm model (Figure 5), the active rolling model (Figure 4) and the destabilising model (Figure 3). In the destabilisation model the DEAD-box helicase binds to single stranded regions adjacent to double stranded regions of the RNA substrate and upon stepping through the nucleotide cycle a conformational change induced in the catalytic core of the enzyme leads to a change of the two RecA core domains relative to each other. Since

both RecA core domains have the ability to bind RNA, this conformational change leads to a local perturbation of the RNA structure[37-38]. Given that the DEAD-box protein binds in close proximity to an ss/ds RNA junction, these structural alterations of the RNA could be enough to destabilise a few base pairs of the duplex region, even if the ss/ds RNA junction is not adjacent to the duplex region[39]. The energy needed for that process could come from ATP hydrolysis or from ATP binding alone. In the latter case, ATP hydrolysis would lead to a reset of the enzyme, preparing it for the next cycle of unwinding activity[15].

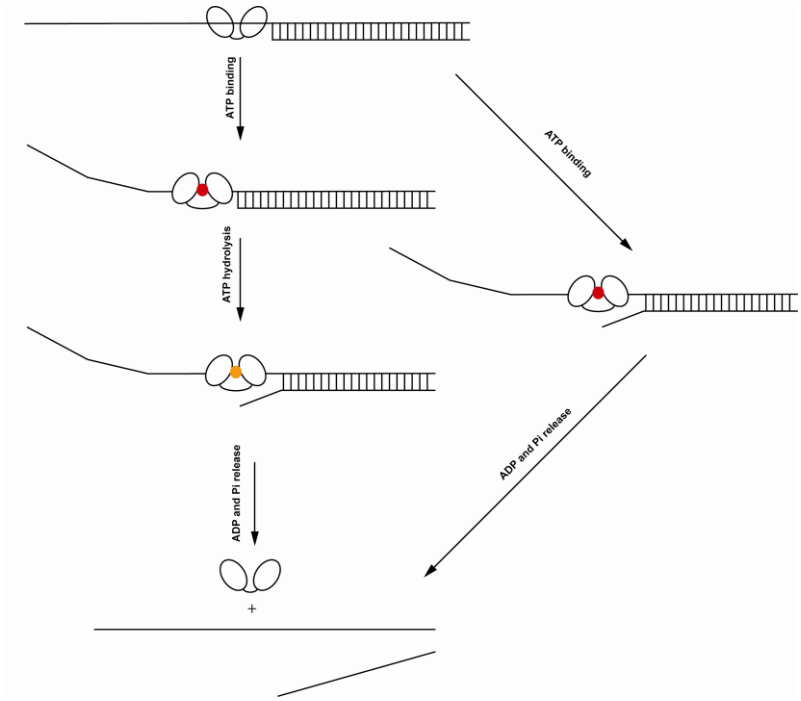

Figure 3

Figure 3 (adapted from[15]): Scheme of the destabilising model. Nucleotides are shown in red for ATP and in orange for ADP. Binding of the DEAD-box protein and a conformational change in the RecA core domains, both binding to RNA, induced in the nucleotide cycle lead to a destabilisation of the RNA duplex region. The energy needed in this process originates from ATP hydrolysis or ATP binding alone therefore also ADP binding could lead to RNA unwinding.

The active rolling model of RNA unwinding requires the DEAD-box protein to be a dimer with one monomer having high affinity for single stranded RNA and one monomer having high affinity for double stranded RNA. The conformational states of the monomers vary upon binding and hydrolysis of ATP. This allows the dimer to act “hand-over-hand” to move along the RNA while unwinding double stranded regions. Nucleotide dependent differences in the RNA binding site of the helicase could induce the required conformational alterations of the RNA by forcing the double stranded phosphate backbone into an energetically unfavourable conformation[22].

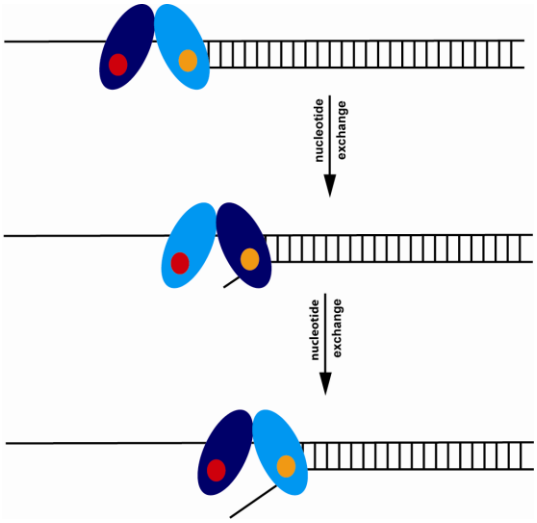

Figure 4

Figure 4: Scheme of the active rolling model. This model requires a DEAD-box protein being active as a dimer. One monomer is shown in light blue and the other is shown in dark blue. ATP is shown in red and ADP in orange. One monomer of the dimer has high affinity for double stranded RNA and one monomer of the dimer has low affinity for double stranded RNA. Upon nucleotide exchanges and conformational changes linked to these exchanges the dimer can move “hand-over-hand” on the RNA strand and induce conformational alterations of the RNA, leading to RNA unwinding.

The inchworm model describes the mode of action of monomeric DEAD-box proteins. Here, the monomer undergoes a conformational change that is associated with the binding and hydrolysis of ATP and brings the two RecA domains of the catalytic core closer to each other,

or further apart. Although both domains are bound to the RNA substrate, they have to temporarily and sequentially dissociate from the substrate. Also here conformational changes of the RNA substrate are induced by forcing the double stranded phosphate backbone in an energetically unfavourable conformation[22]. Since most of the DEAD-box proteins are found to be monomers rather than dimers this model does not have a big impact on explaining unwinding function of DEAD-box proteins.

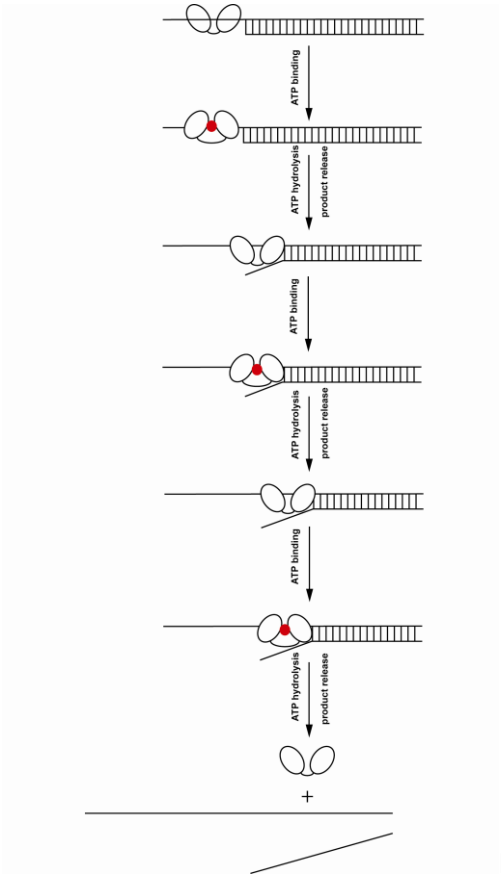

Figure 5

Figure 5: Scheme of the inchworm model. ATP is shown in red. The monomeric DEAD-box protein undergoes a conformational change associated with the binding and hydrolysis of ATP. The catalytic core domains have to temporarily and sequentially dissociate from the RNA substrate and induce conformational alterations of the RNA, leading to RNA unwinding by moving along the RNA strand.

All in all none of the above described models completely describes the unwinding mode of DEAD-box proteins but give a good overview together. Structural evidence points into the

direction that binding of RNA to the RecA domains leads to a kink in the RNA as both the 5'-end and the 3'-end get bent upon structural rearrangements of the core[37]. This kink can be introduced on an ss/ds RNA junction[15], or within a double stranded region[39]. This kinking of the RNA then leads to a destabilisation of the RNA duplex and finally to unwinding.

1.3 DbpA from E.coli and YxiN from B.subtilis

DbpA from *E.coli* and its homolog YxiN from *B.subtilis* are both DEAD-box enzymes with the characteristic catalytic core. In addition to this core, they have a C-terminal domain containing seven highly conserved basic amino acids suggesting a role in RNA binding and thus called the RBD (RNA binding domain)[33]. DbpA is an ATP-dependent RNA helicase with sequence specificity, depending on the presence of hairpin 92 of the 23S rRNA[40]. In contrast to the RBD which demonstrates high substrate specificity and binding affinity for the above mentioned substrate, the catalytic core binds RNA unspecifically and with low affinity. Therefore the RNA binding domain (RBD) is responsible for the substrate specificity to hairpin 92[41]. Binding of a 32mer fragment lacking helix 90 shows a reduced binding affinity to full-length DbpA compared to an RNA substrate containing helix 90[42]. The substrate rRNA containing hairpin 92 spans bases 2496-2588 and is part of the peptidyltransferase center of the ribosome and contains bases involved in interactions with the 3'-terminal adenosines of A- and P-site tRNA. The A-site is the site of the ribosome where the new aminoacyl tRNA binds at the beginning of each translation step and the P-site is the site where the polypeptide chain resides. DbpA thus might be involved in establishing and maintaining the proper structure of the peptidyltransferase center during ribosome biogenesis[40]. This assumption is also supported by the observation that although 23S subunits stimulate ATPase activity of DbpA, neither mature ribosomes nor 50S subunits strongly stimulate this activity, although hairpin 92 is accessible to tRNAs during translation and thus also for the DEAD-box protein[43].

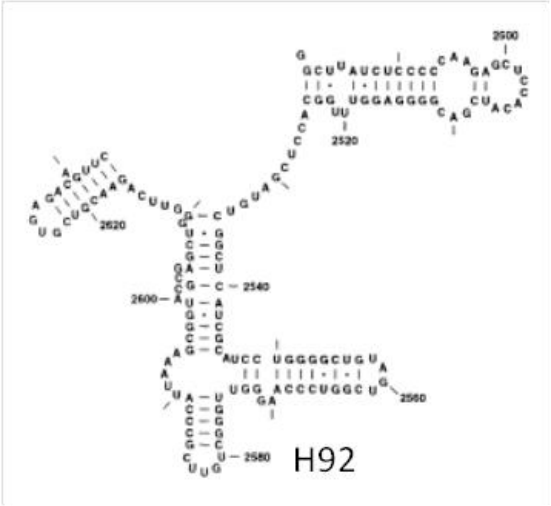

Figure 6: 153mer of 23S rRNA with hairpin 92

As shown in Figure 6, the 23S rRNA does not have long regions of secondary structures or long-ranged tertiary interactions. It is therefore likely, that DbpA disrupts short regions of double stranded RNA in the process of ribosome biogenesis. This is further supported by the fact that DbpA was the first DEAD-box protein shown to have site-specific helicase activity *in vitro*[34]. DbpA is non-processive, being able to unwind double stranded RNA of a length of 9 base pairs, but not 15 base pairs[44]. Although hairpin 92 is the determinant of substrate specificity, it is neither an effective inhibitor nor an activator of ATP hydrolysis activity for DbpA on its own. This suggests that the single-stranded extensions in the 153mer fragment are required for high affinity RNA binding and for stimulation of ATP hydrolysis. Since these extensions have no sequence requirements, it is likely that they contribute to binding through backbone contacts[45].

The *Bacillus subtilis* homolog of DbpA, YxiN also binds to the 153mer fragment of the 23S rRNA and thus might as well function in ribosome biogenesis in *Bacillus subtilis* as DbpA does in *Escherichia coli*[33]. Furthermore YxiN also shows 153mer stimulated ATP hydrolysis[33] and double stranded RNA unwinding activity[46]. In YxiN, the C-terminal extension, the RBD, spans amino acids 404-479, is rich in basic amino acids and linked to the C-terminal domain of the catalytic core by a flexible linker spanning amino acids 369-403. The task of the RBD seems to be to bring the catalytic core to the cellular target, since addition of RBD in trans to the

core does not confer any RNA specificity to the core and also does not affect the ATPase rate[41]. Although the tertiary fold of the YxiN RBD (see Figure 7) is similar to that of RNA recognition motifs (RRM) prevalent in eukaryotes, RNA binding assays of YxiN RBD mutants suggest that the mode of RNA binding differs substantially from that of the eukaryotic RNA recognition motifs[47].

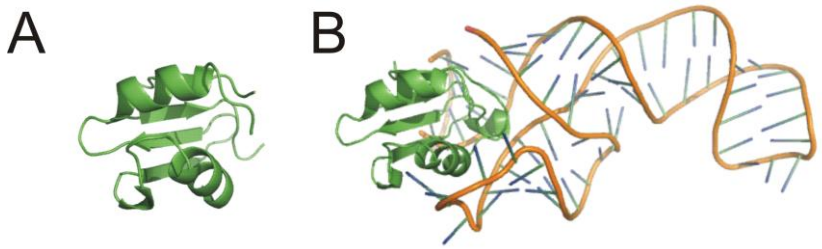

Figure 7

Figure 7: Panel A: 1.7 Å resolution crystal structure of the YxiN RBD (PDB ID: 2G0C). Panel B: 2.9 Å resolution crystal structure of the YxiN RBD bound to a fragment of the 23S rRNA containing hairpin 92 (PDB ID: 3MOJ). The figure was created using PyMOL (DeLano, W.L. The PyMOL Molecular Graphic system, 2002).

To localise the YxiN RBD relative to the YxiN catalytic core, the RBD structure was localised to a homology model of the catalytic core that was created using the crystal structure of DeaD from *Methanococcus jannaschii* as a template using a FRET based orientation approach since there is no structure of the full-length enzyme available. The homology model superimposes well to the crystal structure of the C-terminal RecA domain which shows that the structure of the YxiN catalytic core is well represented by this homology model. (see Figure 8)

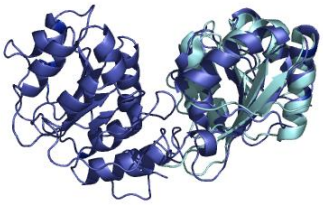

Figure 8

Figure 8: Superimposition of the homology model of the YxiN core using DeaD from *Methanococcus jannaschii* as a template (PDB ID: 1HV8; dark blue) with a 1.95 Å crystal structure of the C-terminal RecA domain of YxiN (PDB ID: 2HJV; light blue).

This approach led to a model where the RBD lies above a slightly concave region of the C-terminal RecA domain (see Figure 9). This region is formed by flexible loops on the surface of the latter domain[48].

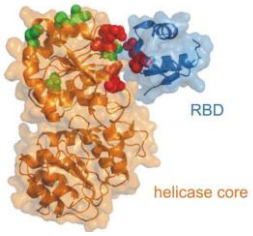

Figure 9

Figure 9[48]: Orientation of the YxiN RBD relative to the homology model of the YxiN catalytic core. Residues highlighted in red are residues that lead to destabilisation upon mutations to cysteine (necessary for the FRET approach) or were not accessible by the malemeide group. Residues highlighted in green are residues that were mutated to cysteine and used for the FRET study and positioning.

Single molecule FRET studies on the YxiN catalytic core show that the two domains are in an open conformation relative to each other in the absence of any substrate, in the presence of ATP, ADP, RNA and ADP+RNA. The presence of ATP+RNA on the other hand induces a closure of the cleft indicating that the ATP-bound and the ADP-bound states of YxiN are only substantially different regarding the structure when also the RNA substrate is bound[49]. The

N-terminal core domain, the C-terminal core domain and the RBD constitute autonomous folding units and it has been proposed that interdomain communication is necessary for efficient helicase activity[49]. This communication includes closure of the cleft between the two core domains upon ATP and/or RNA binding. As previously mentioned, different DEAD-box proteins show different arrangements of the RecA domains in the open state[16, 50-54] but not in the closed state[38,55] suggesting that there must be a need for interdomain communication. Most of the nucleotide binding motifs are located in the N-terminal core domain but the C-terminal domain contributes significantly to tight nucleotide binding, as reflected by the fact, that a covalent connection of the two core domains is essential. A mixture of N-terminal and C-terminal domains without any covalent linkage does not exhibit any ATPase or helicase activity[49]. The study at hand investigates the impact of the linker in the catalytic core on enzyme function.

2. Aim of Research

Previous to this study a lot of research was performed on the mechanistics of enzyme function and on the conformational states of YxiN using different mutations in the conserved motifs. It could be shown that a mutation of the conserved lysine in motif 1 to a glutamic acid (K52Q) leads to a closure of the interdomain cleft in the catalytic core, but does not show any unwinding and ATP hydrolysis activity. A double mutation of the motif III from SAT to AAA leads to a reduced ATP hydrolysis rate and induces a closure of the cleft in the catalytic core. Again, it is unwinding deficient. These results indicate that closure of the cleft is necessary but not sufficient to support helicase activity. Mutating a glycine in motif V to alanine (G303A) prevents complete closure of this interdomain cleft, affects ATP binding and hydrolysis and unwinding activity. Assuming that cooperative binding of ATP and RNA in DEAD-box proteins and the induced closure of the helicase core with extensive interactions across the domain interface leads to a bending in the bound RNA and this distortion of the RNA being the first step towards RNA unwinding, it is possible that the K52Q and motif II mutants still introduce a kink into the backbone, but G303A fails to kink the RNA substrate[56]. These studies show, amongst other things, the importance of functional interdomain communication in the helicase core. This is further supported by the finding, that non-covalently linked subunits of YxiN do not show any enzymatic activity[49]. This study now focuses on the role of the linker providing this covalent linkage of the helicase catalytic core. The impact of linker length and linker sequence on nucleotide and RNA binding properties and enzymatic functions such as ATP hydrolysis and double stranded RNA displacement will be examined. Further investigation will focus on the effect of these linker mutations on the ability to induce the conformational change in the catalytic core. Fluorescence and fluorescence anisotropy spectroscopic methods, photometric methods as well as single molecule FRET techniques will be employed to describe the properties of these linker mutants. We hope to get insight into the role and importance of this linker connecting the two catalytic core domains. Although there is a definite need for a covalent linkage of the two core domains, there seems to be no clear limitation in sequence requirements and length as neither the length nor parts of the sequence of the linker is conserved. The

approach chosen for this work was to start with the native length of the linker between the two catalytic core domains and change its sequence and then gradually increase and decrease the linker length until changes and finally loss of enzymatic properties can be observed.

3. Abstract

DEAD-box RNA proteins are enzymes that bind and unwind RNA. It is assumed that this class of enzymes is involved in the structural conversion and correct folding of complex RNAs such as ribosomal RNA.

YxiN is a DEAD-box RNA protein from *Bacillus subtilis* that recognises hairpin 92 of the 23S rRNA. The protein consists of a catalytic core formed by two RecA domains connected by a linker of 9 amino acids and a C-terminal domain conferring substrate specificity. The sequence motifs for ATP binding, ATP hydrolysis and RNA binding are located in the two RecA domains of the helicase catalytic core and communication between these two domains is crucial for enzymatic function[49].

To investigate the role of the linker between the two RecA domains of the DEAD-box helicase core, its length and sequence were modified. RNA stimulated ATPase activity of YxiN mutants and YxiN wildtype was characterized by a coupled enzymatic steady-state ATPase assay and unwinding assays were performed using a double stranded RNA minimal substrate. Nucleotide binding affinities were determined by displacement titrations of nucleotide with a preformed complex of enzyme with a fluorescently modified nucleotide in the absence and the presence of a minimal RNA substrate. RNA binding affinities were determined by anisotropy titrations of a fluorescently labeled minimal substrate with YxiN wildtype and YxiN mutants. Conformational changes were investigated in confocal smFRET experiments.

This work could show that extension of the linker up to 15 amino acids led to a drastic reduction of ATPase activity. This effect was even more pronounced in mutants with shortened linkers. Reducing the linker length to 4 amino acids resulted in a completely ATPase-deficient enzyme. However nucleotide binding studies of the different mutants showed that ATP affinity is increased in all the mutants when compared to the wildtype enzyme. If additionally an RNA substrate is present the increase in ATP affinity thus can only be observed for the shorter YxiN linker mutants and the longer YxiN linker mutants rather

show a decrease in ATP affinity. The affinities for the pre-hydrolysis ATP-analogue ADP·BeF_x are lower for the YxiN linker mutants compared to YxiN wildtype in the absence of RNA, but similar to YxiN wildtype in the presence of RNA. In the absence of RNA the affinities of the YxiN linker mutants for ADP are similar to those found for YxiN wildtype but are clearly decreased in the presence of RNA. The linker in the catalytic core also has some influence on RNA binding as reflected by the increase in affinity for RNA in the YxiN linker mutants compared to YxiN wildtype in the absence of nucleotide and in the presence of ADP·BeF_x. Changing the linker length leads to lower RNA affinities in the presence of ADPNP and to higher RNA affinities in the presence of ADP. The same trends seen for ATPase activity are observed for unwinding activities of these mutants with the longest and shortest constructs being unwinding deficient. Differences in unwinding rates depending on the nucleotide present could be observed. Unwinding rates with ATP are in general higher than unwinding rates with ADP·BeF_x. Single molecule FRET experiments indicated that mutants with the shortest and the longest linkers did not adopt a closed conformation in the presence of RNA substrate and ATP but in all other YxiN mutants as well as in YxiN wildtype.

These results indicate that the linker between the catalytic core RecA domains of YxiN plays a key role in regulation of the enzyme activity. Furthermore, it is evident that the length of the linker for efficient interdomain communication and thus enzymatic activity between the two core domains lies between 5 and 13 amino acids.

4. Materials and Methods

4.1. Consumables

BD (Franklin Lakes, USA) 50 ml conical tubes, PP; Microlance-3 needles, 0.90 x 40 mm; serological pipettes 1 ml, 10 ml, 25 ml, 50 ml

Bio-Rad Laboratories (Hercules, USA) Micro BioSpin 30 Columns, RNase-free

Brand (Wertheim, D) UV-cuvettes PLASTIBRAND micro, z = 8.5 mm, 2 x 3.5 mm

CODAN Medical (Rødby, DK) single use syringes 2 ml, 10 ml, 50 ml

Eppendorf (Hamburg, D) Safe-Lock tubes ambra 1.5 ml; Safe-Lock tubes 2 ml

G. Kisker (Steinfurt, D) Quali-"Low Retention" tubes, 1.7 ml

Sarstedt (Nürnbrecht, D) 15 ml conical tubes, PP; cuvettes 10 x 4 45 mm; Filtropur S 0.2 µm; Micro Tube 1.5 ml, PP; Multiply-Pro cup, 0.2 ml, PP

Sartorius Stedim Biotech (Aubagne, F) filter Midisart 2000; Vivaspin 20 concentrator 10'000 MWCO PES; Vivaspin 6 concentrator 10'000 MWCO PES; Vivaspin 500 concentrator 10'000 MWCO PES; Vivaspin 15R concentrator 2'000 MWCO

Spectrum Laboratories (Rancho Dominguez, USA) Spectra/Por dialysis membrane 12-14'000 MWCO and 3'500 MWCO

Starlab (Ahrensburg, D) TipOne Tips 10 µl, 200 µl, 1000 µl

Thermo Fisher Scientific (Rockford, USA) Lab-Tek chamber slides, 8 chambers, glass slide

Treff AG (Degersheim, CH) Microtubes ClickFit, 1.5 ml

4.2. Reagents and Enzymes

Aldrich (Steinheim, D) $MgSO_4$

AppliChem (Darmstadt, D) glycerol, anhydrous, p.A.; L-glutathione, reduced

Carl Roth (Karlsruhe, D) NaCl > 99.8 %; peptone; yeast extract, pulv

EPICENTRE Biotechnologies (Madison, USA) T7 RNA and DNA Polymerase

Fermentas (St.Leon-Rot,D) PageRuler Plus prestained protein ladder; 2x RNA loading dye

Fluka (Buchs, CH) activated charcoal, purum;

Invitrogen (Eugene, USA) Alexa Fluor 488 C5-maleimide; Alexa Fluor 546 C5-maleimide; TCEP; TEV protease

Jena Bioscience (Jena, D) mant-ADP, > 95 %

Merck (Darmstadt, D) ethanol, absolute; potassium acetate, puriss.; 2-propanol, p.A.

New England BioLabs (Ipswich, USA) BSA (10 mg/ml); DNA ladder, 1 kb; 100 bp; *Dpn*I (20'000 U/ml)

Pharma Waldhof (Düsseldorf, D) ATP and ADP disodium salt

Promega (Madison, USA) GoTaq DNA polymerase (5 u/µl); *Pfu* DNA polymerase (2-3 U/µl); *Pfu* DNA polymerase 10x reaction buffer; Wizard SV Gel and PCR Clean-Up System

Qiagen (Hilden, D) QIAprep Spin Miniprep Kit (250); QIAquick Nucleotide Removal Kit (50)

Radiant Dyes Laser Acc. (Wermelskirchen, D) *Uranin* (fluorescein)

Reuss-Chemie (Tägerig, CH) 2-propanol, tech.

Roche Diagnostics (Mannheim, D) Complete EDTA-free Protease Inhibitor Cocktail Tablets; hexokinase, from yeast „overproducer"; lactate dehydrogenase from rabbit muscle; NADH

disodium salt; PEP; proteinase K, recombinant, PCR grade; pyruvate kinase from rabbit muscle

Sigma Aldrich (St.Louis, USA) ADPNP tetralithium salt hydrate, ~ 95 % (HPLC); ATP disodium salt, Grade I, ≥ 99 %; $CoCl_2$x6 H_2O; $CuCl_2$x 2 H_2O; CTP disodium salt ≥ 95 %; deoxynucleotide Set (dATP, dCTP, dGTP, dTTP), DMSO ≥ 99.9 %; ethanol, purum; $FeCl_3$x 6 H_2O; GTP sodium salt hydrate, ≥ 95 % (HPLC); Na_2MoO_4x 2 H_2O; spermidine, min. 98 % (GC); UTP trisodium salt hydrate, Type IV, 90-95 %

VWR (Briare, F) glycerol ~ 87 %

Chemicals not listed above, were purchased in p.a. or puriss. Quality from Carl Roth (Karlsruhe, D)

4.3. Instrumentation

Centrifugation Heraeus Biofuge pico with rotor 33258; Sorvall RC 5C plus with rotors SLA3000 and SS34 (both Kendro Laboratory Products, Langenselbold, D); centrifuge 5402 with rotor F-45-18-11 (Eppendorf, Hamburg, D)

Electrophoresis Hoefer multiple gel caster; gel electrophoresis unit Mighty Small II (8 x 7 cm); power supply EPS 300, 301 and 1001 (all of them Amersham Biosciences Europe, Freiburg, D); gel documentation system EDAS 290 (Kodak, Stuttgart, D) equipped with Transilluminator FT-20/254/365 (Herolab, Wiesloch, D)

Fluorescence measurements Fluorimeter Hitachi F-4500 (Hitachi-Hitec, Tokyo, JP); fluorimeter FluoroMax-3 (HORIBA JOBIN YVON, Stanmore, UK) and precision cells made of Quartz SUPRASIL for absorption measurements no. 105.202, path 10 mm (Hellma, Müllheim, D)

Photometric measurements UV/Visible Spectrophotometer Ultraspec 2100pro (Amersham Biosciences Europe, Freiburg, D); UV/Vis photometer BioPhotometer (Eppendorf, Hamburg, D)

Preparative HPLC LC system ÄKTAprime (GE Healthcare, Chalfont St. Giles, UK) equipped with SEC columns HiLoadTM 16/60 Superdex 200 pg, resins Glutathione Sepharose 4 FF and Chelatin Sepharose FF, LC columns XK 16, Superloop 50 ml (all Amersham Biosciences Europe, Freiburg, D)

Electroelution system Elutrap (Schleicher&Schuell, Dassel, D)

Membrane pHmeter HI 8314 (Hanna instruments, Kehl, D)

Microfluidizer M-110L (Microfluidics, Newton, USA)

PCR machine Mastercycler gradient (Eppendorf, Hamburg, D)

Shaker Minitron (Infors, Bottmingen, CH)

Thermostat ThermoStat plus (Eppendorf, Hamburg, D)

Confocal Fluorescence Microscope for SmFRET Measurements FRET events from single molecules freely diffusing in solution were detected on a home-built confocal microscope. The excitation light was generated by a modelocked, solid-state Ti:sapphire laser (Tsunami, Spectra-Physics, Mountain View, USA) that was pumped by a continuous wave Nd:VO_4 diode laser (Millenia pro, Spectra-Physics, Mountain View, USA). The emitted light of 951 nm passed a frequency doubler (Model 3980, Spectra-Physics, Mountain View, USA) and a frequency doubler/tripler (GWU, Spectra-Physics, Mountain View, USA) resulting in light of 475 nm. Passing a $\lambda/2$ plate, an adjustable neutral density filter and a notch filter the beam was directed into an inverted microscope (IX71, Olympus, Tokyo, JP). The beam was then focussed into the sample by a water immersion objective (UPlanApo, N_A = 1.2, Olympus, Tokyo, JP). The fluorescence was collected by the same objective and transmitted to the detection part via a dichroic beam splitter (DM505; Olympus, Tokyo, JP). A lens focussed the light to a pinhole (100 µm) selecting the infocus light only. After passing a second lens the light was split via a dichroic beam splitter to an APD (SPCM-AQR-14, PerkinElmer, Dumberry,

CAN) detecting donor photons and a second APD (SPCM-AQR-14, PerkinElmer, Dumberry, CAN) detecting acceptor photons. The signal from the APDs was sent via a router to a single photon counting card (SPC-630, Becker & Hickl, Berlin, D) and processed.

4.4. Plasmid and bacterial strains

Prior to this work nucleotides 2481-2634 of *B.subtilis* 23S rRNA were cloned into the restriction sites *BamHI/HindII* of pUC18 (Fermentas, St. Leon-Rot, D). This construct was used for *in vitro* transcription. Also prior to this work *yxiN* wildtype was cloned into the restriction sites *NcoI/XhoI* of pETM30 (G. Stier, EMBL, Heidelberg, D). Mutations were then introduced using QuickChange mutagenesis.

All plasmids were propagated in XL1-Blue *E.coli* cells (Stratagene, La Jolla, USA).

recA1 endA1 gyrA96 thi-1 hsdR17 supE44 relA1 lac [F'*proAB lacI*^{q}*ZDM15 Tn10* (Tet^{1})]

All proteins were expressed for purification in Rosetta 2 (DE3) *E.coli* cells (Merck, Darmstadt, D)

F^{-} *ompT hasd* $S_B(r_B^- m_B^-)$ *gal dcm* (DE3) pRARE2 (*argU, argW, argX, glyT, ileX, leuW, metT, proL, thrT, thru, tyrU*; Cam^{1})

4.5. Oligonucleotides

DNA oligonucleotides were purchased from Microsynth (Balgach, CH) or Sigma Aldrich (St. Louis, USA) and RNA oligonucleotides were purchased from PURIMEX (Grebenstein, D).

4.5.1. Primer

YxiN lk 3 forward: 5'-GCATATCGAGGTCGGCTCAGGTATTGAACATGCGG-3'

YxiN lk 3 backward: 5'-CCGCATGTTCAATACCTGAGCCGACCTCGATATGC-3'

YxiN lk 4 forward: 5'-GCATATCGAGGTCGGCTCATCCGGTATTGAACATGCG-3'

YxiN lk 4 backward: 5'-CGCATGTTCAATACCGGATGAGCCGACCTCGATATGC-3'

YxiN lk 5 forward: 5'-GCATATCGAGGTCGGCTCCGGCTCAGGTATTGAACATGCGG-3'

YxiN lk 5 backward: 5'-CCGCATGTTCAATACCTGAGCCGGAGCCGACCTCGATATGC-3'

YxiN lk 7 forward: 5'-GCATATCGAGGTCGGCGGCTCATCCGGCTCAGGTATTGAACATGCGG-3'

YxiN lk 7 backward: 5'-CCGCATGTTCAATACCTGAGCCGGATGAGCCGCCGACCTCGATATGC-3'

YxiN lk 9 forward: 5'-CCCGAGCATATCGAGGTCAAAGCGGCCGGCCTAACCACAAGAAATATTGAACATGCGGTGATTC-3'

YxiN lk 9 backward: 5'-GAATCACCGCATGTTCAATATTTCTTGTGGTTAGGCCGGCCGCTTTGACCTCGATATGCTCGGG-3'

YxiN lk 11 forward: 5'-GAGCATATCGAGGTCGGCGCGGCGGGTTCCGGCTCATCCGGCTCAGGTATTGAACATGCGGTG-3'

YxiN lk 11 backward: 5'-CACCGCATGTTCAATACCTGAGCCGGATGAGCCGGAACCCGCCGCGCCGACCTCGATATGCTC-3'

YxiN lk 13 forward: 5'-GAGCATATCGAGGTCGGCGCGGCGGGCTCAGGTTCCGGCTCATCCGGCTCAGGTATTGAACATGCGGTG-3'

YxiN lk 13 backward: 5'-CACCGCATGTTCAATACCTGAGCCGGATGAGCCGGAACCTGAGCCCGCCGCGCCGACCTCGATATGCTC-3'

YxiN lk 15 forward: 5-'CTAACCACAAGAAGGCTCAGGGTCATCCGGCATATTGAACATGCGGTG-3'

YxiN lk 15 backward: 5-'CACCGCATGTTCAATATGCCGGATGACCCTGAGCCTTCTTGTGGTTAG-3'

YxiN T211A forward: 5-‘GAGGTCAAAGCGGCCGGCCTAGCTACAAGAAATATTGAACATGCGGTG-3’

YxiN T211A backward: 5-‘CACCGCATGTTCAATATTTCTTGTAGCTAGGCCGGCCGCTTTGACCTC-3’

YxiN K52Q forward: 5’-GAC AGG AAG CGG GCA AAC GGC TTC GTT CGG G-3’

YxiN K52Q backward: 5’-CCC GAA CGA AGC CGT TTG CCC GCT TCC TGT C-3’

YxiN C61A forward: 5’-CGG GAT TCC TCT CGC GGA GCT GGC GAA TTG GG-3’

YxiN C61A backward: 5’-CCC AAT TCG CCA GCT CCG CGA GAG GAA TCC CG-3’

YxiN S108C forward: 5’-CAGCC GTA TTT GGA AAA TGC TCC TTT GAT AAA CAA A-3’

YxiN S108C backward: 5’-TTTGTT TAT CAA AGG AGC ATT TTC CAA ATA CGG CTG-3’

YxiN A115C forward: 5’-CCT TTG ATA AAC AAA AAT GTG AGC TTA AGC AAA AAA GCC-3’

YxiN A115C backward: 5’-GGC TTT TTT GCT TAA GCT CAC ATT TTT GTT TAT CAA AGG-3’

YxiN S229C forward: 5’- GAA GAG AAT AAG TTT TGC TTG CTG AAA GAT GTG-3’

YxiN S229C backward: 5’-CAC ATC TTT CAG CAA GCA AAA CTT ATT CTC TTC-3’

YxiN C267A forward: 5’-GGG ATA TCC AGC GGA TAA AAT TCA CGG CGG-3’

YxiN C267A backward: 5’-CCG CCG TGA ATT TTA TCC GCT GGA TAT CCC-3’

YxiN R330A forward: 5’-CCG CAC GGG CGC AAC GGG ACG CGC AGG-3‘

YxiN R330A backward: 5’-CCT GCG CGT CCC GGT GCG CCC GTG CGG-3’

pGEX forward: 5’-GGGCTGGCAAGCCACGTTTGGTG-3’

T7 terminator: 5’-GCTAGTTATTGCTCAGCGG-3’

IVT 154mer forward: 5’-TAA TAC GAC TCA CTA TAG GC-3’

IVT 154mer backward: 5’-GAA CTG TCT CAC GAC GTT C-3’

4.5.2. RNA substrates

9mer: 5´-UUGGGACCU-3´

Cy3-9mer: 5´-UUGGGACCU(Cy3) -3´

32mer: 5´-CGAGGUCCCAAGGGUUGGGCUGUUCGCCCAUU-3´

Cy5-32mer: 5´- (Cy5)CGAGGUCCCAAGGGUUGGGCUGUUCGCCCAUU-3´

32mer_fluorescein: 5´- (FAM)GCAGGUCCCAAGGGUUGGGCUGUUCGCCCAUU-3´

4.6. List of YxiN mutants and abbreviations

YxiN AAAS: YxiN wildtype for smFRET measurements. C61 and C267 exchanged to alanine; A115 and S229 exchanged to cysteine for labelling

YxiN K52Q: Walker A (motif I) mutant, shown to be ATPase deficient [56]

YxiN R330A: motif VI mutant, uncoupling mutant

YxiN lk 3: mutant with a linker length of 3 amino acids (linker between the two RecA core domains)

YxiN lk 4: mutant with a linker length of 4 amino acids (linker between the two RecA core domains)

YxiN lk 5: mutant with a linker length of 5 amino acids (linker between the two RecA core domains)

YxiN lk 7: mutant with a linker length of 7 amino acids (linker between the two RecA core domains)

YxiN lk 9: mutant with a linker length of 9 (wt length) amino acids (linker between the two RecA core domains)

YxiN lk 11: mutant with a linker length of 11 amino acids (linker between the two RecA core domains)

YxiN lk 13: mutant with a linker length of 13 amino acids (linker between the two RecA core domains)

YxiN lk 15: mutant with a linker length of 15 amino acids (linker between the two RecA core domains)

YxiN core: YxiN 1-404; mutant consisting of the two RecA domains

YxiN GST-RBD: YxiN 404-478; RNA binding domain of YxiN fused to GST

4.7. General Methods

4.7.1. Agarose Gel Electrophoresis

DNA fragments of up to 1 kb were separated on 2 % agarose gels, DNA fragments with a size bigger than 1 kb were separated on 0.8 % agarose gels. 6x loading buffer (10 mM Tris/HCl, pH 7.6; 60 mM EDTA; 0.03 % (w/v) bromphenol blue; 0.03 % (w/v) xylencyanole; 60 % (v/v) glycerol) was added to the samples prior to gel loading. The electrophoresis was performed at 160 V for 20 min. Gels were stained in ethidium bromide solution and DNA bands visualised using a UV light source.

4.7.2. SDS-Polyacrylamide Gel Electrophoresis

Stacking gel:	125 mM Tris/HCl, pH 6.8; 4.5 % acrylamide; 0.1 % (v/v) *N,N'* – methylenbisacrylamide; 0.06 % (w/v) SDS; 0.1 % (w/v) APS and 0.1 % (v/v) TEMED
Resolving gel:	375 mM Tris/HCl, pH 8.8; 15 % acrylamide; 0.4 % (v/v) *N,N'* – methylenbisacrylamide; 0.1 % (w/v) SDS; 0.086 % (w/v) APS and 0.06 % (v/v) TEMED
Running buffer:	24 mM Tris base; 0.1 % (w/v) SDS; 200 mM glycine
4x loading buffer:	130 mM Tris/HCl, pH 6.8; 200 mM DTT; 4 % (w/v) SDS; 20 % glycerine; 0.01 % bromphenol blue
Staining solution:	50 % (v/v) methanol; 10 % (v/v) acetic acid; 0.1 % (w/v) Brilliant Blue R-250
Destaining solution:	20 % (v/v) ethanol; 10 % (v/v) acetic acid

Protein samples were analysed on denaturing polyacrylamide gels consisting of a stacking gel with lager pockets and a resolving gel. This method established by Laemmli[57] allows better resolution since the bands get focussed in the stacking gel before entering the resolving gel, where proteins get separated according to their size. The electrophoresis was performed at 30 mA until the front reached the end of the gel. Gels were then stained in staining solution for approximately 30 min and destained with destaining solution for approximately 15 min and kept in water. All gels were photographed for documentation.

4.7.3. Preparation of ADP·BeF_x

ADP·BeF_x nucleotides were prepared by mixing stock solutions of $BeCl_2$, NaF and ADP to a final concentration of 14.3 mM ADP, 71.5 mM $BeCl_2$, and 751 mM NaF[39, 58].

4.7.4. Absorption measurements

To determine concentrations of RNA, protein and labelled protein, absorption spectra were recorded (Ultraspec 2100 pro) or a single wavelength value at A_{280} was recorded (BioPhotometer). Absorption values were corrected for buffer contributions and concentrations calculated according to the Beer-Lambert law (eq.1)

$$A_x = c * \varepsilon_x * d \qquad \text{eq.1}$$

A_x – absorption at wavelength x; c – concentration; ε_x – extinction coefficient at wavelength x; d – path length (1 cm)

The following extinction coefficients were used:

For DNA: A_{260} = 50 ng/ml

153mer RNA: ε_{260} = 1425000 $M^{-1}cm^{-1}$

32mer RNA: ε_{260} = 2112000 $M^{-1}cm^{-1}$

32mer_fl RNA: ε_{260} = 2112000 $M^{-1}cm^{-1}$

Cy5-32mer RNA: ε_{260} = 29889000 $M^{-1}cm^{-1}$

9mer RNA: ε_{260} = 846000 $M^{-1}cm^{-1}$

Cy3-9mer RNA: ε_{260} = 846000 $M^{-1}cm^{-1}$

A488: ε_{493} = 72000 $M^{-1}cm^{-1}$ (ε_{280} = 7922 $M^{-1}cm^{-1}$ taken into account when calculating labelled protein concentration)

A546: ε_{554} = 93000 $M^{-1}cm^{-1}$ (ε_{493} = 7025 $M^{-1}cm^{-1}$; ε_{280} = 10538 $M^{-1}cm^{-1}$ taken into account when calculating double labelled protein concentration)

YxiN: ε_{280} = 23540 $M^{-1}cm^{-1}$ [59]

4.7.5. Mutagenesis

For the generation of all mutations of the linker between the two Rec-domains of YxiN, YxiN wildtype previously cloned in a pETM30 vector was used as a starting point. The mutations were introduced following the *QuickChange™ Site-directed mutagenesis* protocol from Stratagene. According to this protocol complementary DNA-primer strands were designed containing the respective mutations with a melting temperature of about 80°C. 200 nM of each primer, 200 µM dNTPs mix and 2-3 units of *Pfu* DNA polymerase were added to 90 ng of plasmid DNA. This mixture was subject to the following PCR cycle: 5 min of initial heating at 95 °C, 95 °C for 30 sec, different temperatures according to the mutations for 60 sec, 68 °C for 14 min 30 sec, 68 °C for 10 min. Steps 2-4 were repeated 25 times. Success of this reaction was analysed using 0.8% agarose gels. Successful reactions were incubated with 10 units of DpnI at 37 °C for 1 hour. This leads to digestion of hemimethylated template plasmids. After digestion the mutated plasmids were transformed into *E.coli* XL-1 blue cells. (section 4.7.6). Transformants were selected on antibiotic containing LB plates. As there can occur multiple primer-insertions in the PCR reaction, a screening PCR was performed to exclude those clones. Primers for this reaction were selected to bind in proximity of the mutation on each strand. As a positive control a plasmid with the correct length was included. 500 nM of each primer, 200 µM dNTPS and 0.5 units *GoTaq* polymerase were

added to bacterial cells in 20 µl of sterile water. This mixture was subject to the following PCR cycle: 5 min of initial heating at 95 °C, 95 °C for 30 sec, 55 °C for 30 sec, 72 °C for 1 min, steps 2-4 were repeated 30 times. PCR products were analysed using 2% agarose gels. Of the clones without any inserts, overnight LB-cultures were grown for plasmid isolation following the QIAprep Miniprep protocol (elution was done with only 20% EB though). Plasmid DNA was then sent for sequencing with Microsynth (Balgach, CH).

4.7.6. Transformation

100 ng of plasmid DNA or PCR samples were added to $CaCl_2$ competent *E.coli* cells. The cells were kept on ice for 10 min and after 90 s incubation at 42 °C put on ice for another 2 min. 900 µl of LB were added to the cells, which were then incubated at 37 °C for 1 hour. Cells were then harvested by centrifugation (2 min; 3000 rpm) and plated on LB plates supplemented with the respective antibiotics, allowing for selection of transformants.

4.7.7. Labelling of YxiN Constructs with Fluorophores

Buffer A: 50 mM Tris/HCl pH 8.5 at 4 °C; 500 mM NaCl; 500 µM TCEP

Buffer B: 50 mM Tris/HCl pH 8.5 at 4 °C; 500 mM NaCl; 2 mM 2-Mercaptomethanol

The storage buffer of the protein was exchanged to Buffer A, prior to the labelling reaction using P30 MicroSpin columns and the protein diluted to 30 - 40 µM. Maleimide-functionalised donor (Alexa 488) and acceptor (A 546) dyes were mixed and added to the

protein. Donor dye was added in a 3-fold excess over protein and acceptor dye in a 4-fold excess. The labelling reaction was performed in low-retention tubes at 25 °C for 1 hour in the dark. Removal of free dye was performed using P30 MicroSpin columns afore equilibrated with Buffer B, passing the labelling reaction over the column two times. Concentration of protein and dyes and the respective labelling efficiencies were determined using a Spectrophotometer.

4.7.8. In vitro transcription

IVT-Buffer:	80 mM Tris/HCl, pH 7.5; 22 mM $MgCl_2$; 1 mM spermidine; 5 mM DTT; 0.12 mg/ml BSA
TBE Buffer:	89 mM Tris; 89 mM boric acid; 10.7 mM EDTA
8 M Urea 10% PA gel:	8 M Urea; 89 mM Tris; 89 mM boric acid; 10.7 mM EDTA; 10% (v/v) acrylamide; 0.267 (v/v) *N,-N'*-methylenebisacrylamide; polymerised by addition of 0.045% (w/v) APS and 0.113% (v/v) TEMED

A 153 bp fragment of *B.subtilis* 23S rRNA (nucleotides 2483-2635) cloned into pUC18 was amplified using PCR with a forward primer containing the T7 promoter sequence to generate a template for *in vitro* transcription[49]. The following PCR cycle was used: 1 min at 95 °C initial heating; 30 sec at 95 °C; 30 sec at 48 °C; 20 sec at 72 °C; steps 2-4 were repeated 35 times. The PCR product was EtOH precipitated and used as a template for *in vitro* transcription (80 mM Tris/HCl, pH 7.5; 22 mM $MgCl_2$; 1 mM spermidine; 5 mM DTT; 0.12 mg/ml BSA; 20 mM ATP; 20 mM UTP; 20 mM CTP; 20 mM GTP; 1.5 µM template DNA; 2 U T7 polymerase; 37 °C; 4h). Stopping of the reaction was achieved by addition of 1/10 volume 0.5 M EDTA (pH 8), 1/10 volume 3 M sodiume acetate and 3 volumes ethanol. RNA was precipitated at -20 °C for 20 min and centrifuged (13'000 rpm; 14 °C; 1h). Pellets were

washed with 70 % ethanol and dissolved in water and 2xFermentas RNA loading dye. Samples were loaded on an 8 M Urea 10 % polyacrylamide gel and run at 500 V/ 20 W for 2 h 20 min in TBE buffer. Product bands were visualised with UV (λ = 254 nm), excised and kept in TBE buffer. RNA was eluted in TBE at 100 mA/250 V for 4h at 4 °C and precipitated by addition of 1/10 volume 0.5 M EDTA (pH 8), 1/10 volume 3 M sodiume acetate and 3 volumes ethanol at -20 °C over night. Precipitate was pelleted by centrifugation at 13'000 rpm at 14 °C for 1h. The pellet was washed with 70 % ethanol, dried for a few hours and dissolved in 20 mM HEPES/NaOH pH, 7.2. The concentration was determined by absorption spectroscopy.

4.8. Protein Expression and Purification

4.8.1. Protein Expression

A single *E.coli* clone was used to inoculate a 20 ml LB medium culture containing Chloramphenicol (10 µg/ml) and Kanamycine (20 µg/ml) that was incubated overnight at 37 °C. This culture was then used to inoculate a 4 l culture of auto inducing medium (AIM[60]), which was incubated for 24 h at 30 °C. Cells were harvested by centrifugation (10 min; 4 °C; 4800 rpm; SLA3000 rotor) and resuspended in a total volume of 50 ml buffer (50 mM Tris/HCl, pH 8.5 at 4°C; 500 mM NaCl; 2 mM 2-Mercaptoethanol). Cell disruption was performed by the use of a microfluidizer. To remove cell-debris the disrupted cell solution was centrifuged (40 min; 13000 rpm; SS30 rotor).

4.8.2. Purification

Buffer A: 50 mM Tris/HCl, pH 8.5 at 4 °C; 500 mM NaCl; 2 mM 2-Mercaptoethanol

Buffer B: 50 mM Tris/HCl, pH 8.5 at 4 °C; 500 mM NaCl; 20 mM glutathione; 2 mM 2-Mercaptoethanol

Buffer C: 50 mM Tris/HCl, pH 8.5 at 4 °C; 500 mM NaCl; 20 mM imidazole; 2 mM 2-Mercaptoethanol

Buffer D: 50 mM Tris/HCl, pH 8.5 at 4 °C; 500 mM NaCl; 500 mM imidazole; 2 mM 2-Mercaptoethanol

All purification steps were performed at 4 °C to ensure optimal protein stability. The protein solution was loaded on a glutathione-affinity column at a flow rate of 0.5 ml/min. The protein was eluted with Buffer B at a flow rate of 0.5 ml/min. The eluted protein was dialysed over night in 1 l Buffer A. At the same time the GST-affinity tag was removed by a TEV protease digest. Since the GST-affinity tag is fused to a His-Tag, it can be removed by a Nickel metal affinity chromatography. 20 mM imidazole was added to the dialysed protein solution, which was loaded on a Nickel metal affinity column at a flow rate of 1 ml/min. The flow-through with the protein of interest was collected and the two tags as well as uncleaved protein were eluted with Buffer D from the column. An ammonium sulphate precipitation with 80% ammonium sulphate followed. Ammonium sulphate was added at room temperature, and the protein solution with ammonium sulphate was stirred for 2 h at 4 °C. The precipitated protein was collected by centrifugation (40 min; 13000 rpm; SS30). The gained pellet was resuspended in 1.4 ml Buffer A, and loaded at a flow rate of 1 ml/min on a S200 size exclusion chromatography column. Eluted protein was collected in fractions of 1 ml. Pure fractions were pooled and concentrated using a Vivaspin (Vivaspin 6; 10'000 MCWO) concentrator. Protein concentration was determined using a spectrophotometer with an extinction coefficient of ε_{280} = 23540 M^{-1} cm^{-1} (as calculated by the ExPaSy -

ProtParam tool of the SIB Bioinformatics Resource Portal). After shock-freezing the proteins were stored at -80 °C.

4.9. Steady state ATPase activity assay

Assay Buffer: 50 mM HEPES/KOH, pH 7.5; 175 mM KCl; 10 mM $MgCl_2$; 200 µM NADH; 400 µM PEP; 13 µg/ml lactate dehydrogenase; 23 µg/ml pyruvate kinase

ATPase activity of YxiN was monitored in an enzymatically coupled spectroscopic assay[61]. Steady state ATP conditions were achieved by the conversion of ADP and PEP to pyruvate and ATP by the enzymatic activity of pyruvate kinase. Pyruvate is further reduced to lactate by the oxidation of NADH to NAD^+ by lactate dehydrogenase. The consumption of NADH can be followed spectroscopically by measuring the absorbance at A_{380}. The decrease in NADH concentration is linked to the decrease in ATP concentration. Therefore the velocity of NADH consumption corresponds to the velocity of ATP turnover. The reactions were performed at varying 153mer RNA concentrations; 5 mM ATP and 10 nM to 1 µM YxiN (depending on the mutant) at 37 °C. Buffer and ATP were equilibrated for 5 min and the reaction started by the addition of RNA and YxiN. As the RNA substrate concentration is in the same range as the YxiN concentration, the explicit binding equation was used to analyse the data. (eq.2)

$$k = \frac{k_{cat}}{[YxiN]}\left[\frac{[S]_0 + [YxiN] + K_{app,RNA}}{2} - \sqrt{\left(\frac{[S]_0 + [YxiN] + K_{app,RNA}}{2}\right)^2 - [S]_0[YxiN]}\right] \quad \text{eq.2}$$

$[S]_0$ – substrate concentration; k_{cat} – turnover number; $K_{app,RNA}$ – apparent dissociation constant for RNA

4.10. mantADP Fluorescence Titrations

Buffer: 50 mM Tris/HCl, pH 8.5 at 4 °C; 150 mM NaCl, 10 mM $MgCl_2$; 2 mM 2-Mercaptoethanol

Assay conditions:

Equilibrium titrations: 1 µM mantADP; λ_{exc} = 360 nm (bandwidth 5 nm); λ_{em} = 440 nm (bandwidth 5 nm); 20 °C; Hitachi F-4500

Displacement titrations: 1 µM mantADP; 10 µM YxiN; λ_{exc} = 360 nm (bandwidth 5 nm); λ_{em} = 440 nm (bandwidth 5 nm); 20 °C; Hitachi F-4500

To determine binding constants of YxiN wildtype and YxiN mutants, a fluorescent ADP analogue, mantADP as well as ATP, ADP and the non hydrolysable ATP-analogue ADP·BeF_x were used. mantADP changes its fluorescent signal according to its environment[62]. In a rather hydrophilic environment the signal is weaker than in a hydrophobic environment thus mantADP fluorescent increases upon binding to YxiN. The dissociation constant of YxiN wildtype was determined using the following equation (eq.3):

$$F = F_{0+}\Delta F_{\max}\frac{\frac{[YxiN]_{tot}+[mADP]_{tot}+K_d}{2}-\sqrt{\left(\frac{[YxiN]_{tot}+[mADP]_{tot}+K_d}{2}\right)^2-[YxiN]_{tot}[mADP]_{tot}}}{[mADP]_{tot}}$$

Eq.3: F – fluorescent signal; F_0 – initial fluorescent signal; ΔF_{max} – maximal change of fluorescent signal; Kd – dissociation constant

Dissociaton constants of YxiN mutants could not be determined directly by fluorescent equilibrium titrations due to aggregation issues. Therefore initial slope values were determined and compared to wildtype values.

To determine dissociation constants of ATP, ADP and the non-hydrolisable ATP-analogue ADP·BeF_x competitive displacement titrations with a pre-formed mantADP/YxiN complex were performed. The solution of the cubic equation (eq.3) describing the competitive titration was evaluated numerically using the program Scientist (Micromath) to yield the Kd of the respective nucleotide complex.

4.11. Anisotropy measurements

Buffer: 50 mM Tris/HCl, pH 7.5; 150 mM NaCl; 5 mM $MgCl_2$

Assay conditions: λ_{exc} = 495 nm (slit 10 nm); λ_{em} = 530 nm (slit 10 nm); time increment 12 s; total time 120 s; 5 nM RNA substrate; 25 °C

Anisotropy measurements were performed to determine binding constants of YxiN wildtype and YxiN mutants to a minimal RNA substrate of 32 bp labelled with fluorescein. In anisotropy measurements linear polarised light is used to excite the fluorescent dye. The emitted light is polarised as well and detected on two polarisation filters. One is placed parallel to the exciting polarisation filter and the other one is placed perpendicular to the exciting polarisation filter. With the two intensities detected the anisotropy can be defined as:

$$r = \frac{I_{\parallel} - I_{\perp}}{I_{\parallel} + 2I_{\perp}} \qquad \text{eq.4}$$

r - anisotropy; $I_{\parallel}$ - parallel intensity; $I_{\perp}$ - perpendicular intensity

Given the fluorescent molecule is immobile, the anisotropy values is 1. Thus, the more mobile the fluorescent molecule gets, the smaller the anisotropy value. A fluorescein labelled 32mer RNA substrate was present in buffer, and YxiN wildtype or YxiN mutants

were titrated to this RNA. RNA binding to YxiN lead to an increase in anisotropy which allowed determination of the dissociation constant Kd using equation 5.

$$r = r_0 + \left(\frac{\Delta r}{[RNA]} * \frac{[YxiN] + [RNA] + Kd}{2} - \sqrt{\left(\frac{[YxiN] + [RNA] + Kd}{2} \right)^2 - [YxiN] * [RNA]} \right) \quad \text{eq.5}$$

r - anisotropy; r_0 - initial anisotropy; Δr - change in anisotropy; Kd - dissociation constant

4.12. Double stranded RNA unwinding assay

4.12.1 Spectroscopic unwinding assay

Buffer: 50 mM HEPES, pH 7.2; 50 mM KCl; 5 mM $MgCl_2$; 5% Glycerol; 0.1 mM DTT; 0.1 mg/ml BSA

Assay conditions: 500 nM dsRNA; 5 µM 9mer trap; 500 µM ATP or 200 µM ADP·BeF_x; λ_{exc} = 554 nm (slit 1 nm); λ_{em} = 666 nm (slit 1 nm); 25 °C

dsRNA substrate generation: 25 µM Cy3-9mer; 50 µM Cy5-32mer; 50 mM HEPES,pH 7.2; 25 °C; 1h

Unwinding of a fluorescently labelled Cy5-32mer/Cy3-9mer minimal dsRNA substrate was monitored by observing FRET decay of the acceptor labelled strand. In order to inhibit reannealing of the two fluorescently labelled substrate RNA strands, a non-labelled 9mer strand (trap) was present in the reaction in excess. The dsRNA substrate and the trap strand were equilibrated in buffer at 25 °C for 5 min, and the unwinding reaction started by the

addition of YxiN and ATP or ADP·BeF_x respectively. FRET signal of the acceptor strand was measured for 30 minutes and evaluated with a single exponential to get unwinding rate constants.

4.12.2 Polyacrylamide gel-based unwinding assay

TB(E) Buffer: 500 mM Tris, pH 8.0; 500 mM Boric acid, 5 mM EDTA

2-fold stopping buffer:	2% SDS; 100mM DTT; 10% glycerine; 0.1% Bromphenolblue; 50 mM Tris, pH 6.8
5-fold activity Buffer:	250 mM HEPES, pH 7.2; 750 mM KCl; 25% glycerine; 0.5 mM DTT; 25 mM $MgCl_2$; 0.5 mg/ml BSA
Gel run conditions:	100 V; 10 mA; 4°C; 2h

Unwinding assays were performed with 5 µM RNA and 10 µM YxiN in activity buffer and in the presence of 10 mM ATP or ADP, or 5.5 mM ATP analogues at 25°C for 30 minutes, and unwinding products were analyzed by native polyacrylamide gel electrophoresis.

4.13. Fluorescence resonance energy transfer (FRET)

Fluorescence resonance energy transfer (FRET) is based on a non-radiative energy transfer from a donor fluorophor to an acceptor fluorophor via dipole-dipole interactions. This transfer can only take place, if there is a spectral overlap of donor emission and acceptor excitation. The efficiency of this transfer heavily depends on the distance between the two

fluorophores and can be calculated from the transfer efficiency (eq.6). This technique thus is widely used in biochemistry and biophysics as a molecular ruler.

$$E = \frac{R_0^6}{R_0^6 + r^6} \qquad \text{eq.6}$$

E - FRET efficiency; R_0 - Förster distance; r - inter-dye distance

The Förster-distance is the distance between the two fluorophores at which E = 0.5 and depends on the spectral properties of the dye-pair used, the relative orientation of the dipoles for donor and acceptor and the refractive index. Therefore the Förster-distance has to be determined for every dye-pair under the conditions used in the experiment (attached to protein and in activity buffer). (described in section 4.13.3).

4.13.1 Confocal smFRET set-up

Substrate binding and enzymatic properties are widely determined using ensemble techniques that measure an average value of all molecules present. Transient states or rare events are not observable using such techniques since they disappear in the average signal. Single molecule techniques allow detection of such rare events or transient states. Determination of a large number of single molecules gives the distribution within the population. Single molecule conditions for FRET studies are achieved by extremely diluted samples (picomolar concentrations) and a minimised observation volume (in the range of 10^{-15} l). In a confocal microscope, the donor fluorophores are excited by a laser beam that is focused into the confocal volume using an objective. Fluorescence emitted by the donor and acceptor fluorophores within the confocal volume is collected by the same objective.

The detection beam is transferred to a pin-hole to block out all “out-of-focus” light and split up into the acceptor and donor contributions by the use of accordant beam-splitters and detected.

4.13.2. Determination of correction parameters

Buffer A: 50 mM Tris/HCl, pH 7.5; 150 mM NaCl; 5 mM $MgCl_2$ (treated with charcoal to remove fluorescent impurities)

Buffer B: 50 mM Tris/HCl, pH 7.5; 500 mM NaCl; 2 mM 2-Mercaptoethanol

Data obtained in the confocal smFRET set-up needs to be corrected for direct excitation of the acceptor (δ), for acceptor bleed-through into the donor-channel (β) and donor bleed-through into the acceptor channel (α). To determine these correction parameters respective single cysteine mutants of each FRET pair were labelled with donor or acceptor and free dye removed as described in section 4.7.7. Since correction parameters for measurements with RNA present in RNA binding domain studies were determined, a 5 times excess of 32mer RNA was present in all measurements. Correction parameters for all other smFRET experiments were determined prior to this work by Bettina Theissen and Anne Karow[46, 59]. To determine δ, absorbance spectra (400 - 900 nm) of 5 µM of donor or acceptor only labelled single cysteine mutants in Buffer B were recorded three times at 25 °C. A mean of the absorbance at 475 nm was taken and δ calculated. (eq. 7)

$$\delta = \frac{A_{acceptor} / [acceptor]}{A_{donor} / [donor]} \qquad \text{eq.7}$$

δ - direct acceptor excitation; A - mean absorbance at 475 nm

To determine donor and acceptor leakage, 100 nM of donor or acceptor only labelled single cysteine mutants in Buffer A and Buffer A only were measured in saturated cuvettes at 75 µW for 5 min using neutral filters. Counting rates were normalised to dye concentrations and α, β and γ were calculated. (eqs. 8, 9, 10)

$$\alpha = \frac{I_A^{Donor} - I_A^{Buffer}}{I_D^{Donor} - I_D^{Buffer}} \qquad \text{eq.8}$$

$$\beta = \frac{I_D^{Acceptor} - I_D^{Buffer}}{I_A^{Donor} - I_A^{Buffer}} \qquad \text{eq.9}$$

$$\gamma = \frac{I_A^{Acceptor} - I_A^{Buffer}}{I_D^{Donor} - I_D^{Buffer}} * \delta^{-1} \qquad \text{eq.10}$$

I_A - counting rate in the acceptor channel; I_D - counting rate in the donor channel

4.13.3. Determination of Förster distances

For conversion of FRET efficiencies into distances between the fluorophores attached to the protein a Förster distance R_0 specific for the mutant is needed. R_0 for a double-cysteine mutant XY can be determined as followed, if assumed that the donor dye is at position X and the acceptor dye is at position Y and the other way around. (eq.11)

$$R_0 = \sqrt[6]{\frac{9000 * \ln 10}{128 * \pi^5 N_A} * \phi_D * \kappa^2 * n^{-4} * J} \qquad \text{eq.11}$$

R_0 - Förster distance; N_A - Avogadro number; ϕ_D - donor quantum yield; κ^2 - orientation factor; n - index of refraction; J - overlap integral

The orientation factor κ^2 was assumed to be 2/3, which corresponds to a freely rotating dye and the index of refraction was set to n_{water} = 1.33 since all proteins were measured in aqueous solution. The overlap integral *J* and donor quantum yield ϕ_D were determined as follows: An absorption spectrum of the acceptor-labelled species was recorded and dye concentration determined. A fluorescence emission spectrum of a 10 nM solution of the corresponding donor-labelled species was recorded (λ_{exc} = 460 nm; excitation slit 5 nm; emission slit 5 nm; integration time 0.5 s; Buffer A) and normalised to have an integrated area of 1. The acceptor spectrum and the normalised donor emission spectrum were then used to calculate the overlap integral *J*. (eq.12)

$$J(\lambda) = \int_0^\infty F_D(\lambda) * \varepsilon_A * \lambda^4 d\lambda \qquad \text{eq.12}$$

J - overlap integral; $F_D(\lambda)$ - normalised area of donor fluorescence; ε_A - extinction coefficient of acceptor at wavelength λ

The concentration, A_{460} and the fluorescence spectrum of fluorescein in 0.1 M NaOH (λ_{exc} = 460 nm; excitation slit 5 nm; emission slit 5 nm; integration time 0.5 s) were determined and the donor quantum yield ϕ_D was determined relative to fluorescein. (eq.13)

$$\phi_D = \frac{F_D * E_R * \phi_R}{F_R * E_D} \qquad \text{eq.13}$$

ϕ_D – donor quantum yield; F_D – normalised area of donor fluorescence; E_D – donor absorbance at 460 nm; F_R – normalised area of fluorescein fluorescence; E_R – fluorescein absorbance at 460 nm; ϕ_R = 0.92 [63]

4.13.4. Confocal smFRET experiments

Buffer A: 50 mM Tris/HCl, pH 7.5; 150 mM NaCl; 5 mM $MgCl_2$ (treated with charcoal to remove fluorescent impurities)

SmFRET was measured in a home-built confocal set up (see section 4.3) in cuvettes (Lab-Tek chamber slides) which were pre-incubated with 10 µM $YxiN_{1-368}$ for 1h at RT for saturation. YxiN mutants were diluted in Buffer to 80 pM donor concentration and substrates added as indicated. Donor was excited at 475 nm with 75 µM and single molecule fluorescence was recorded until 20 million events were recorded.

Since not only the labelled proteins passing the confocal volume cause photon counts but also small fluorescent impurities, an algorithm calculating the noise and detecting bursts was applied to the raw data and bursts with more than 50 (or 100 if indicated) photons were selected[64]. FRET efficiencies for each burst were calculated using eq. 14. The correction parameters α and β account for crosstalk of donor and acceptor respectively, γ accounts for the difference in quantum yield and detection efficiencies of donor and acceptor and δ accounts for direct excitation of acceptor at 475nm.

$$E = \frac{(1+\beta\gamma\delta)*\left(I_A - \frac{\alpha+\gamma\delta}{1+\beta\gamma\delta}*I_D\right)}{(1+\beta\gamma\delta)*\left(I_A - \frac{\alpha+\gamma\delta}{1+\beta\gamma\delta}*I_D\right)+(\gamma+\gamma\delta)(I_D-\beta I_A)} \qquad \text{eq.14}$$

E - FRET efficiency; I_A - counting rate in acceptor channel; I_D - counting rate in donor channel; α, β, γ, δ - correction parameters

5. Results

5.1. - Part I wildtype

In order to have reference values to compare the data obtained for the YxiN catalytic core linker constructs, YxiN wildtype properties were studied. In addition, these studies give insights into the nucleotide cycle of YxiN previously not known.

5.1.1. Nucleotide binding affinities of YxiN wildtype and YxiN R330A

It is important to know binding affinities of YxiN to different nucleotides in order to have saturating conditions in all experiments that are performed in the presence of nucleotides. Furthermore these numbers hold important information concerning the enzymatic cycle. For the YxiN R330A mutant, a motif VI mutant, it was interesting to determine, whether there is an influence on nucleotide binding, as mutations in motif VI uncouple nucleotide binding and hydrolysis from unwinding actions. Nucleotide binding affinities of YxiN wildtype and YxiN R330A were determined by displacement titrations of a preformed mantADP/YxiN complex by the respective nucleotide. The experimental procedure is described in section 4.10.

Figure 10: Nucleotide binding of YxiN wildtype

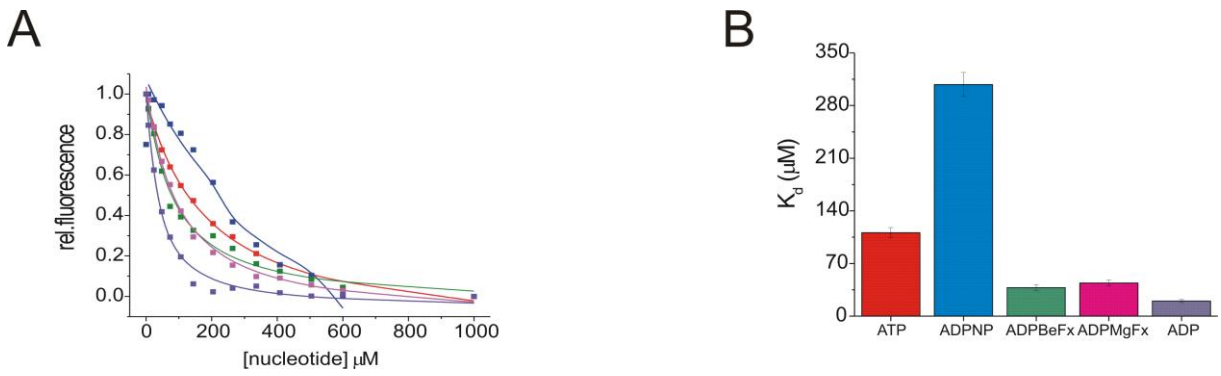

Figure 10: Nucleotide binding of YxiN wildtype

Figure 10 shows displacement titrations of YxiN wildtype for ATP (red, 111 ± 7 µM), ADPNP (blue, 308 ± 16 µM), ADP·BeF_x (green, 38 ± 4 µM), ADP·MgF_x (magenta, 44 ± 4 µM) and ADP (violet, 20 ± 2 µM). Kd values were determined by displacement titrations of mantADP/YxiN complexes with the respective nucleotides as described in section 4.10.

The affinity of YxiN wildtype for ATP was determined to be 111 ± 7 µM. The affinity of ADPNP is clearly lower as reflected by the Kd value of 308 ± 16 µM. The affinities for the pre-hydrolysis analogue ADP·BeF_x[65-67] is clearly higher as seen in the Kd value of 38 ± 4 µM. For the post-hydrolysis analogue ADP·MgF_x[65-67] the affinity is in the same range as the affinity for ADP·BeF_x (Kd = 44 ± 4 µM). The affinity for ADP is also found to be higher than the one for ATP and the Kd value is determined to be 20 ± 2 µM.

The YxiN R330A mutant shows a Kd value of 38 ± 5 µM for ATP. This value is a bit lower for the pre-hydrolysis analogue ADP·BeF_x and found to be 82 ±21 µM. The Kd value for ADP again is a bit higher and determined to be 27 ± 4 µM.

Figure 11: Nucleotide binding of YxiN R330A

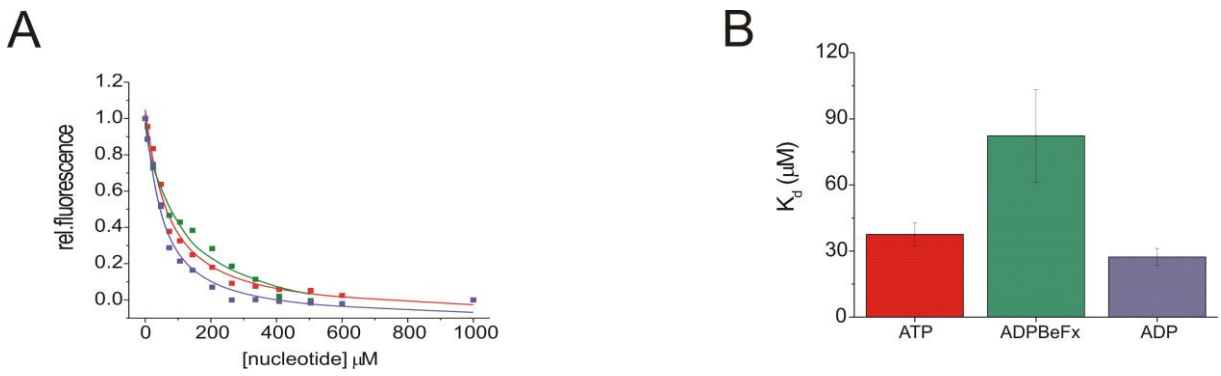

Figure 11: Nucleotide binding of YxiN R330A

Figure 11 shows displacement titrations of YxiN R330A for ATP (red, 38 ± 5 µM), ADP·BeF_x (green, 82± 21 µM), and ADP (violet, 27± 4 µM). Kd values were determined by displacement titrations of mantADP/YxiN complexes with the respective nucleotides as described in section 4.10.

Comparing YxiN wildtype to YxiN R330A it can be seen, that the affinity for ATP is much higher for YxiN R330A than for YxiN wildtype. This is different in the case of ADP·BeF_x. Here the affinity for YxiN R330A is clearly lower than for YxiN wildtype. In the case of ADP there is no dramatic change in affinity to be observed.

Figure 12: Comparison of nucleotide binding of YxiN R330A and YxiN wildtype

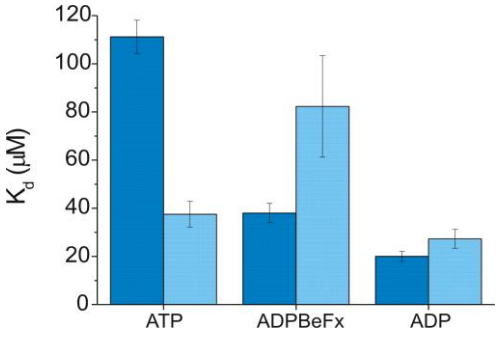

Figure 12: Comparison of nucleotide binding of YxiN R330A and YxiN wildtype

Figure 12 shows a comparison of the displacement titrations of YxiN R330A and YxiN wildtype. YxiN wildtype values are shown in dark blue and Kd values for YxiN R330A are shown in light blue.

For YxiN wildtype it can be seen, that the differences in the enzymatic cycle are reflected also by differences in nucleotide affinities. The motif VI mutant YxiN R330A definitively shows differences in nucleotide binding compared to YxiN wildtype, which could play a role in uncoupling nucleotide binding and hydrolysis from unwinding activity.

5.1.2. Nucleotide binding of YxiN wildtype in the presence of RNA

Binding affinities of YxiN wildtype to different nucleotides were also determined in the presence of a minimal RNA substrate. Nucleotide binding affinities of YxiN wildtype were determined by displacement titrations of a preformed mantADP/YxiN complex in the presence of a 32mer RNA minimal substrate by the respective nucleotide. The experimental procedure is described in section 4.10.

Figure 13: Nucleotide binding of YxiN wildtype with an RNA substrate

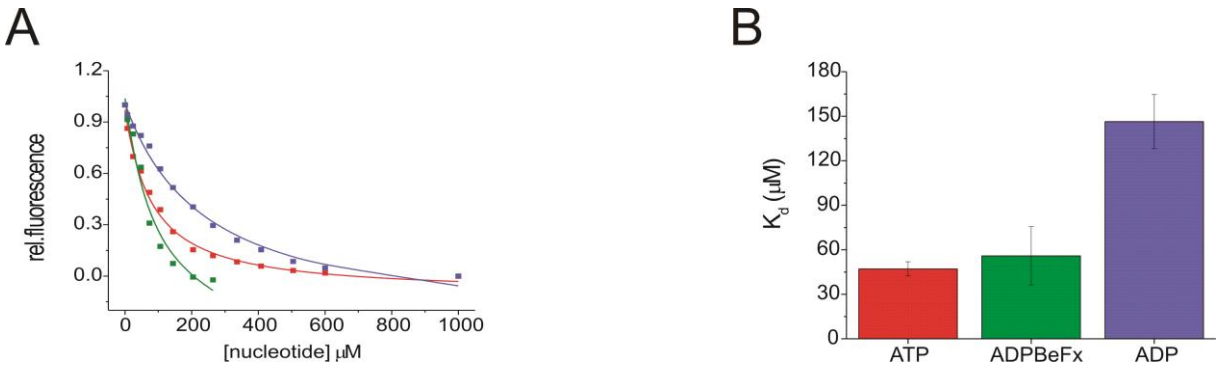

Figure 13: Nucleotide binding of YxiN wildtype with an RNA substrate

Figure 13 shows the nucleotide binding of YxiN wildtype in the presence of a 32mer RNA substrate. Graphs shown originate from taking a mean value of at least two independent measurements and fitting of them. Experimental procedure of these displacement titrations is described in section 4.10. ATP is shown in red, ADP·BeF_x is shown in green and ADP is shown in violet. Panel A shows nucleotide affinities of YxiN wildtype for ATP (47 ± 5 µM), ADP·BeF_x (56 ± 20 µM) and ADP (146 ± 18 µM). Panel B shows a comparison of the respective nucleotide affinities.

The affinity of YxiN wildtype for ATP was determined to be 47 ± 5 µM. The affinity for the pre-hydrolysis analogue ADP·BeF_x[65-67] is in the same range as reflected by the Kd value of 56 ± 20 µM. The affinity for ADP is clearly lower as the affinity for ATP as reflected by the Kd value of 146 ± 18 µM. In comparison to the nucleotide affinities determined without any RNA substrate it is evident, that there is a change in nucleotide specificity. In the presence of an RNA substrate, the affinity for ATP is dramatically increased, and the affinity for ADP is dramatically decreased. In the presence of an RNA substrate high affinity nucleotide binding is observed in the beginning of the catalytic cycle and low affinity nucleotide binding is observed at the end of the catalytic cycle. Thus there is a positive cooperativity of RNA and ATP and a negative cooperativity of RNA and ADP.

5.1.3. RNA binding of YxiN wildtype and two motive mutants in the nucleotide cycle

Knowing affinities for nucleotides throughout the enzymatic cycle, the next question arising is if affinities for a minimal RNA substrate correlates with nucleotide affinities. To determine these RNA binding affinities of YxiN wildtype as well as of the two motive mutants YxiN K52Q and YxiN R330A, an ATPase deficient and a presumably uncoupling mutant, fluorescence anisotropy titrations with a fluorescein labelled minimal RNA substrate were performed as

described in section 4.11. The Kd value of YxiN wildtype in the absence of nucleotide is determined to be 375 ± 96 nM, reflecting a tight binding. There is a slight increase in affinity in the presence of ADPNP, ADP·BeF_x and ADP to Kd values of 206 ± 19 nM, 276 ± 65 nM and 276 ± 58 nM respectively. In the presence of ADP·MgF_x there is a slight decrease in affinity to a Kd value of 524 ± 230 nM. These findings show that there is an increase in affinity upon nucleotide binding, which is abolished after ATP hydrolysis and finally reset after P_i release.

Figure 14: RNA binding of YxiN wildtype in the nucleotide cycle

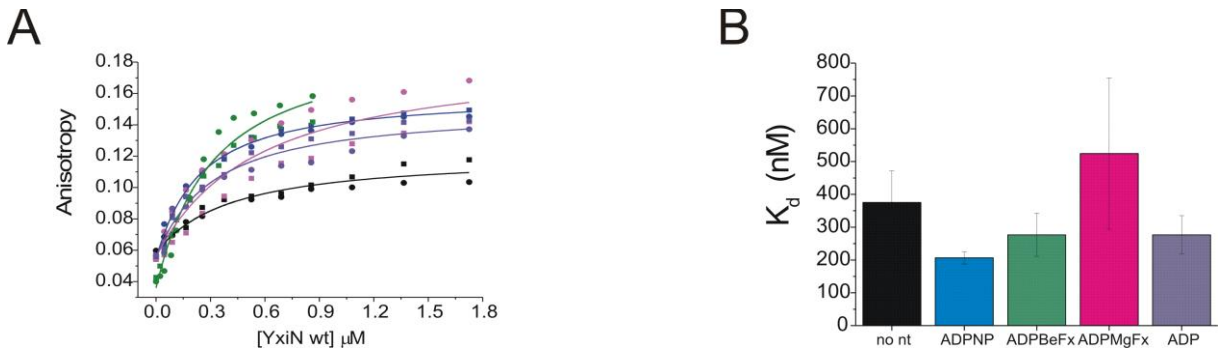

Figure 14: RNA binding of YxiN wildtype in the nucleotide cycle

Affinities of a minimal 32mer RNA substrate to YxiN wildtype were determined by fluorescence anisotropy titrations as described in section 4.11. Panel A shows two independent datasets for each nucleotide (same colour) and the global fitting thereof. Panel B shows RNA binding of YxiN wildtype in the presence of ADPNP (blue; Kd = 206 ± 19 nM); ADP·BeF_x (green; Kd = 276 ± 65 nM); ADP·MgF_x (magenta; Kd = 524 ± 230 nM) and ADP (violet; Kd = 276 ± 58 nM) as well as in the absence of nucleotide (black; Kd = 375 ± 96 nM).

For the ATPase deficient motif I mutant K52Q the Kd value for the 32mer minimal RNA substrate is found to be 638 ± 6 nM. There is a drastic decrease in the Kd values in the presence of ATP, ADPNP, ADP·BeF_x and ADP to 170 ± 49 nM, 268 ± 141 nM, 74 ± 16 nM and 127 ± 22 nM respectively

Figure 15: RNA binding of the YxiN motif I mutant K52Q in the nucleotide cycle

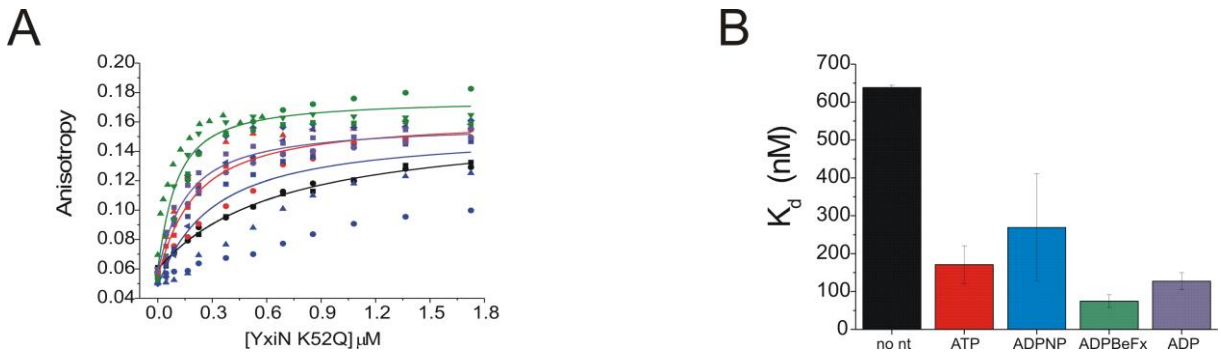

Figure 15: RNA binding of YxiN motif I mutant K52Q in the nucleotide cycle

Affinities of a minimal 32mer RNA substrate to YxiN motif I mutant K52Q were determined by fluorescence anisotropy titrations as described in section 4.11. Panel A shows two independent datasets for each nucleotide (same colour) and the global fitting thereof. Panel B shows RNA binding of the ATPase deficient motif I mutant K52Q in the presence of ATP (red; Kd = 170 ± 49 nM); ADPNP (blue; Kd = 268 ± 141 nM); ADP·BeF_x (green; Kd = 74 ± 16 nM) and ADP (violet; Kd = 127 ± 22 nM) as well as in the absence of nucleotide (black; Kd = 638 ± 6 nM).

The Kd value for the uncoupling mutant R330A is found to be 1383 ± 645 nM. A slight drop in this value to 995 ± 582 nM is seen in the presence of ADPNP and a drastic drop to Kd values of 120 ± 1 nM and 253 ± 81 nM for ADP·BeF_x and ADP respectively.

Figure 16: RNA binding of YxiN motif VI mutant R330A in the nucleotide cycle

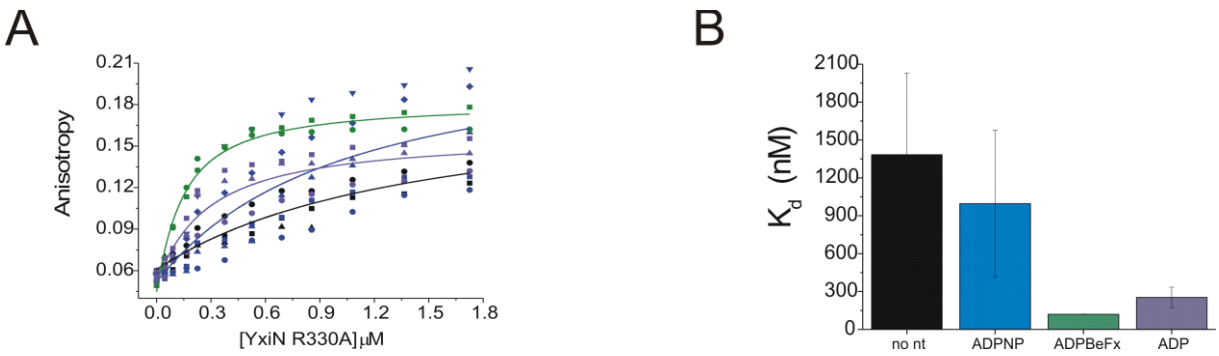

Figure 16: RNA binding of YxiN motif VI mutant R330A in the nucleotide cycle

Affinities of a minimal 32mer RNA substrate to YxiN wildtype were determined by fluorescence anisotropy titrations as described in section 4.11. Panel A shows two independent datasets for each nucleotide (same colour) and the global fitting thereof. Panel B shows RNA binding of the uncoupling motif VI mutant R330A in the presence of ADPNP (blue; Kd = 995 ± 582 nM); ADP·BeFx (green; Kd = 120 ± 1 nM) and ADP (violet; Kd = 253 ± 81 nM) as well as in the absence of nucleotide (black; Kd = 1383 ± 645 nM).

Figure 17: Comparison of YxiN wildtype to the motif mutants in the presence of different nucleotides

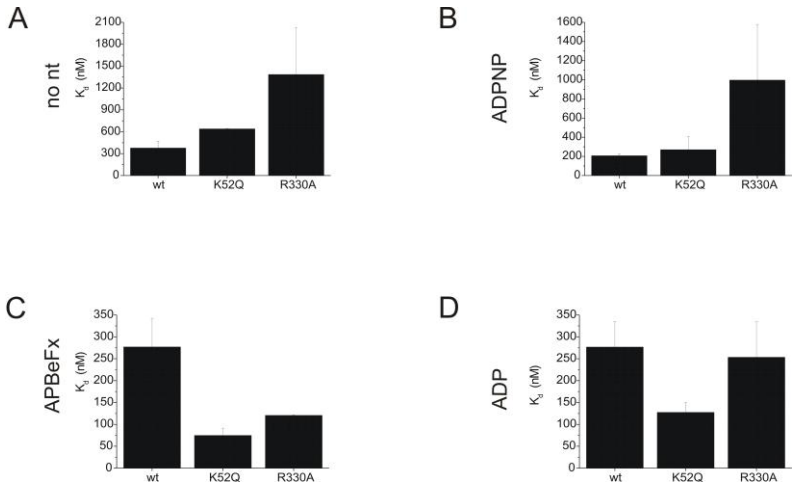

Figure 17: Comparison of YxiN wildtype to the YxiN motif mutants in the presence of different nucleotides

Figure 17 shows a comparison of the two motif mutants YxiN K52Q and YxiN R330A to wildtype in the presence of ADPNP (Panel B); ADP·BeF_x (Panel C); ADP (Panel D) and no nucleotide (Panel A). Kd values are shown in a bar plot and error bars arise from a global fitting of two independent measurements.

Table 1: RNA affinities of YxiN wildtype and two motif mutants

YxiN mutant	no nucleotide (nM)	ATP (nM)	ADPNP (nM)	ADP·BeF_x (nM)	ADP·MgF_x (nM)	ADP (nM)
wildtype	375 ± 96	n.d.	206 ± 19	276 ± 65	524 ± 230	276 ± 59
R330A	1383 ± 645	n.d.	995 ± 582	120 ± 1	n.d.	253 ± 81
K52Q	638 ± 6	170 ± 49	268 ± 141	74 ± 16	n.d.	127 ± 22

In the beginning of the enzymatic cycle, in the absence of any nucleotide YxiN wildtype shows a clearly higher affinity for the 32mer minimal substrate than the motif VI mutant R330A that shows an approximately 3.5-fold reduction in affinity. The motif I mutant K52Q also shows an approximately 1.5-fold reduction in affinity compared to YxiN wildtype. Stepping further in the enzymatic cycle, in the presence of the ATP-analogue ADPNP the motif VI mutant still shows a drastic approximately 5-fold reduction in RNA affinity. The motif I mutant as well still shows an approximately 1.5-fold reduction in RNA affinity. In the activated nucleotide-bound state, in the presence of the ATP-analogue ADP·BeF_x this is different. Now RNA binding of the motif VI mutant is approximately 2.5-fold tighter than for YxiN wildtype, and the motif I mutant even shows an increase in RNA affinity of about 3.5-fold compared to YxiN wildtype. At the end of the nucleotide cycle, in the presence of ADP, the motif VI mutant shows an RNA affinity comparable to YxiN wildtype, but the motif I mutant shows an approximate 2-fold increase in affinity. The mutations in the two motifs thus not only lead to changes in the affinity of nucleotides, as expected since the two motifs are involved in nucleotide binding[24, 26], but also lead to severe differences in RNA binding in all steps of the enzymatic cycle.

5.1.4. Steady state ATP hydrolysis activity of YxiN wildtype and the two motif mutants

Having determined nucleotide and RNA binding affinities of YxiN wildtype and the two motif mutants YxiN K52Q and YxiN R330A, we next wanted to determine the enzymatic properties of these proteins. The first enzymatic property investigated was the ability to hydrolyse ATP. The rate of ATP hydrolysis for YxiN wildtype and YxiN R330A was determined by an enzymatically coupled steady state assay as described in section 4.9. For the determination of the rate constant for YxiN wildtype an enzyme concentration of 10 nM was used, the enzyme concentration for the R330A mutant was 1 µM. The RNA stimulated rate constant k_{cat} of YxiN wildtype was determined to be 5.2 ± 0.3 s^{-1}. The YxiN K52Q mutant was shown to be ATPase deficient[56] and the uncoupling mutant YxiN R330A was ATPase deficient even with an enzyme concentration of 1 µM.

Figure 18: Steady state ATP hydrolysis activity of YxiN wildtype

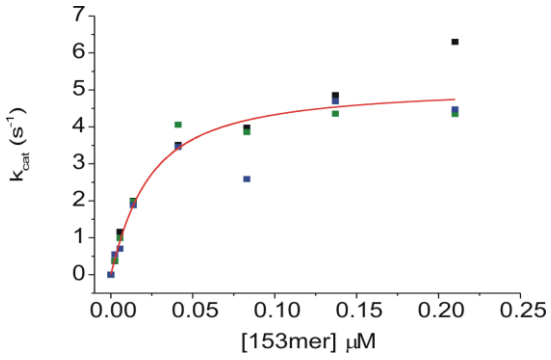

Figure 18: Steady state ATP hydrolysis activity of YxiN wildtype

The ATPase activity of YxiN wildtype was determined by steady state ATPase assays, as described in section 4.9. For YxiN wildtype an enzyme concentration of 10 nM was used. The figure shows three independent measurements and global fitting of them.

5.1.5. Unwinding of a double stranded RNA substrate by YxiN wildtype

Displacement or unwinding of the double stranded RNA region in the hairpin 92 of the 23S rRNA is the enzymatic task of YxiN wildtype. To monitor this reaction a FRET based assay was established (section 4.12.1). In the presence of ATP this displacement reaction can take place at an unwinding rate constant of $7.7*10^{-3} \pm 6.8*10^{-5}$ s^{-1}. Also in the presence of ADP·BeF_x displacement of the double stranded RNA substrate can be observed, which is in good agreement to earlier findings with Ded1 from yeast[39]. Surprisingly the unwinding rate constant determined to be $1.9*10^{-2} \pm 2.3*10^{-4}$ s^{-1} for ADP·BeF_x is even a bit higher than for ATP. Unwinding rates for YxiN wildtype were also determined in a polyacrylamide gel based assay. The observed rate constant k_{obs} is 0.012 ± 0.001 s^{-1} for ATP and 0.004 ± 0.001 s^{-1} for ADP·BeF_x. Unwinding in the presence of ADP·BeF_x is 3-fold slower than in the presence of ATP. Here the unwinding is 3-fold faster in the presence of ATP than for ADP·BeF_x and in agreement with the findings for Ded1 from yeast[39].

Figure 19: double stranded RNA unwinding by YxiN wildtype

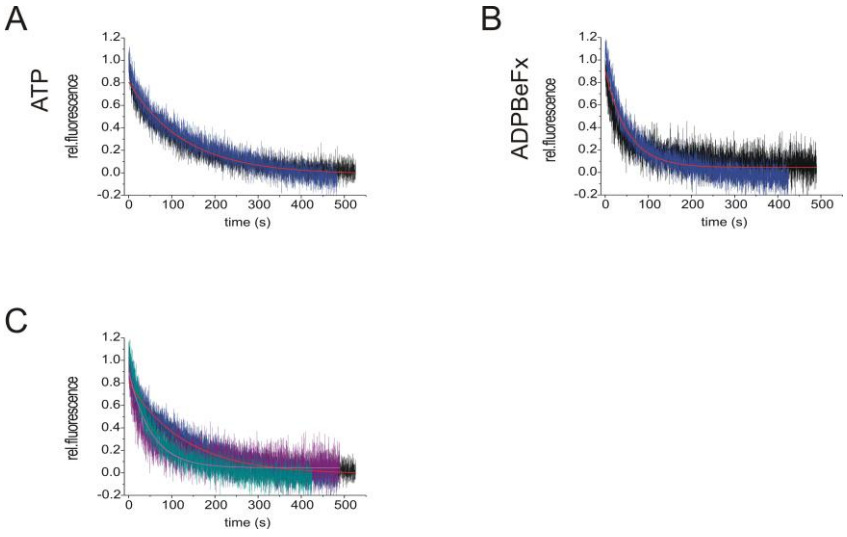

Figure 19: double stranded RNA unwinding by YxiN wildtype

Figure 19 shows the capability of YxiN wildtype to unwind a minimal RNA substrate consisting of a Cy5-32mer and a Cy3-9mer of the hairpin 92 of the 23S rRNA. The experimental procedure is described in section 4.12.1. Panel A shows two independent measurements (one in black, one in blue) with a global fitting of the respective data with ATP. YxiN wildtype shows an unwinding rate constant of $7.7*10^{-3} \pm 6.8*10^{-5}$ s^{-1}. Panel B shows independent measurements (one in black, one in blue) with a global fitting of the respective data with ADP·BeF_x. YxiN wildtype shows an unwinding rate constant of $1.9*10^{-2} \pm 2.3*10^{-4}$ s^{-1}. Panel C shows an overlay of the datasets for ATP (black/blue) and ADP·BeF_x (cyan/wine).

Figure 20: double stranded RNA unwinding by YxiN wildtype with a polyacrylamide gel assay

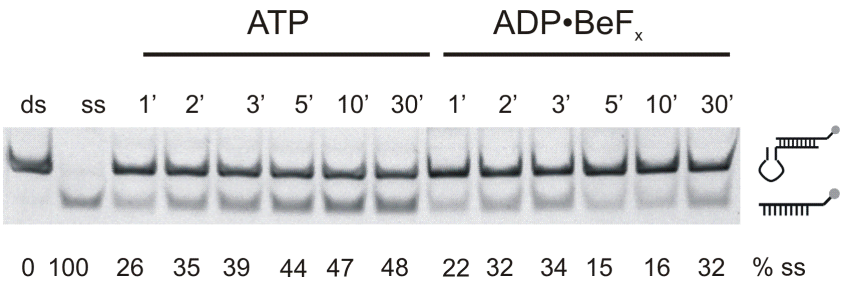

Figure 20: double stranded RNA unwinding by YxiN wildtype with a polyacrylamide gel assay

Figure 20 shows the capability of YxiN wildtype to unwind a minimal RNA substrate consisting of a Cy5-32mer and a Cy3-9mer of the hairpin 92 of the 23S rRNA with a polyacrylamide gel assay. The experimental procedure is described in section 4.12.2. Both nucleotides tested, ATP and ADP·BeF_x support unwinding of the 32/9mer model substrate. The observed rate constant k_{obs} is $1.2*10^{-3} \pm 1*10^{-4}$ s^{-1} for ATP and $4*10^{-4} \pm 1*10^{-4}$ s^{-1} for ADP·BeF_x. Unwinding in the presence of ADP·BeF_x is 3-fold slower than in the presence of ATP.

Although the motif I mutant K52Q is ATP hydrolysis deficient it still shows double stranded RNA unwinding activity[56]. The rate constant of unwinding with ATP is determined to be $2.8*10^{-3} \pm 7.2*10^{-5}$ s^{-1} and thus similar to the unwinding rate constant of YxiN wildtype determined to be $7.7*10^{-3} \pm 6.8*10^{-5}$ s^{-1}. The unwinding rate constant of $1.9*10^{-3} \pm 3.4*10^{-5}$ s^{-1} for YxiN K52Q with ADP·BeF_x is lower than the unwinding rate of YxiN wildtype of $1.9*10^{-2} \pm 2.3*10^{-4}$ s^{-1}. The unwinding rate constants for both nucleotides, ATP and ADP·BeF_x are virtually identical, which can be expected, since the K52Q mutant does not hydrolyse ATP and therefore ATP and ADP·BeF_x act similar in activating enzyme activity.

Figure 21: double stranded RNA unwinding by YxiN motif I mutant K52Q

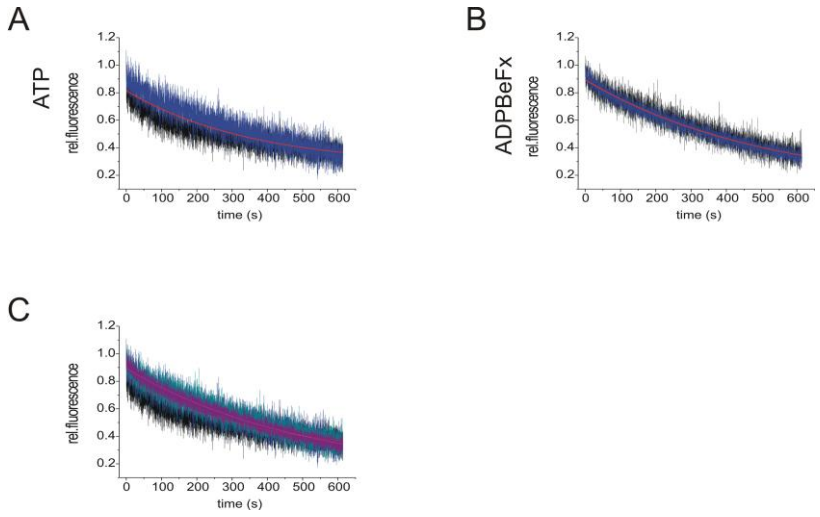

Figure 21: double stranded RNA unwinding by YxiN motif I mutant K52Q

Figure 21 shows the capability of YxiN motif I mutant K52Q to unwind a minimal RNA substrate consisting of a Cy5-32mer and a Cy3-9mer of the hairpin 92 of the 23S rRNA. The experimental procedure is described in section 4.12.1. Panel A shows two independent measurements (one in black, one in blue) with a global fitting of the respective data with ATP. YxiN K52Q shows an unwinding rate constant of $2.8*10^{-3} \pm 7.2*10^{-5}$ s^{-1}. Panel B shows independent measurements (one in black, one in blue) with a global fitting of the respective data with ADP·BeF_x. YxiN K52Q shows an unwinding rate constant of $1.9*10^{-3} \pm 3.4*10^{-5}$ s^{-1}. Panel C shows an overlay of the datasets for ATP (black/blue) and ADP·BeF_x (cyan/wine)

The YxiN motif VI mutant R330A unwinds a double stranded RNA substrate, despite being ATPase deficient. The unwinding rate constant for ATP is determined to be $4.6*10^{-4} \pm 1.1*10^{-4}$ s^{-1} and thus significantly lower than the unwinding rate constant of YxiN wildtype of $7.7*10^{-3} \pm 6.8*10^{-5}$ s^{-1}. This might originate from lower RNA binding constants. In the presence of ADP·BeF_x the unwinding rate constant is $2.2*10^{-3} \pm 6.7*10^{-5}$ s^{-1} which is significantly higher than the unwinding rate in the presence of ATP. Compared to the unwinding rate constant of YxiN wildtype of $1.9*10^{-2} \pm 2.3*10^{-4}$ s^{-1}, the unwinding rate is still rather low. The higher unwinding rate for ADP·BeF_x might originate from the fact, that RNA is bound tighter in the presence of ADP·BeF_x than in the presence of ATP.

Figure 22: double stranded RNA unwinding by YxiN motif VI mutant R330A

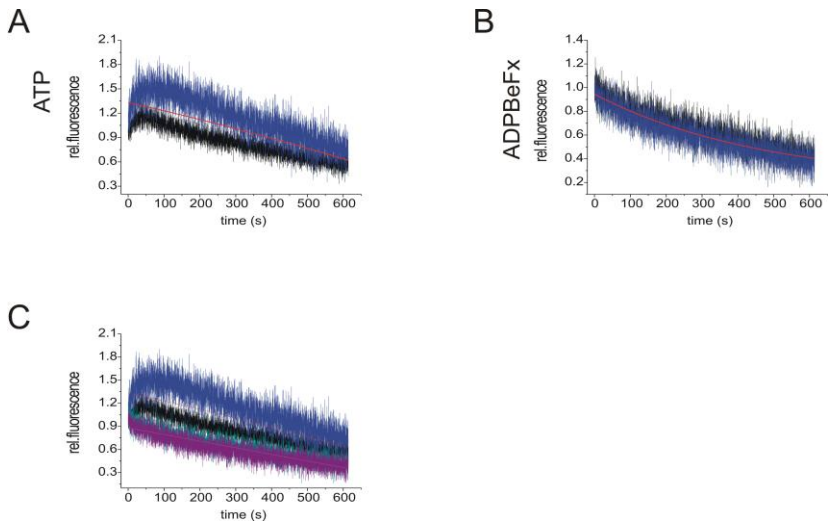

Figure 22: double stranded RNA unwinding by YxiN motif VI mutant R330A

Figure 22 shows the capability of YxiN motif VI mutant R330A to unwind a minimal RNA substrate consisting of a Cy5-32mer and a Cy3-9mer of the hairpin 92 of the 23S rRNA. The experimental procedure is described in section 4.12.1. Panel A shows two independent measurements (one in black, one in blue) with a global fitting of the respective data with ATP. YxiN R330A shows an unwinding rate constant of $4.6*10^{-4} \pm 1.1*10^{-4}$ s^{-1}. Panel B shows independent measurements (one in black, one in blue) with a global fitting of the respective data with

ADP·BeF_x. YxiN R330A shows an unwinding rate constant of $2.2*10^{-3} \pm 6.7*10^{-5}$ s^{-1}. Panel C shows an overlay of the datasets for ATP (black/blue) and ADP·BeF_x (cyan/wine).

Both motif mutants as well as YxiN wildtype are able to unwind a double stranded minimal RNA substrate. The unwinding rates found nicely reflect RNA binding constants as well as ATP hydrolysis capabilities.

5.1.6. Conformational state of YxiN wildtype in the nucleotide cycle

After determination of substrate affinities and enzymatic properties of YxiN wildtype and the two motif mutants YxiN K52Q and YxiN R330A it was interesting to test, whether enzymatic and substrate binding properties are also reflected in the conformational states of the respective enzyme. To determine the conformational state of YxiN wildtype in the nucleotide cycle donor and acceptor dye labelled protein (described in section 4.7.7) was used to measure FRET on a confocal set-up. (described in section 4.13.4). The dyes were attached on opposite sites of the cleft between the two RecA domains. In the absence of RNA substrate and nucleotides a major FRET efficiency of 0.35 was observed, which corresponds to an open conformation of the helicase core as reported by Theissen et al.[46]. Since ATP gets readily hydrolysed in the presence of the 153mer RNA substrate, non-hydrolysable analogues such as ADPNP and ADP·BeF_x had to be used. Upon addition of ADPNP and 153mer RNA, the observed FRET peak shifts to a higher FRET efficiency of 0.75 (Figure 23) corresponding to a closed conformation as reported by Theissen et al.[46]. In the presence of ADP·BeF_x, which represents a pre-hydrolysis state of ATP[65-67] and is thought to favour an "activated" enzyme state[39] and 153mer RNA there is also this shift to a higher FRET efficiency of 0.75 to be observed (Figure 23). If the 153mer RNA substrate and ADP·MgF_x, representing a post-hydrolysis state of ATP[65-67], are present, again this shift to a higher FRET efficiency of 0.75 can be observed (Figure 23). At the end of the nucleotide cycle in the presence of ADP and the 153mer RNA substrate there is a re-opening of the helicase core cleft, reflected in the major FRET peak at 0.3 FRET efficiency (Figure 23). These results

show that in the course of the catalytic cycle, the catalytic core of YxiN starts in an open conformation. Upon binding of the nucleotide and RNA substrate, the YxiN catalytic core undergoes a conformational change and closes its cleft. This closure is persistent until both, the hydrolysis products, and both RNA strands are released.

Figure 23: Conformational state of YxiN wildtype in the nucleotide cycle

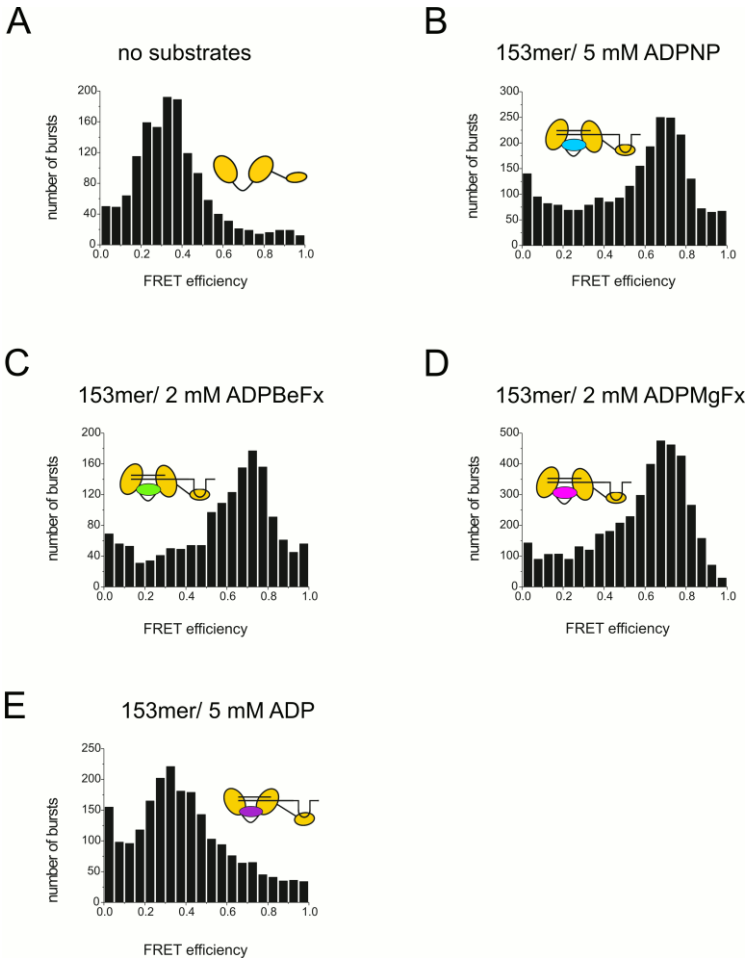

Figure 23: Conformational state of YxiN wildtype in the nucleotide cycle

Figure 23 shows the conformational state of YxiN wildtype throughout the nucleotide cycle. FRET histograms of 80 pM YxiN wildtype without substrates (panel A); of 80 pM YxiN wildtype, 5 mM ADPNP and 200 nM 153mer RNA (panel B); of 80 pM YxiN wildtype, 2 mM ADP·BeF_x and 200 nM 153mer RNA (panel C); of 80 pM YxiN wildtype, 2 mM ADP·MgF_x 153mer RNA (panel D) and of 80 pM YxiN wildtype, 5 mM ADP and 153mer RNA were recorded on a home-built confocal microscope set-up. The cartoons depict the conformational state of the helicase core, the respective nucleotide and the RNA substrate bound to the RBD.

5.1.7. Dissection of the putative high-FRET ADP population

Although YxiN wildtype bound to RNA and ADP shows a major FRET population at FRET efficiencies corresponding to an open conformation of the catalytic core, in almost all measurements with 153mer and ADP there was a minor population at FRET efficiencies corresponding to a closed conformation to be observed. To determine, whether this appearance of an additional peak originates from a subpopulation of enzymes being in a closed conformation and to rule out a measurement artefact, FRET experiments were performed with increasing concentrations of ADP (200 µM - 10 mM ADP). Up to 2 mM ADP there is no appearance of a population at higher FRET states (Figure 24, panel B – E). Upon addition of 5 mM ADP (concentrations used in all FRET experiments) there is this small peak at a FRET efficiency of 0.75, indicating that the peak represents a subpopulation of enzymes in a closed conformation of the catalytic core (Figure 24, panel F). Upon addition of 10 mM ADP the population size does not increase though (Figure 24, panel G). This might be due to the fact that a very small subset of proteins is in this closed conformation. All in all, even in the last step of the catalytic cycle, when YxiN is reset to an open and ligand-free state, there is a small subpopulation of proteins to be found in a closed conformation. Since there is no increase in population size after addition of more than 5 mM, appearance of this population can not be assigned to traces of other nucleotides in the ADP nucleotide solution, but reflects the ability of the protein to induce a closed catalytic core in the presence of 153mer and ADP.

Figure 24: Dissection of the putative high-FRET ADP population

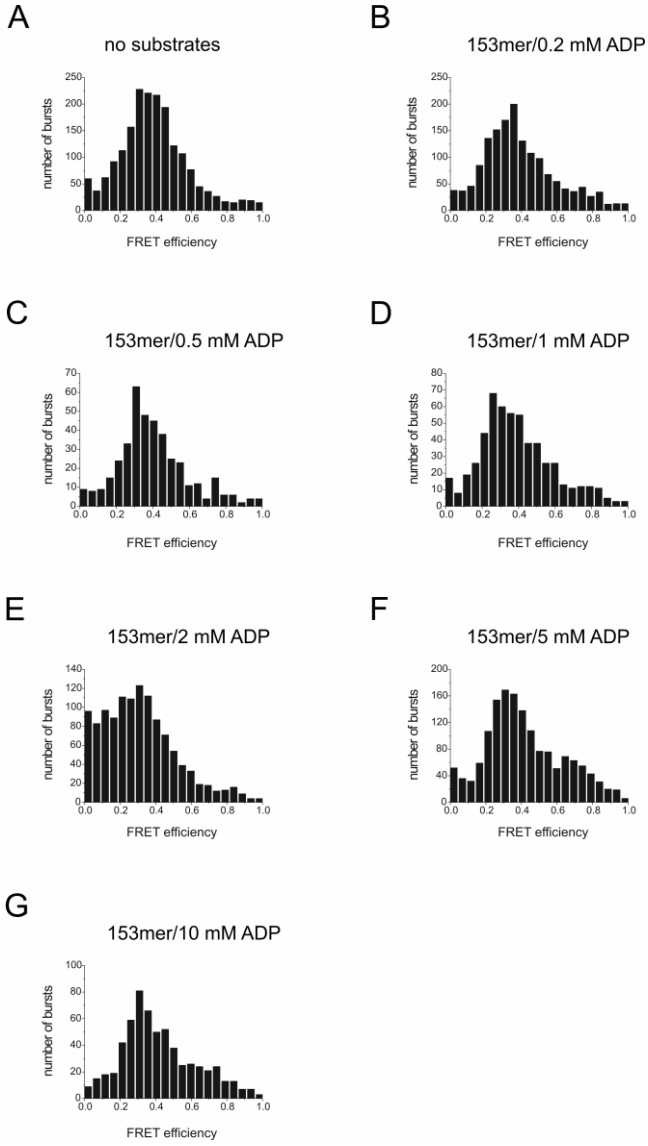

Figure 24: Dissection of the putative high-FRET ADP population

Figure 24 shows an ADP titration to YxiN wildtype in the presence of 153mer substrate. 200 µM ADP (Panel B); 500 µM ADP (Panel C); 1 mM ADP (Panel D); 2 mM ADP (Panel E); 5 mM ADP (Panel F) and 10 mM ADP (Panel G) were added to 80 pM of YxiN wildtype and 200 nM 153mer RNA and FRET efficiencies recorded.

5.1.8. Conformational state of the uncoupling mutant R330A

The motif VI mutant R330A shows an inverted preference in nucleotide binding compared to YxiN wildtype, ATP is bound with higher affinity than ADP·BeF_x. In addition the RNA affinities are also rather different than affinities found for YxiN wildtype. In the absence of any nucleotide or in the presence of ADPNP affinities for a minimal 32mer RNA substrate are lower than for YxiN wildtype. On the other hand there is a higher affinity for the minimal 32mer RNA substrate in the presence of ADP·BeF_x or ADP. ATP hydrolysis of this mutant is totally impaired, and also unwinding reactions are slower than the rates observed for YxiN wildtype. It was therefore interesting to see whether these effects are also reflected in changes in conformational states. In the absence of any substrate this mutant shows the same FRET efficiency peak as wildtype at 0.35 FRET efficiency. In the presence of 153mer RNA and ATP two populations are observed, one at 0.35 FRET efficiency and one at 0.75 FRET efficiency reflecting open and closed states. Upon addition of ADP·BeF_x and 153mer RNA there is a shift towards higher FRET efficiencies of 0.75. The effects found for substrate binding, and enzymatic properties such as ATP hydrolysis and double stranded RNA unwinding are therefore not reflected in the movements of the helicase core.

Figure 25: Conformational state of the uncoupling mutant R330A

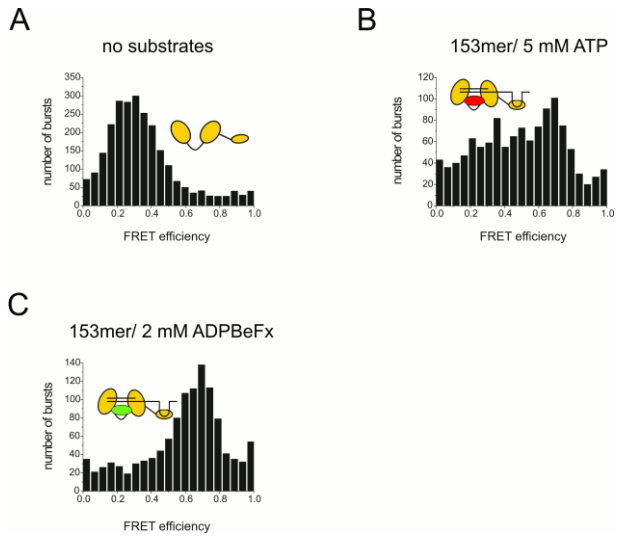

Figure 25: Conformational state of the uncoupling mutant R330A

Figure 25 shows the FRET histograms of the uncoupling mutant R330A in the presence and absence of RNA substrate and nucleotides. Panel A shows 80 pM YxiN R330A without substrates; Panel B shows 80 pM YxiN R330A with 200 nM 153mer RNA and ATP and Panel C shows 80 pM YxiN R330A with 200 nM and ADP·BeF_x.

In the first part of this work, the catalytic cycle of YxiN wildtype and two motif mutants is investigated. Substrate binding studies as well as enzymatic activity assays and smFRET studies delineate the conformational states and the respective binding affinities of substrates throughout the enzymatic cycle. It could be shown that YxiN wildtype undergoes a closure of the catalytic core upon binding of ATP or pre-hydrolysis analogues of ATP, unwinds a double stranded minimal RNA substrate in the presence of ATP and ADP·BeF_x and upon release of the hydrolysis products and the unwound RNA reopens the catalytic core. Binding affinities of RNA and nucleotides reflect these steps of the cycle. The same stepping through the catalytic cycle is also demonstrated for the two motif mutants. Differences in enzymatic activities are reflected by the different binding constants of the mutants as well as by ATPase deficiency.

5.2. - Part II Impact of the linker in the catalytic core on enzyme function

5.2.1. Mutations of the linker between the two RecA core domains of YxiN

In order to examine the influence of the linker between the two RecA catalytic core domains of the DEAD-box protein YxiN, this sequence was changed in sequence and length. In a first step the original length of the linker of nine amino acids was maintained but the amino acid sequence was changed into a sequence a bit more flexible. This flexible sequence was then shortened and prolonged. The mutations in the catalytic core were then tested for RNA and nucleotide binding properties, for enzymatic properties such as ATP hydrolysis activity and double stranded RNA unwinding activity, as well as for conformational states in different stages of the nucleotide cycle of YxiN. Due to redundancy in the nucleotide sequence of the linker, which leads to multiple annealing possibilities for the mutation primers in the longer sequences, the longest YxiN linker construct has the original sequence maintained and additional amino acids added. The respective amino acid sequences are shown in Figure 26.

Figure 26: Mutations in the linker between the two RecA domains of YxiN

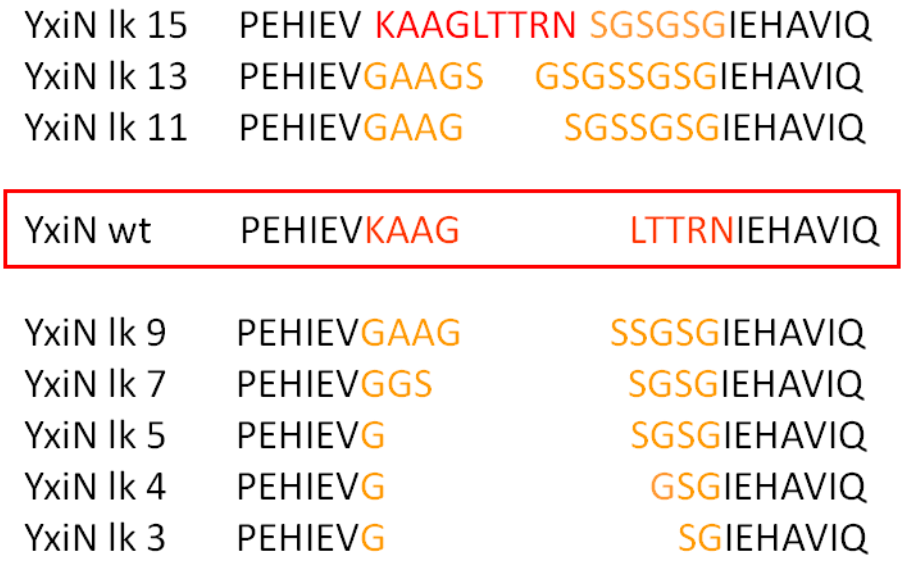

Figure 26: Mutations in the linker between the two RecA domains of YxiN

Figure 26 shows the mutations introduced into the linker between the two RecA domains of YxiN. All mutations were introduced following the mutagenesis procedure described in section 4.7.5. The original linker sequence KAAGLTTRN (highlighted in red) was in a first step changed to GAAGSSGSG in order to get the sequence a bit more flexible and then shortened and prolonged to the sequences shown in orange. Since mutagenesis starting from the YxiN lk 13 sequence to get the YxiN lk 15 sequence was not possible due to the redundancy in the nucleotide sequence, these amino acids were introduced into the original linker sequence.

5.2.2. Nucleotide binding of YxiN linker mutants without an RNA substrate

In order to determine the nucleotide binding affinities of the YxiN linker mutants to ATP, ADP·BeF_x and ADP displacement titrations of a mantADP/YxiN complex were performed as described in section 4.10. YxiN wildtype has a rather low affinity for ATP with a Kd value of 111 ± 6 µM. The affinities for the pre-hydrolysis state analogue ADP·BeF_x[65-67] with a Kd value of 38 ± 4 µM and also for ADP with a Kd value of 20 ± 2 µM are much higher. Changes in the linker in the catalytic core also lead to changes of nucleotide affinities. Reducing the linker length to seven (YxiN lk 7), five (YxiN lk 5), four (YxiN lk 4) or three (YxiN lk 3) amino acids leads to gradual increase in ATP affinity as reflected by the respective binding constants. The binding constant of 111 ± 6 µM for YxiN wildtype is increased to 74 ± 17 µM for YxiN lk 7, to 37 ± 11 µM for YxiN lk 5, to 21 ± 7 µM for YxiN lk 4 and to 12 ± 3 µM for YxiN lk 3 (see Table 2). Stepping further in the nucleotide cycle the binding constant for the non-hydrolysable ATP-analogue ADP·BeF_x[65-67] for YxiN wildtype is determined to be 38 ± 4 µM and thus much higher than the binding constant for ATP. Reducing the length of the linker in the catalytic core leads to a decrease in affinity for ADP·BeF_x as reflected by the binding constants for YxiN lk 7, determined to be 93 ± 16 µM, for YxiN lk 5, determined to be 147 ± 42 µM, for YxiN lk 4, determined to be 113 ± 24 µM and for YxiN lk 4, determined to be 93 ± 29 µM (see Table 2). At the end of the catalytic cycle the binding constant for YxiN wildtype for ADP of 20 ± 2 µM reflects a high affinity. Different to ATP and its non-hydrolysable ATP-analogue ADP·BeF_x[65-67] there is no change in the binding constants of the shorter linker mutants for ADP. YxiN lk 7 has a binding constant of 59 ± 11 µM, YxiN lk 5 has a binding constant of 41 ± 9 µM and YxiN lk 4 has a binding constant of 46 ± 11 µM. The only mutant showing any change in ADP affinity is YxiN lk 3 with a increased binding constant of 14 ± 9 µM (see Table 2).

Figure 27: Nucleotide binding of the short YxiN linker mutants without an RNA substrate

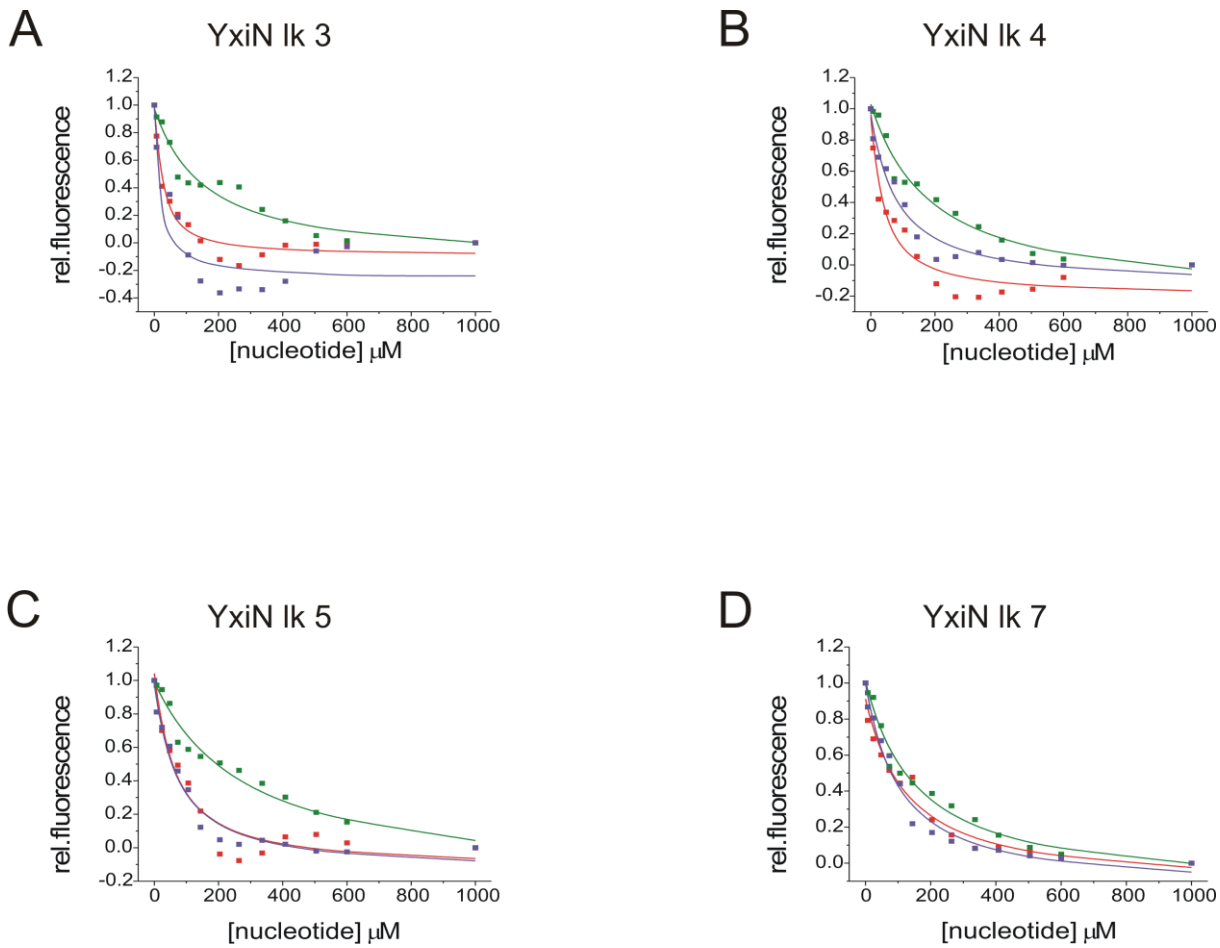

Figure 27: Nucleotide binding of the short YxiN linker mutants without an RNA substrate

Figure 27 shows the nucleotide binding of the different short mutants of the linker between the two RecA core domains of YxiN. Graphs shown originate from taking a mean value of at least two independent measurements and fitting of them. Experimental procedure of these displacement titrations is described in section 4.10. ATP is shown in red, ADP·BeF_x is shown in green and ADP is shown in violet. Panel A shows nucleotide affinities of YxiN lk 3 for ATP (12 ± 3 µM), ADP·BeF_x (93 ± 29 µM) and ADP (14 ± 9 µM). Panel B shows nucleotide affinities of YxiN lk 4 for ATP (21 ± 7 µM), ADP·BeF_x (113 ± 23 µM) and ADP (46 ± 11 µM). Panel C shows nucleotide affinities of YxiN lk 5 for ATP (36 ± 11 µM), ADP·BeF_x (174 ± 42 µM) and ADP (41 ± 9 µM). Panel D shows nucleotide affinities of YxiN lk 7 for ATP (73 ± 17 µM), ADP·BeF_x (93 ± 16 µM) and ADP (59 ± 11 µM).

Table 2: Nucleotide binding constants of the shorter linker mutants

YxiN linker mutant	ATP (µM)	ADP·BeF_x (µM)	ADP (µM)
lk 3	12 ± 3	93 ± 29	14 ± 9
lk 4	21 ± 7	113 ± 24	46 ± 11
lk 5	37 ± 11	174 ± 42	41 ± 9
lk 7	74 ± 17	93 ± 16	59 ± 11
wildtype	111 ± 7	38 ± 4	20 ± 2

Increasing the linker length of the linker in the catalytic core also leads to a gain in affinity for ATP but in the longest linker construct as is reflected by the binding constants of 49 ± 7 µM for YxiN lk 9, 74 ± 11 µM for YxiN lk 11 and 26 ± 5 µM for YxiN lk 13. In contrast to the other longer linker constructs, YxiN lk 15 shows a reduction in ATP binding as seen in the binding constant of 132 ± 11 µM (see Table 3). Stepping further in the nucleotide cycle to ADP·BeF_x a loss in nucleotide affinity can be observed. YxiN lk 9 has a binding constant for ADP·BeF_x of 33 ± 9 µM, YxiN lk 11 has a binding constant of 71 ± 11 µM and YxiN lk 13 has a binding constant of 136 ± 26 µM. The longest linker, YxiN lk 15, shows an affinity for ADP·BeF_x that is comparable to YxiN wildtype with a binding constant of 55 ± 6 µM (see Table 3). At the end of the catalytic cycle the high affinity for ADP as seen in YxiN wildtype is also seen for the mutants with a longer catalytic core linker. YxiN lk 9 has a binding constant for ADP of 37 ± 9 µM, YxiN lk 11 has a binding constant of 52 ± 6 µM, YxiN lk 13 has a binding constant of 53 ± 10 µM and YxiN lk 15 has a binding constant of 49 ± 5 µM (see Table 3).

Figure 28: Nucleotide binding of the long YxiN linker mutants without an RNA substrate

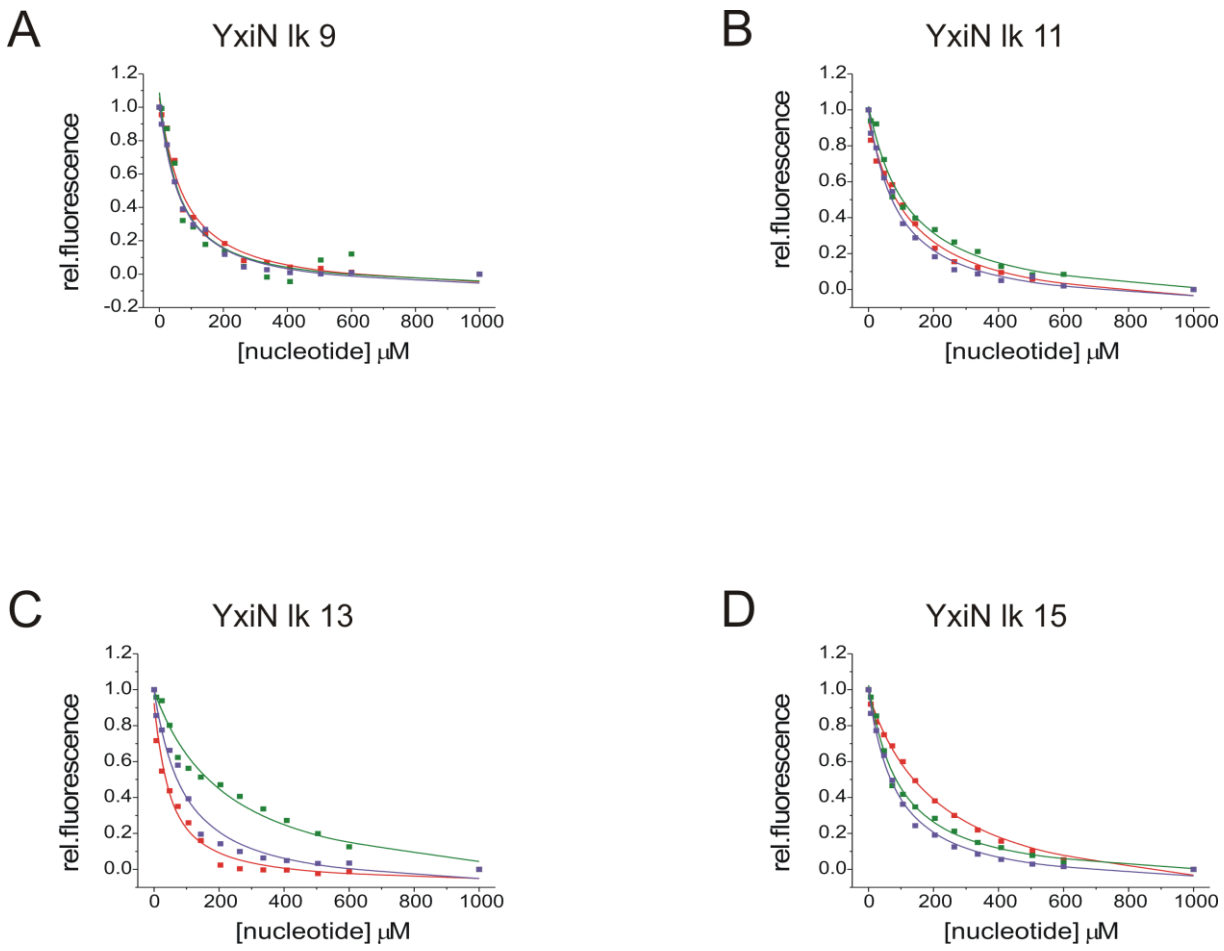

Figure 28: Nucleotide binding of the long YxiN linker mutants without an RNA substrate

Figure 28 shows the nucleotide binding of the different long mutants of the linker between the two RecA core domains of YxiN. Graphs shown originate from taking a mean value of at least two independent measurements and fitting of them. Experimental procedure of these displacement titrations is described in section 4.10. ATP is shown in red, ADP·BeF_x is shown in green and ADP is shown in violet. Panel A shows nucleotide affinities of YxiN lk 9 for ATP (43 ± 8 µM), ADP·BeF_x (33 ± 9 µM) and ADP (37 ± 4 µM). Panel B shows nucleotide affinities of YxiN lk 11 for ATP (74 ± 11 µM), ADP·BeF_x (71 ± 11 µM) and ADP (53 ± 6 µM). Panel C shows nucleotide affinities of YxiN lk 13 for ATP (26 ± 5 µM), ADP·BeF_x (136 ± 26 µM) and ADP (53 ± 10 µM). Panel D shows nucleotide affinities of YxiN lk 15 for ATP (132 ± 11 µM), ADP·BeF_x (55 ± 6 µM) and ADP (49 ± 5 µM).

Table 3: Nucleotide binding constants of the shorter linker mutants

YxiN linker mutant	ATP (µM)	ADP·BeF_x (µM)	ADP (µM)
lk 9	43 ± 8	33 ± 9	37 ± 4
wildtype	111 ± 7	38 ± 4	20 ± 2
lk 11	74 ± 11	71 ± 11	53 ± 6
lk 13	26 ± 5	136 ± 26	53 ± 10
lk 15	132 ± 11	55 ± 6	49 ± 5

Figure 29: Comparison of nucleotide binding of the YxiN linker mutants to YxiN wildtype

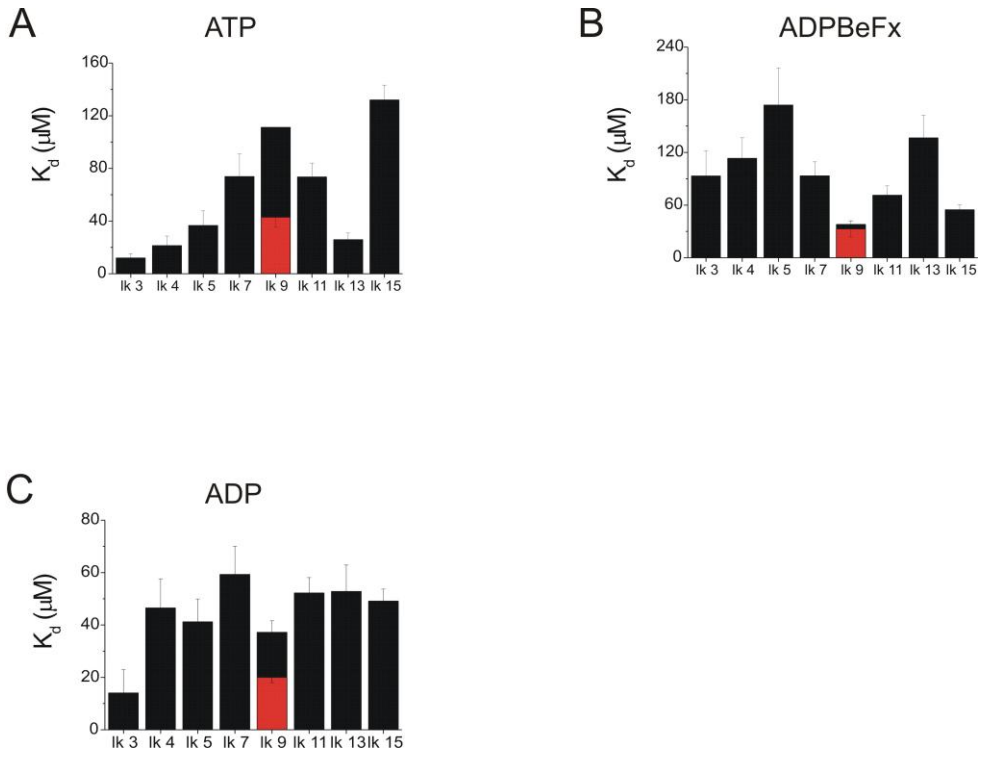

Figure 29: Comparison of nucleotide binding of the YxiN linker mutants to YxiN wildtype

Figure 29 shows a comparison of the YxiN linker mutants to YxiN wildtype concerning nucleotide binding. Panel A shows the Kd values of all mutants for ATP. The Kd value for wildtype is shown as a black bar in the lk 9 section. Panel B shows the Kd values of all mutants for ADP·BeF_x. Again, the Kd value for wildtype is shown as a black bar in the lk 9 section. Panel C shows the Kd values of all mutants for ADP. The Kd value for wildtype is shown as a red bar in the lk 9 section.

In the absence of any RNA substrate there is an effect of the mutations of the linker in the catalytic core on the enzymatic cycle to be observed. Binding of ATP gets tighter if the linker is shortened or prolonged, on the other hand binding of the non-hydrolysable ATP-analogue ADP·BeF_x[65-67] gets less tight. There is no such effect to be observed at the end of the enzymatic cycle, on binding of ADP to the YxiN linker mutants.

5.2.3. Nucleotide binding of YxiN linker mutants with an RNA substrate

In order to determine the nucleotide binding affinities of the YxiN linker mutants to ATP, ADP·BeF_x and ADP in the presence of a minimal RNA substrate displacement titrations of a mantADP/YxiN complex in presence of a 32mer RNA substrate were performed as described in section 4.10. YxiN wildtype has a rather high affinity for ATP with a Kd value of 47 ± 5 µM. The affinity for the pre-hydrolysis state analogue ADP·BeF_x[65-67] with a Kd value of 56 ± 20 µM is in the same range as for ATP. The affinity for ADP with a Kd value of 146 ± 18 µM is significantly reduced. Changes in the linker in the catalytic core also lead to changes of nucleotide affinities. Reducing the linker length to seven (YxiN lk 7), five (YxiN lk 5), four (YxiN lk 4) or three (YxiN lk 3) amino acids leads to a gradual increase in ATP affinity as reflected by the respective binding constants. The binding constant of 47 ± 5 µM for YxiN wildtype is increased to 26 ± 5 µM for YxiN lk 7, to 25 ± 4 µM for YxiN lk 5, to 12 ± 4 µM for YxiN lk 4 and to 19 ± 4 µM for YxiN lk 3 (see Table 4). Stepping further in the nucleotide cycle the binding constant for the non-hydrolysable ATP-analogue ADP·BeF_x for YxiN wildtype is determined to be 56 ± 20 µM very similar to the binding constant for ATP. Reducing the length of the linker in the catalytic core leads to small changes in affinity for ADP·BeF_x as reflected by the binding constants for YxiN lk 7, determined to be 45 ± 18 µM, for YxiN lk 5, determined to be 27 ± 13 µM, for YxiN lk 4, determined to be 43 ± 33 µM and for YxiN lk 3, determined to be 36 ± 9 µM (see Table 4). At the end of the catalytic cycle the binding constant for YxiN wildtype for ADP of 146 ± 18 µM reflects a rather low affinity. As seen for

ATP and its non-hydrolysable ATP-analogue ADP·BeF_x[65-67] there is a change in the binding constants of the shorter linker mutants for ADP. Minor increases in nucleotide affinities can be observed. YxiN lk 7 has a binding constant of 161 ± 36 µM, YxiN lk 5 has a binding constant of 93 ± 23 µM, YxiN lk 4 has a binding constant of 52 ± 17 µM and YxiN lk 3 has a binding constant of 103 ± 29 µM (see Table 4).

Figure 30: Nucleotide binding of the short YxiN linker mutants with an RNA substrate

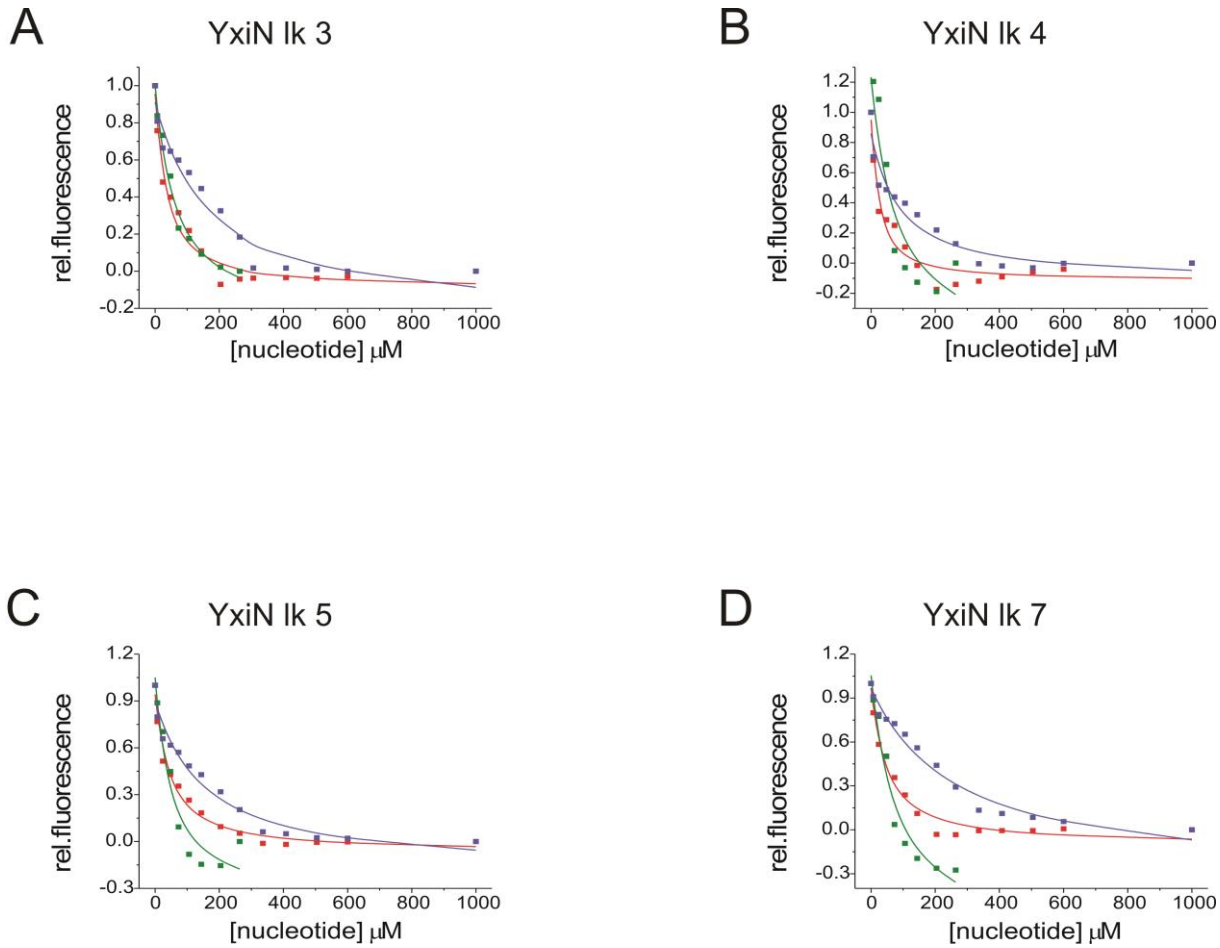

Figure 30: Nucleotide binding of the short YxiN linker mutants with an RNA substrate

Figure 30 shows the nucleotide binding of the different short mutants of the linker between the two RecA core domains of YxiN in the presence of a 32mer RNA substrate. Graphs shown originate from taking a mean value of at least two independent measurements and fitting of them. Experimental procedure of these displacement

titrations is described in section 4.10. ATP is shown in red, ADP·BeF_x is shown in green and ADP is shown in violet. Panel A shows nucleotide affinities of YxiN lk 3 for ATP (19 ± 4 µM), ADP·BeF_x (36 ± 9 µM) and ADP (103 ± 29 µM). Panel B shows nucleotide affinities of YxiN lk 4 for ATP (12 ± 4 µM), ADP·BeF_x (43 ± 33 µM) and ADP (52 ± 17 µM). Panel C shows nucleotide affinities of YxiN lk 5 for ATP (25 ± 4 µM), ADP·BeF_x (27 ± 13 µM) and ADP (93 ± 23 µM). Panel D shows nucleotide affinities of YxiN lk 7 for ATP (26 ± 5 µM), ADP·BeF_x (24 ± 13 µM) and ADP (150 ± 27 µM).

Table 4: Nucleotide binding constants of the shorter linker mutants in the presence of RNA

YxiN linker mutant	ATP (µM)	ADPBeFx (µM)	ADP (µM)
lk 3	19 ± 4	36 ± 9	103 ± 29
lk 4	12 ± 4	43 ± 33	52 ± 17
lk 5	25 ± 4	27 ± 13	93 ± 23
lk 7	26 ± 5	45 ± 18	161 ± 36
wildtype	47 ± 5	56 ± 20	146 ± 18

Increasing the linker length of the linker in the catalytic core leads to similar affinities for ATP but for the longest YxiN linker mutant, where there is a loss in affinity to be observed as is reflected by the binding constants of 48 ± 6 µM for YxiN lk 9, 47 ± 8 µM for YxiN lk 11 and 53 ± 9 µM for YxiN lk 13. In contrast to the other longer linker constructs, YxiN lk 15 shows a reduction in ATP binding as seen in the binding constant of 86 ± 14 µM (see Table 5). Stepping further in the nucleotide cycle to ADP·BeF_x a very small increase in nucleotide affinity can be observed. YxiN lk 9 has a binding constant for ADP·BeF_x of 24 ± 13 µM, YxiN lk 11 has a binding constant of 39 ± 26 µM, YxiN lk 13 has a binding constant of 42 ± 13 µM and YxiN lk 15 has a binding constant of 44 ± 8 µM (see Table 5). At the end of the catalytic cycle the low affinity for ADP as seen in YxiN wildtype is also seen for the mutants with a longer catalytic core linker. YxiN lk 9 has a binding constant for ADP of 150 ± 27 µM, YxiN lk 11 has a binding constant of 182 ± 45 µM, YxiN lk 13 has a binding constant of 212 ± 60 µM and YxiN lk 15 has a binding constant of 128 ± 18 µM (see Table 5).

Figure 31: Nucleotide binding of the long YxiN linker mutants with an RNA substrate

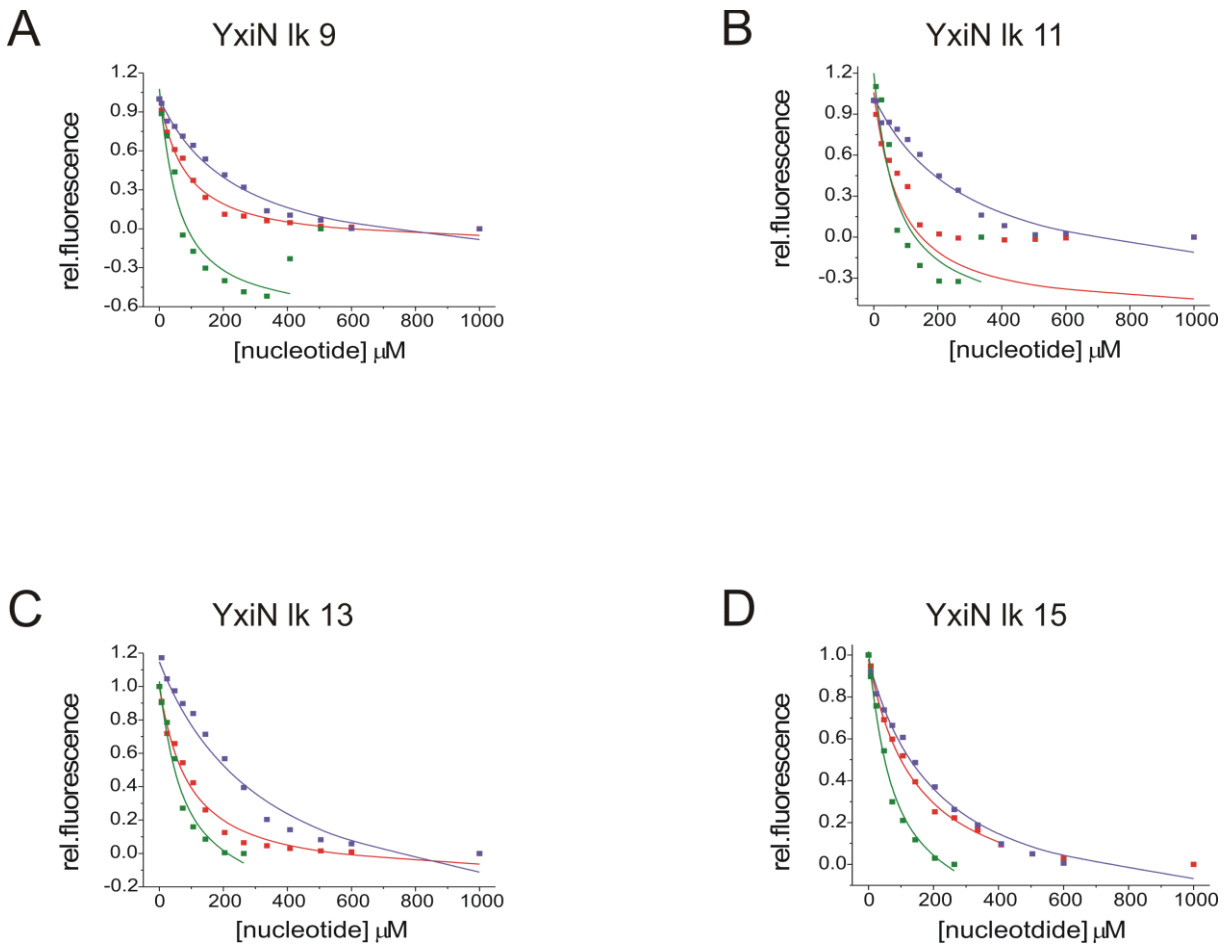

Figure 31: Nucleotide binding of the long YxiN linker mutants with an RNA substrate

Figure 31 shows the nucleotide binding of the different long mutants of the linker between the two RecA core domains of YxiN in the presence of a 32mer RNA substrate. Graphs shown originate from taking a mean value of at least two independent measurements and fitting of them. Experimental procedure of these displacement titrations is described in section 4.10. ATP is shown in red, ADP·BeF_x is shown in green and ADP is shown in violet. Panel A shows nucleotide affinities of YxiN lk 9 for ATP (48 ± 6 µM), ADP·BeF_x (24 ± 13 µM) and ADP (150 ± 27 µM). Panel B shows nucleotide affinities of YxiN lk 11 for ATP (47 ± 8 µM), ADP·BeF_x (39 ± 26 µM) and ADP (182 ± 45 µM). Panel C shows nucleotide affinities of YxiN lk 13 for ATP (53 ± 9 µM), ADP·BeF_x (42 ± 13 µM) and ADP (212 ± 60 µM). Panel D shows nucleotide affinities of YxiN lk 15 for ATP (86 ± 14 µM), ADP·BeF_x (44 ± 8 µM) and ADP (128 ± 18 µM).

Table 5: Nucleotide binding constants of the longer linker mutants in the presence of RNA

YxiN linker mutant	ATP (µM)	ADPBeFx (µM)	ADP (µM)
lk 9	48 ± 6	24 ± 13	150 ± 27
wildtype	47 ± 5	56 ± 20	146 ± 18
lk 11	47 ± 8	39 ± 26	182 ± 45
lk 13	53 ± 9	42 ± 13	212 ± 60
lk 15	86 ± 14	44 ± 8	128 ± 18

Figure 32: Comparison of nucleotide binding of the YxiN linker mutants to YxiN wildtype in the presence of RNA

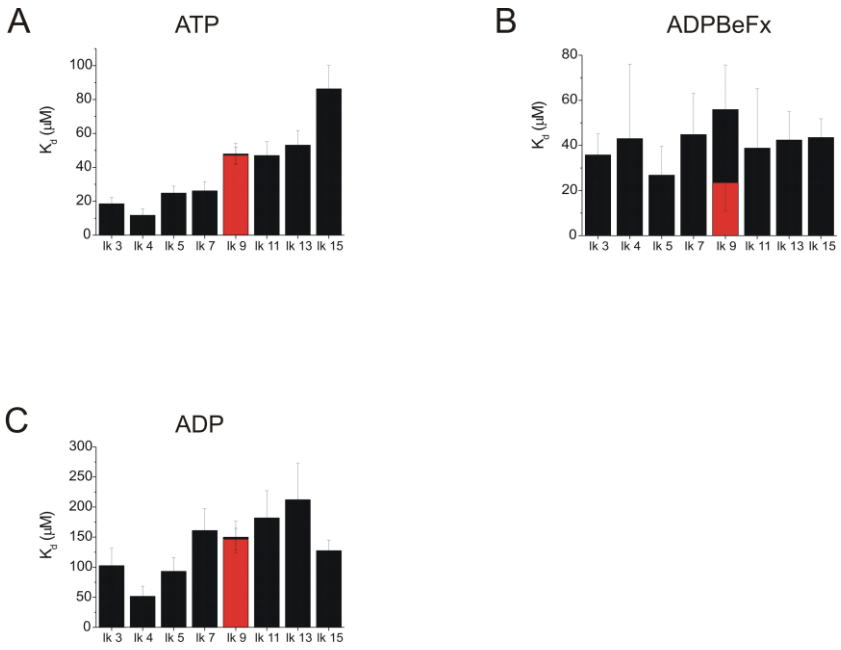

Figure 32: Comparison of nucleotide binding of the YxiN linker mutants to YxiN wildtype

Figure 32 shows a comparison of the YxiN linker mutants to YxiN wildtype concerning nucleotide binding in the presence of RNA. Panel A shows the Kd values of all mutants for ATP. The Kd value for wildtype is shown as a red bar in the lk 9 section. Panel B shows the Kd values of all mutants for ADP·BeF_x. The Kd value for wildtype is shown as a black bar in the lk 9 section. Panel C shows the Kd values of all mutants for ADP. The Kd value for wildtype is shown as a red bar in the lk 9 section.

In general the nucleotide binding affinities are higher in the presence of a 32mer RNA substrate than in the absence of an RNA substrate. The trend towards higher affinities for ATP in the catalytic core linker mutations is also present if looking at the shortened constructs. If looking at the prolonged constructs, this trend is reversed into a trend of loosing ATP affinity. The trend to lose affinity for ADP·BeF_x observed for the catalytic core linker mutations in the absence of RNA is also lost. There rather is a fuzzy trend towards increasing affinities, which is also observed for ADP affinities that are virtually the same as for YxiN wildtype in the absence of an RNA substrate. Binding of RNA together with binding of nucleotide thus influences the nucleotide affinities.

5.2.4. Comparison of the ability to bind RNA of YxiN wildtype to YxiN linker mutants throughout the nucleotide cycle

As it is important to know binding affinities for nucleotides throughout the nucleotide cycle for further activity assays, it is also important to know RNA binding affinities in the presence of different nucleotides, or in the absence of them. Furthermore, binding affinities of RNA also gives insight into the catalytic cycle of YxiN. To examine the effect of the mutations in the linker in the catalytic core of YxiN on RNA binding, fluorescence anisotropy measurements were performed as described in section 4.11 and globally fitted with equation 5. In the absence of any nucleotide YxiN wildtype shows a binding constant for the fluorescently labeled 32mer minimal substrate of 351 ± 93 nM. A slight reduction of this affinity is seen for YxiN lk 9 and is found to be 244 ± 140 nM. For the YxiN linker mutant with the shortest sequence, YxiN lk 3, the same slight reduction to a Kd of 240 ± 55nM is observed. Also for the YxiN linker mutant with the longest sequence, YxiN lk 15, there is this slight decrease in Kd to 204 ± 236 nM. In the absence of nucleotide, the influence of the linker upon RNA binding therefore is neglectable.

Figure 33: Comparison of RNA binding of YxiN wildtype and YxiN linker mutants without nucleotide

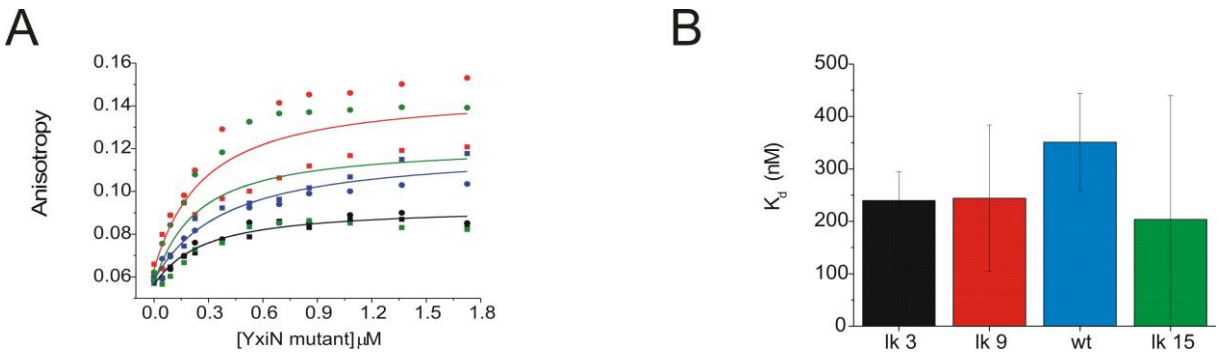

Figure 33: Comparison of RNA binding of YxiN wildtype and YxiN linker mutants without nucleotide

Figure 33 shows the ability of the YxiN linker mutants to bind RNA compared to the wildtype enzyme without nucleotide. RNA binding was determined by fluorescence anisotropy titrations of a fluorescently labeled 32mer with the respective YxiN construct (see section 4.11). Panel A shows two independent measurements for each construct and a global fitting thereof (lk 3 in black, lk 9 in red, wt in blue and lk 15 in green). Panel B shows the respective Kd values.

If ADPNP is present, the binding constant for YxiN wildtype of 195 ± 18 nM is reduced to a binding constant of 82 ± 15 nM for YxiN lk 9. For the shortest linker construct, YxiN lk 3 the binding constant is significantly increased to 487 ± 351 nM reflecting a loss in RNA binding ability. The same holds true for the construct with the longest linker sequence, YxiN lk 15 where the binding constant is increased to 500 ± 482 nM. Presence of an ATP-analogue thus influences binding capacities of RNA.

Figure 34: Comparison of RNA binding of YxiN wildtype and YxiN linker mutants in the presence of ADPNP

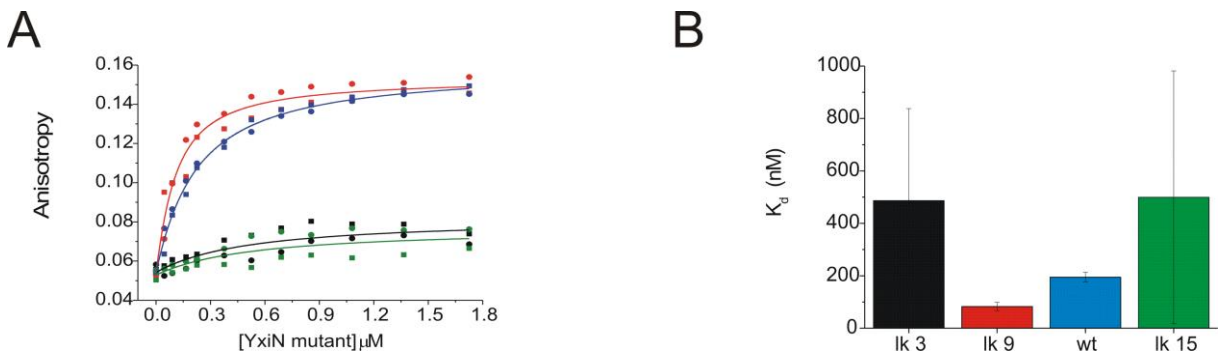

Figure 34: Comparison of RNA binding of YxiN wildtype and YxiN linker mutants in the presence of ADPNP

Figure 34 shows the ability of the YxiN linker mutants to bind RNA compared to the wildtype enzyme in the presence of ADPNP. RNA binding was determined by fluorescence anisotropy titrations of a fluorescently labeled 32mer with the respective YxiN construct (see section 4.11). Panel A shows two independent measurements for each construct and a global fitting thereof (lk 3 in black, lk 9 in red, wt in blue and lk 15 in green). Panel B shows the respective Kd values.

In the presence of the non-hydrolysable pre-hydrolysis state ATP analogue ADP·BeF_x, the binding constant of 277 ± 66 nM for YxiN wildtype is slightly decreased to 180 ± 100 nM for YxiN lk 9. While the YxiN construct with the shortest linker sequence, YxiN lk 3 shows a drastic decrease in affinity to a Kd value of 770 ± 280 nM the YxiN construct with the longest linker sequence, YxiN lk 15 exhibits a dramatic increase in affinity to a Kd value of 32 ± 6 nM. Again, presence of a pre-hydrolysis state ATP-analogue[65-67] influences RNA binding affinities of the mutants.

Figure 35: Comparison of RNA binding of YxiN wildtype and YxiN linker mutants in the presence of ADP·BeF$_x$

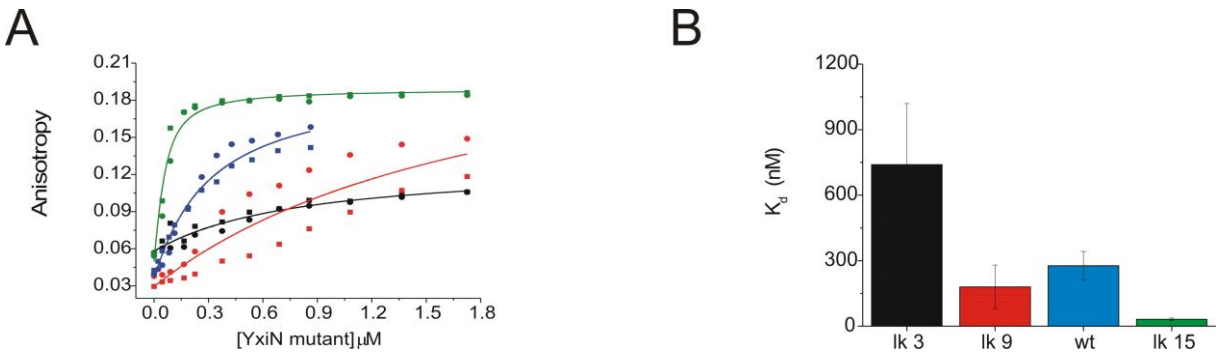

Figure 35: Comparison of RNA binding of YxiN wildtype and YxiN linker mutants in the presence of ADP·BeF$_x$

Figure 35 shows the ability of the YxiN linker mutants to bind RNA compared to the wildtype enzyme in the presence of ADP·BeF$_x$. RNA binding was determined by fluorescence anisotropy titrations of a fluorescently labeled 32mer with the respective YxiN construct (see section 4.11). Panel A shows two independent measurements for each construct and a global fitting thereof (lk 3 in black, lk 9 in red, wt in blue and lk 15 in green). Panel B shows the respective Kd values.

At the end of nucleotide cycle, in the presence of ADP, there is a drastic loss in affinity for the YxiN lk 9 mutant to an RNA binding constant of 1120 ± 343 nM. For the YxiN construct with the shortest (YxiN lk 3) and the longest (YxiN lk 15) linker sequence, there is a slight increase in affinity as reflected by the RNA binding constants of 192 ± 61 nM and 138 ± 132 nM respectively. Also in the reset state of the nucleotide cycle, presence of a nucleotide, being ADP, influences affinities for RNA in the YxiN linker mutants.

Figure 36: Comparison of RNA binding of YxiN wildtype and YxiN linker mutants in the presence of ADP

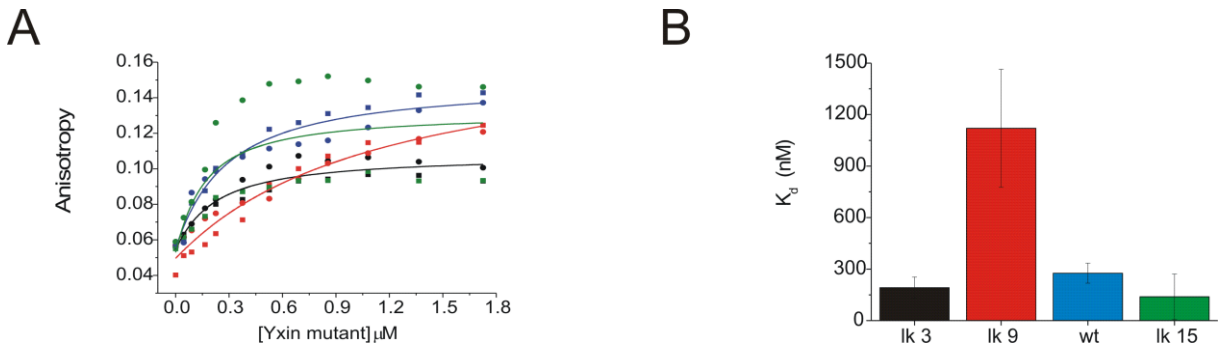

Figure 36: Comparison of RNA binding of YxiN wildtype and YxiN linker mutants in the presence of ADP

Figure 36 shows the ability of the YxiN linker mutants to bind RNA compared to the wildtype enzyme in the presence of ADP. RNA binding was determined by fluorescence anisotropy titrations of a fluorescently labeled 32mer with the respective YxiN construct (see section 4.11). Panel A shows two independent measurements for each construct and a global fitting thereof (lk 3 in black, lk 9 in red, wt in blue and lk 15 in green). Panel B shows the respective Kd values.

Taken together, the most pronounced changes in RNA binding affinity are observed for the pre-hydrolysis state for the YxiN mutants with the shortest and the longest linker sequence and in the ADP state for the YxiN lk 9 mutant. These differences in RNA binding could have an impact on the catalytic cycle. Both YxiN linker mutants, YxiN lk 3 and YxiN lk 15 are double stranded RNA unwinding deficient. The ATP hydrolysis deficiency of these mutants cannot be the reason for this deficiency, since ATP hydrolysis is needed for enzyme reset, but not for the enzymatic double stranded RNA unwinding[39]. Thus it might be, that RNA binding in the activated RNA state, present in the ADP·BeF_x state, is strictly controlled, as gain or loss in affinity leads to a loss in double stranded RNA unwinding ability. Impacts of the loss in RNA affinity of YxiN lk 9 in the presence of RNA cannot be observed from these experiments, since the unwinding assay performed is a single-turnover assay, and differences in enzyme

reset thus cannot be detected. But it can be observed, that the conformational state of YxiN lk 9 in the presence of RNA and ADP does not differ from YxiN wildtype. If there is an impact of this loss in RNA affinity, it is not reflected in the conformational state.

5.2.5. RNA stimulated ATPase activity of YxiN wildtype compared to YxiN linker mutants.

To investigate the ability of YxiN catalytic core linker mutants to hydrolyse ATP an enzymatically coupled RNA stimulated ATPase assay was carried out as described in section 4.9. YxiN wildtype shows a moderate ATP hydrolysis rate constant of 4.7 ± 0.7 s^{-1}. Reducing the linker of the catalytic core leads to a stepwise reduction of ATP hydrolysis rate constants as reflected by the values determined for the YxiN linker mutants YxiN lk 7, YxiN lk 5, YxiN lk 4 and YxiN lk 3. YxiN lk 7 has an ATP hydrolysis rate constant of 3.6 ± 0.4 s^{-1}, YxiN lk 5 has an ATP hydrolysis rate constant of 1.03 ± 0.02 s^{-1} and the YxiN lk 4 and YxiN lk 3 mutants are completely ATPase deficient. Increasing of the linker length in the catalytic core also leads to a reduction of ATP hydrolysis rate constants as reflected by the values determined for the YxiN linker mutants YxiN lk 11, YxiN lk 13 and YxiN lk 15. YxiN lk 11 has an ATP hydrolysis rate constant of 4.6 ± 0.3 s^{-1} and YxiN lk 13 has an ATP hydrolysis rate constant of 2.1 ± 0.3 s^{-1}. Again the longest linker in the catalytic core is ATP hydrolysis deficient.

Table 6: RNA stimulated ATPase activity of YxiN wildtype compared to YxiN linker mutants

YxiN linker mutant	K_M (µM)	k_{cat} (s^{-1})
lk 3	not detected	not detected
lk 4	not detected	not detected
lk 5	0.0015 ± 0.001	1.03 ± 0.0013
lk 7	0.018 ± 0.001	3.58 ± 0.38
lk 9	0.017 ± 0.008	4.17 ± 0.43
wildtype	0.012 ± 0.001	4.66 ± 0.69
lk 11	0.021 ± 0.006	4.56 ± 0.28
lk 13	0.054 ± 0.018	2.11 ± 0.23
lk 15	not detected	not detected

Figure 38: RNA stimulated ATPase activity of YxiN wildtype compared to YxiN linker mutants

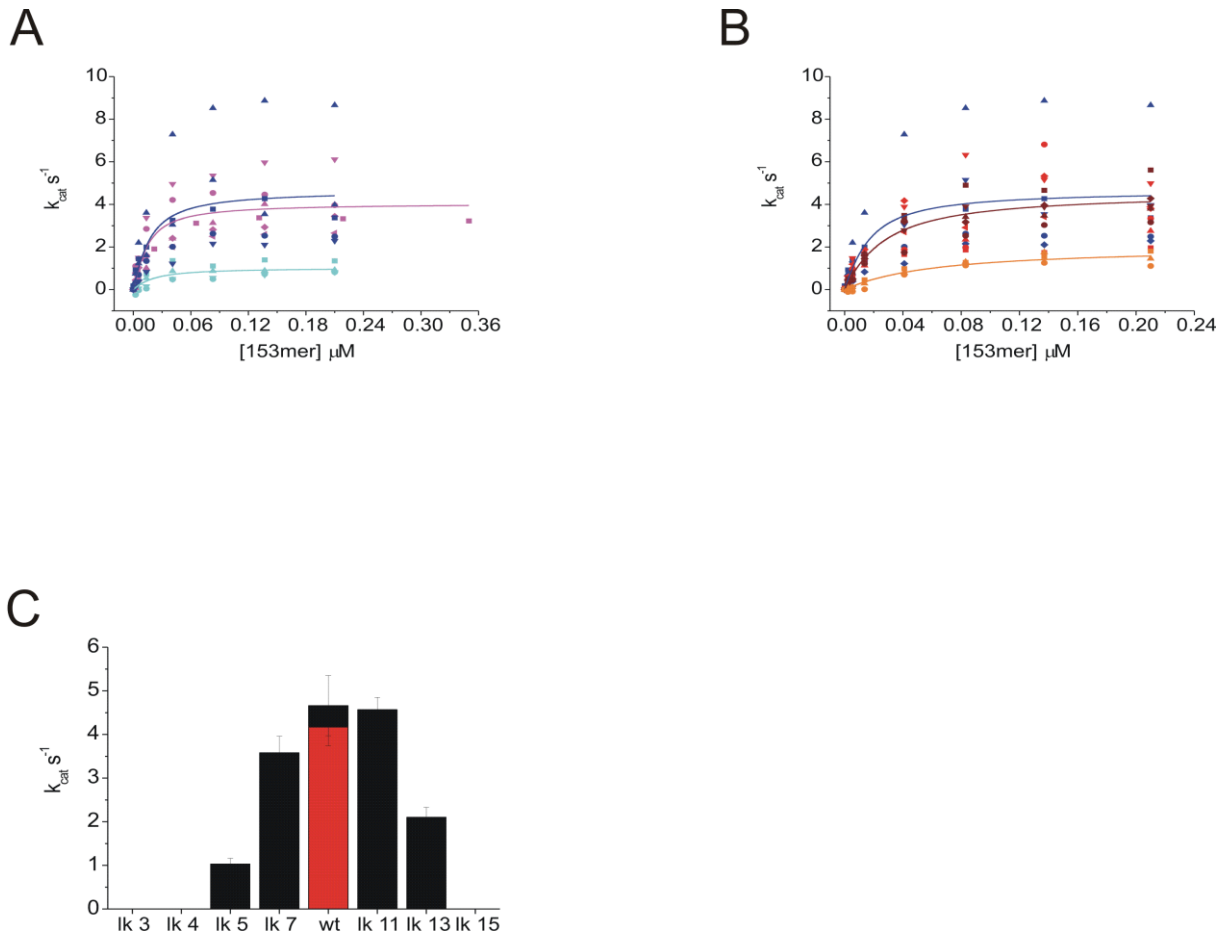

Figure 38: RNA stimulated ATPase activity of YxiN wildtype compared to YxiN linker mutants

Figure 38 shows the ATP hydrolysis activity of YxiN wildtype compared to YxiN linker mutants as determined by an enzymatically coupled ATPase assay (described in section 4.9). Panel A shows at least three independent measurements of RNA stimulated ATPase activity of YxiN wildtype and the YxiN short linker mutants and a global fitting of them according to equation 2. YxiN wildtype is shown in blue, YxiN lk 5 in cyan, YxiN lk 7 in magenta. Panel B shows at least three independent measurements of RNA stimulated ATPase activity of YxiN wildtype and the YxiN long linker mutants and a global fitting of them according to equation 2. YxiN lk 9 is shown in red, YxiN lk 11 in wine, YxiN lk 13 in orange and YxiN lk 15 in green. Panel C shows the respective reaction constants k_{cat}. The YxiN lk 9 construct is shown as wildtype in red.

These results indicate that the length of the linker in the catalytic core is strictly controlled. If the linker is too long and allows too much flexibility in the movement of the two core RecA domains relative to each other, ATP can no longer be hydrolysed. The same effect is also seen if the linker in the catalytic core is too short allowing too little flexibility of the two core RecA domains relative to each other.

5.2.6. Influence of the YxiN linker mutations on double stranded RNA unwinding

Having determined RNA and nucleotide affinities and ATP hydrolysis rates for the YxiN linker mutants, testing the ability to unwind double stranded RNA was needed and we next tested, whether the influences on substrate binding and ATP hydrolysis rates are also present in the second enzymatic process, the unwinding of double stranded RNA. To examine this influence of the linker in the catalytic core of YxiN on the unwinding activity of the respective mutants FRET based unwinding assays were performed as described in section 4.12.1. Unwinding reactions were performed with a minimal double stranded RNA substrate Cy3-9mer hybridised to a Cy5-32mer of the hairpin 92 of the 23S rRNA in the presence of ATP and the non-hydrolysable pre-hydrolysis state ATP-analogue ADP·BeF_x [65-67] with YxiN wildtype and the YxiN linker mutants. In the presence of ATP YxiN wildtype shows an unwinding rate constant of $7.7*10^{-3} \pm 6.8*10^{-5}$ s^{-1}. Reducing the length of the linker to seven (YxiN lk 7), five (YxiN lk 5), four (YxiN lk 4) and three (YxiN lk 3) amino acids leads to a reduction in unwinding rates, after an increase in unwinding rate for YxiN lk 7. The rate constant determined for YxiN lk 7 is $2.2*10^{-2} \pm 4.9*10^{-5}$ s^{-1}. The rate constant determined for YxiN lk 5 is $3.5*10^{-3} \pm 3.2*10^{-5}$ s^{-1}. The rate constant determined for YxiN lk 4 is $1.3*10^{-3} \pm 1.3*10^{-5}$ s^{-1} and the rate constant determined for YxiN lk 3 is $6.1*10^{-4} \pm 1.7*10^{-5}$ s^{-1}.

Table 7: double stranded RNA unwinding rate constants of the short YxiN linker mutants compared to YxiN wildtype in the presence of ATP

YxiN linker mutant	rate constant with ATP (s^{-1})
lk 3	$6.1 * 10^{-4} \pm 1.7 * 10^{-5}$
lk 4	$1.3 * 10^{-3} \pm 1.3 * 10^{-5}$
lk 5	$3.5 * 10^{-3} \pm 3.2 * 10^{-5}$
lk 7	$2.2 * 10^{-3} \pm 4.9 * 10^{-5}$
wildtype	$7.7 * 10^{-3} \pm 6.8 * 10^{-5}$

Figure 39: double stranded RNA unwinding rate constants of the short YxiN linker mutants compared to YxiN wildtype in the presence of ATP

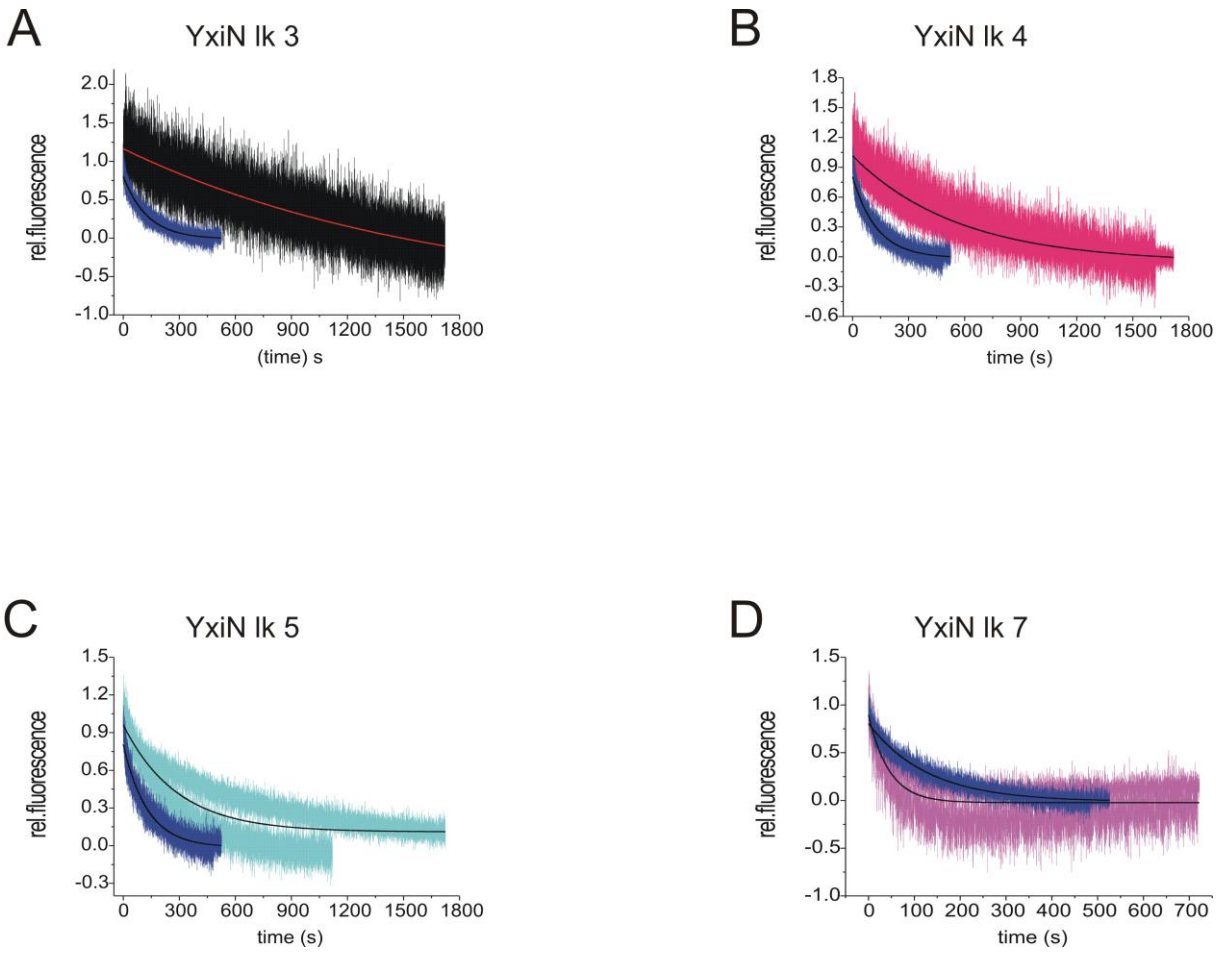

Figure 39: double stranded RNA unwinding rate constants of the short YxiN linker mutants compared to YxiN wildtype in the presence of ATP

Figure 39 shows the capability of the short YxiN linker mutants to unwind a minimal RNA substrate consisting of a Cy3-9mer and a Cy5-32mer of the hairpin 92 of the23S rRNA in the presence of ATP. The experimental procedure is described in section 4.12.1. For comparison, YxiN wildtype (blue curve) is included in all graphs. All panels show two independent measurements and a global fit thereof. The unwinding rate constant determined are as follows: $6.1*10^{-4} \pm 1.7*10^{-5}$ s^{-1} for YxiN lk 3 (black curve, panel A); $1.3*10^{-3} \pm 1.3*10^{-5}$ s^{-1} for YxiN lk 4 (pink curve, panel B); $3.5*10^{-3} \pm 3.2*10^{-5}$ s^{-1} for YxiN lk 5 (cyan curve, panel C); $2.2*10^{-2} \pm 4.9*10^{-5}$ s^{-1} for YxiN lk 7 (magenta curve, panel D)

Increasing the length of the linker in the catalytic core to eleven (YxiN lk 11), thirteen (YxiN lk 13) and fifteen (YxiN lk 15) amino acids first leads to a drastic increase in double stranded RNA unwinding rate (YxiN lk 11), but then again to a decrease (YxiN lk 13) and a complete loss (YxiN lk 15). Changing of the sequence of the linker in the catalytic core does not change the double stranded RNA unwinding rates. The rate constant determined for YxiN lk 9 is $8.2*10^{-3} \pm 7.5*10^{-5}$ s^{-1}. The rate constant determined for YxiN lk 11 is $5.8*10^{-2} \pm 1.2*10^{-3}$ s^{-1}. The rate constant determined for YxiN lk 13 is $7.1*10^{-3} \pm 7.1*10^{-5}$ s^{-1} and the rate constant determined for YxiN lk 15 is $1.3*10^{-3} \pm 1.3*10^{-5}$ s^{-1}.

Table 8: double stranded RNA unwinding rate constants of the long YxiN linker mutants compared to YxiN wildtype in the presence of ATP

YxiN linker mutant	rate constant with ATP (s^{-1})
lk 9	$8.2 * 10^{-3} \pm 7.5 * 10^{-5}$
wildtype	$7.7 * 10^{-3} \pm 6.8 * 10^{-5}$
lk 11	$5.8 * 10^{-2} \pm 1.2 * 10^{-3}$
lk 13	$7.1 * 10^{-3} \pm 7.1 * 10^{-5}$
lk 15	$1.3 * 10^{-3} \pm 1.3 * 10^{-5}$

Figure 40: double stranded RNA unwinding rate constants of the long YxiN linker mutants compared to YxiN wildtype in the presence of ATP

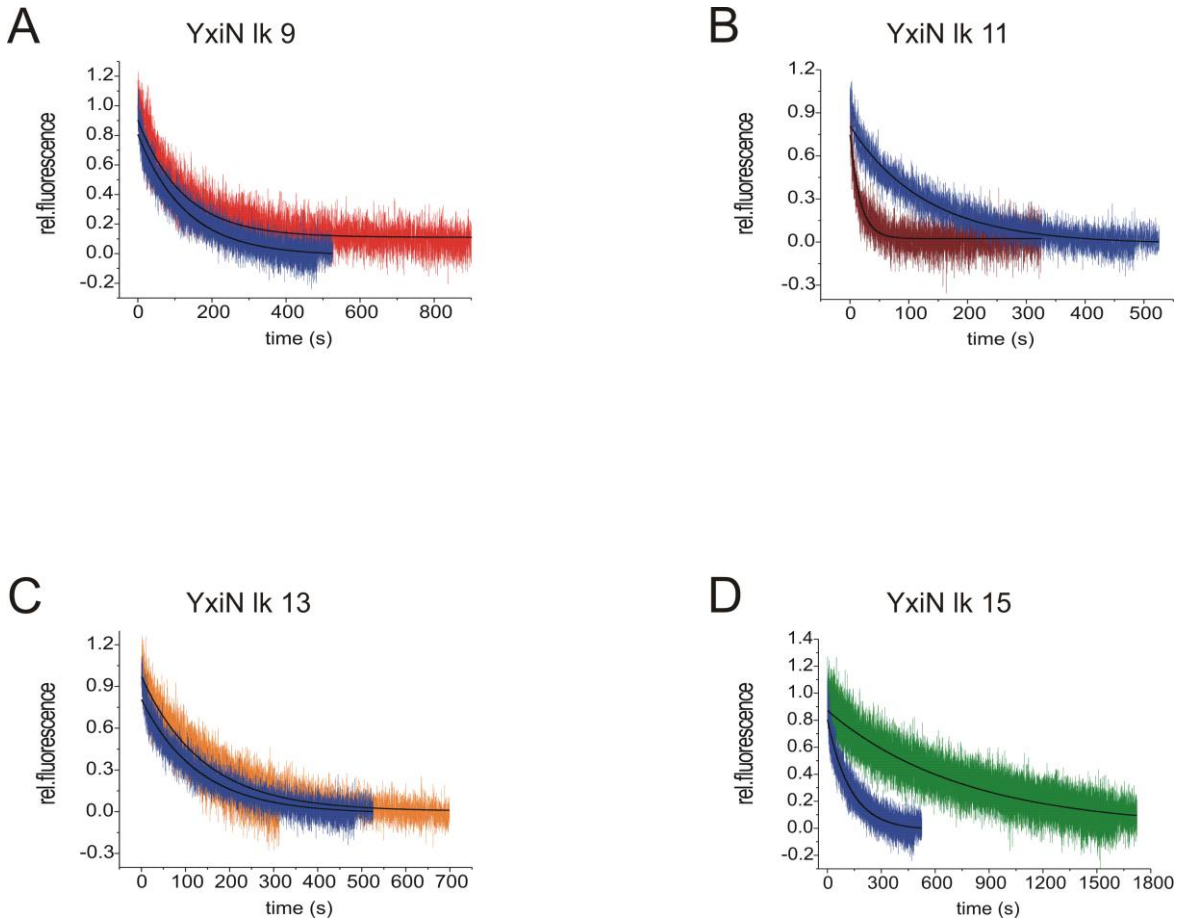

Figure 40: double stranded RNA unwinding rate constants of the long YxiN linker mutants compared to YxiN wildtype in the presence of ATP

Figure 40 shows the capability of the long YxiN linker mutants to unwind a minimal RNA substrate consisting of a Cy5-32mer and a Cy3-9mer of the hairpin 92 of the23S rRNA in the presence of ATP. The experimental procedure is described in section 4.12.1. For comparison, YxiN wildtype (blue curve) is included in all graphs. All panels show two independent measurements and a global fit thereof. The unwinding rate constant determined are as follows: $8.2*10^{-3} \pm 7.5*10^{-5}$ s^{-5} for YxiN lk 9 (red curve, panel E); $5.8*10^{-2} \pm 1.2*10^{-3}$ s^{-1} for YxiN lk 11 (wine curve, panel F); $7.1*10^{-3} \pm 7.\ 1*10^{-5}$ s^{-1} for YxiN lk 13 (orange curve, panel G); $1.3*10^{-3} \pm 1.27*10^{-5}$ s^{-1} for YxiN lk 15 (green curve, panel H). The rate constant of YxiN wildtype is $7.7*10^{-3} \pm 6.8*10^{-5}$ s^{-1}.

In the presence of ADP·BeF_x YxiN wildtype shows an unwinding rate constant of $1.9*10^{-2} \pm 2.3*10^{-4}$ s^{-1}. Reducing the length of the linker to seven (YxiN lk 7), five (YxiN lk 5), four (YxiN lk 4) and three (YxiN lk 3) amino acids leads to a reduction in unwinding rates. The rate constant determined for YxiN lk 7 is $6.5*10^{-3} \pm 6.7*10^{-5}$ s^{-1}. The rate constant determined for YxiN lk 5 is $1.4*10^{-3} \pm 2.4*10^{-5}$ s^{-1}. The rate constant determined for YxiN lk 4 is $1.2*10^{-3} \pm 2.3*10^{-5}$ s^{-1} and the rate constant determined for YxiN lk 3 is $3.2*10^{-4} \pm 2.4*10^{-5}$ s^{-1}.

Table 9: double stranded RNA unwinding rate constants of the short YxiN linker mutants compared to YxiN wildtype in the presence of ADP·BeF_x

YxiN linker mutant	rate constant with ADP·BeFx (s^{-1})
lk 3	$3.2 * 10^{-4} \pm 2.4 * 10^{-5}$
lk 4	$1.2 * 10^{-3} \pm 2.3 * 10^{-5}$
lk 5	$1.4 * 10^{-3} \pm 2.4 * 10^{-5}$
lk 7	$6.5 * 10^{-3} \pm 6.7 * 10^{-5}$
wildtype	$1.9 * 10^{-2} \pm 2.3 * 10^{-4}$

Figure 41: double stranded RNA unwinding rate constants of the short YxiN linker mutants compared to YxiN wildtype in the presence of ADP·BeF$_x$

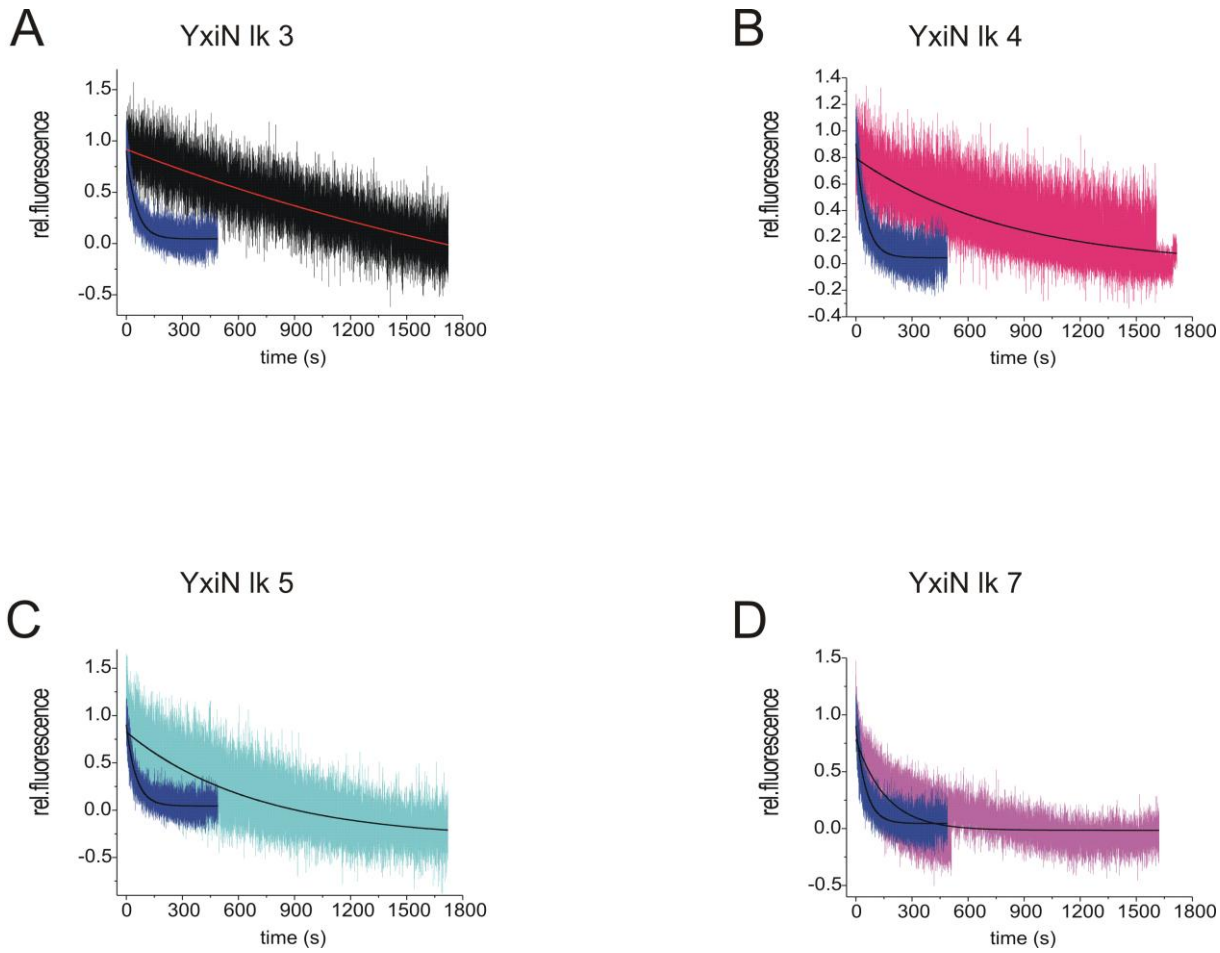

Figure 41: double stranded RNA unwinding rate constants of the short YxiN linker mutants compared to YxiN wildtype in the presence of ADP·BeF$_x$

Figure 41 shows the capability of the short YxiN linker mutants to unwind a minimal RNA substrate consisting of a Cy3-9mer and a Cy5-32mer of the hairpin 92 of the23S rRNA in the presence of ADP·BeF$_x$. The experimental procedure is described in section 4.12. For comparison, YxiN wildtype (blue curve) is included in all graphs. All panels show two independent measurements and a global fit thereof. The unwinding rate constant determined are as follows: $3.2*10^{-4} \pm 2.4*10^{-5}$ s^{-1} for YxiN lk 3 (black curve, panel A); $1.2*10^{-3} \pm 2.3*10^{-5}$ s^{-1} for YxiN lk 4 (pink curve, panel B); $1.4*10^{-3} \pm 2.4*10^{-5}$ s^{-1} for YxiN lk 5 (cyan curve, panel C); $6.5*10^{-3} \pm 6.7*10^{-5}$ s^{-1} for YxiN lk 7 (magenta curve, panel D)

Increasing the length of the linker in the catalytic core to eleven (YxiN lk 11), thirteen (YxiN lk 13) and fifteen (YxiN lk 15) amino acids or changing the sequence of the linker in the catalytic core leads to a decrease in double stranded RNA unwinding rate or even a complete loss (YxiN lk 15). The rate constant determined for YxiN lk 9 is $6.1*10^{-3} \pm 6.3*10^{-5}$ s^{-1}. The rate constant determined for YxiN lk 11 is $2.3*10^{-3} \pm 2.4*10^{-5}$ s^{-1}. The rate constant determined for YxiN lk 13 is $5.5*10^{-3} \pm 7.4*10^{-5}$ s^{-1} and the rate constant determined for YxiN lk 15 is $1*10^{-3} \pm 2.1*10^{-4}$ s^{-1}.

Table 10: double stranded RNA unwinding rate constants of the long YxiN linker mutants compared to YxiN wildtype in the presence of ADP·BeF_x

YxiN linker mutant	rate constant with ADP·BeFx (s^{-1})
lk 9	$6.1 * 10^{-3} \pm 6.3 * 10^{-5}$
wildtype	$1.9 * 10^{-2} \pm 2.3 * 10^{-4}$
lk 11	$2.3 * 10^{-3} \pm 2.4 * 10^{-5}$
lk 13	$5.5 * 10^{-3} \pm 7.4 * 10^{-5}$
lk 15	$1 * 10^{-3} \pm 2.1 * 10^{-5}$

Figure 42: double stranded RNA unwinding rate constants of the long YxiN linker mutants compared to YxiN wildtype in the presence of ADP·BeF$_x$

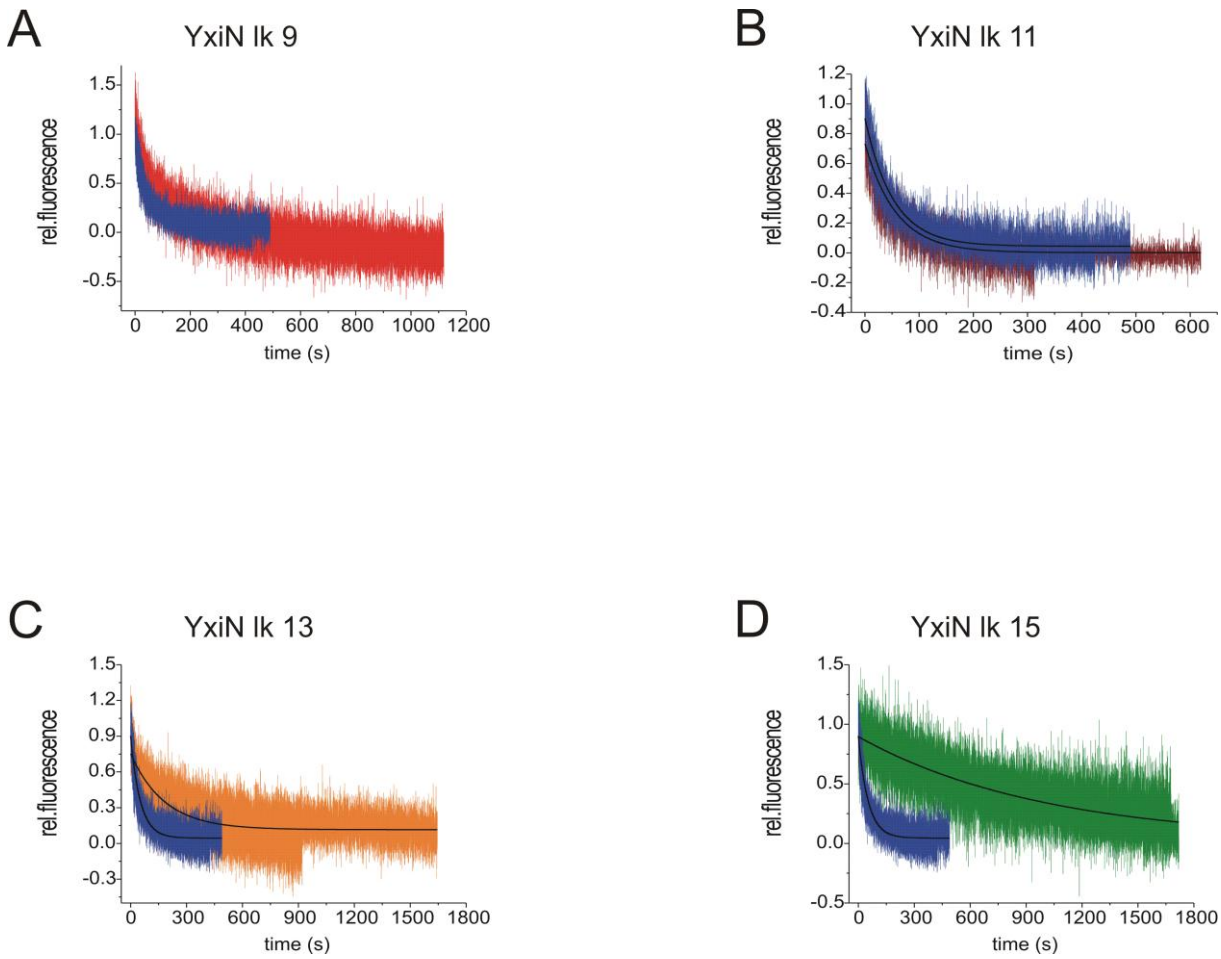

Figure 42: double stranded RNA unwinding rate constants of the long YxiN linker mutants compared to YxiN wildtype in the presence of ADP·BeF$_x$

Figure 42 shows the capability of the long YxiN linker mutants to unwind a minimal RNA substrate consisting of a Cy5-32mer and a Cy3-9mer of the hairpin 92 of the23S rRNA in the presence of ADP·BeFx. The experimental procedure is described in section 4.12. For comparison, YxiN wildtype (blue curve) is included in all graphs. All panels show two independent measurements and a global fit thereof. The unwinding rate constant determined are as follows: $6.1*10^{-3} \pm 6.3*10^{-5}$ s^{-1} for YxiN lk 9 (red curve, panel E); $2.3*10^{-3} \pm 2.4*10^{-4}$ s^{-1} for YxiN lk 11 (wine curve, panel F); $5.5*10^{-3} \pm 7.4*10^{-5}$ s^{-1} for YxiN lk 13 (orange curve, panel G); $1*10^{-3} \pm 2.1*10^{-5}$ s^{-1} for YxiN lk 15 (green curve, panel H). The rate constant of YxiN wildtype is $1.9*10^{-2} \pm 2.3E^{-4}$ s^{-1}.

Figure 43: double stranded RNA unwinding rate constants of the YxiN linker mutants compared to YxiN wildtype

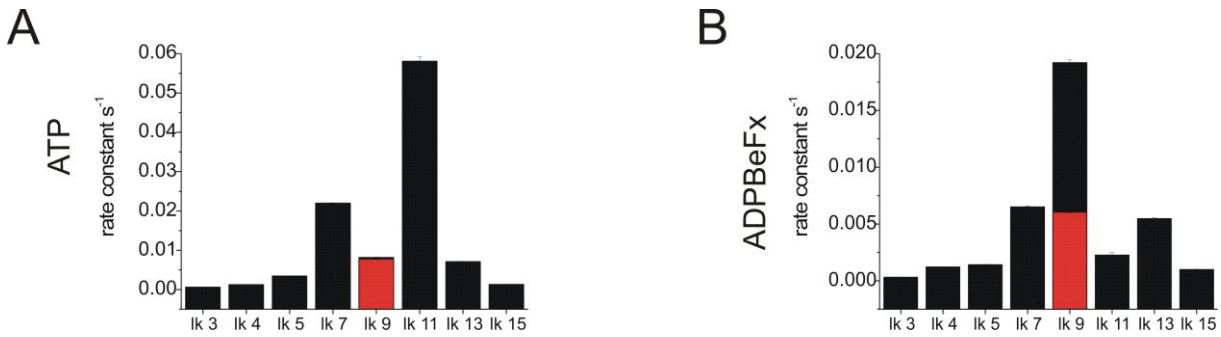

Figure 43: double stranded RNA unwinding rate constants of the YxiN linker mutants compared to YxiN wildtype

Figure 43 shows the capability of the YxiN linker mutants to unwind a minimal RNA substrate compared to YxiN wildtype. Rate constants are represented on a bar plot and error bars originate from a global fitting of two independent measurements. Panel A shows the comparison of the YxiN linker mutants to YxiN wild type in the presence of ATP (wildtype shown as lk 9 in red) and panel B shows the comparison of the YxiN linker mutants compared to YxiN wild type in the presence of ADP·BeF_x (wildtype shown as lk 9 in black).

These findings display a clear dependency of the unwinding activity in the presence of both nucleotides ATP and its non-hydrolysable pre-hydrolysis state analogue ADP·BeF_x [65-67] on the length of the linker in the catalytic core.

5.2.7. Propensity to undergo a conformational change of the YxiN linker mutants throughout the nucleotide cycle

Having determined binding constants and enzymatic properties of the mutants in the linker in the catalytic core of YxiN it was interesting to investigate, whether the effects seen in the binding properties or the enzymatic function are also reflected in the conformational state of the respective mutants. To investigate this impact single molecule fluorescence energy transfer (smFRET) experiments were performed as described in section 4.13.4. YxiN wildtype undergoes a conformational change towards a closed cleft in the catalytic core in the presence of both substrates, ADPNP and 153mer RNA[46]. In the presence of ATP and 153mer RNA the YxiN linker mutant YxiN lk 9 exhibits two major FRET distributions at a FRET efficiency of 0.3, corresponding to an open conformation[46] and at a FRET efficiency of 0.7, corresponding to a closed conformation[46]. The observation of two distinct FRET efficiency distributions reflects the fact, that this mutant is enzymatically fully active, and thus both states of the catalytic cycle can be observed. The same two distinct FRET efficiency distributions can also be observed for the enzymatic active YxiN linker mutants YxiN lk 7, YxiN lk 11 and YxiN lk 13. In the presence of the non-hydrolysable ATP-analogues ADPNP or ADP·BeF_x[65-67] and 153mer RNA all these mutants show a FRET efficiency of 0.7 corresponding to a closed conformation. The reason for this single distribution to be seen is that ADPNP and ADP·BeF_x cannot be hydrolysed and the catalytic cycle cannot be finished, thus no reopening of the cleft in the catalytic core can be observed.

Figure 44: Conformational states of the YxiN linker mutant lk 7

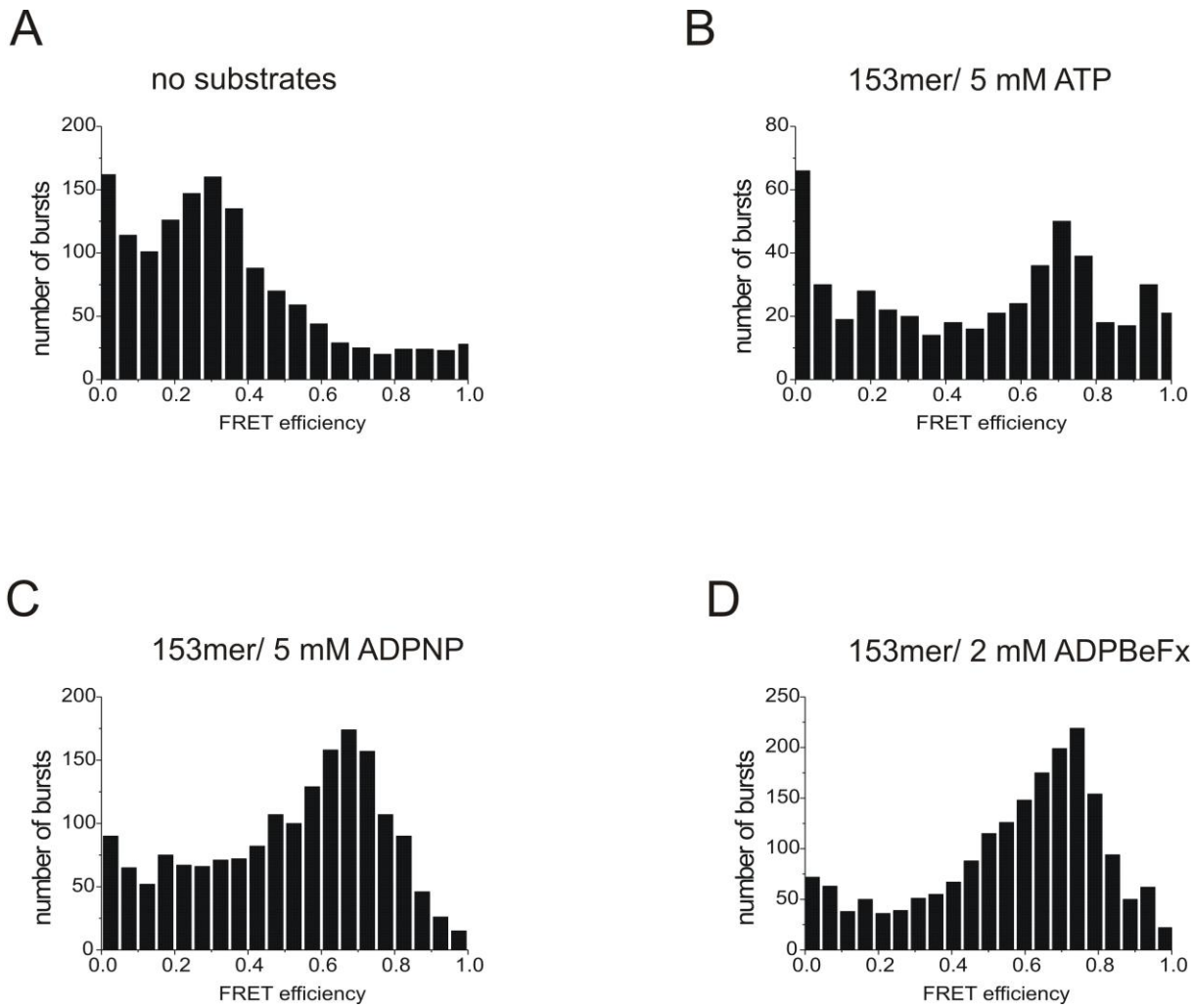

Figure 44: Conformational states of the YxiN linker mutant lk 7

Figure 44 shows the conformational states of the YxiN linker mutant lk 7 with the 153mer RNA substrate and different nucleotides as well as with no substrate. Single molecule FRET experiments were carried out as described in section 4.13.4. Panel A shows the conformational state of lk 7 in the absence of any substrate, which is an open conformation. Panel B shows the conformational state of lk 7 in the presence of ATP and 153mer RNA. There is a pronounced population at a FRET efficiency corresponding to a closed conformation, but also a very small population at a FRET efficiency corresponding to an open conformation. Panel C shows the conformational state of lk 7 in the presence of ADPNP and panel D shows the conformational state of lk 7 in the presence of ADP·BeF_x. In these cases, the FRET efficiency measured corresponds to a closed conformation.

Figure 45: Conformational states of the YxiN linker mutant lk 9

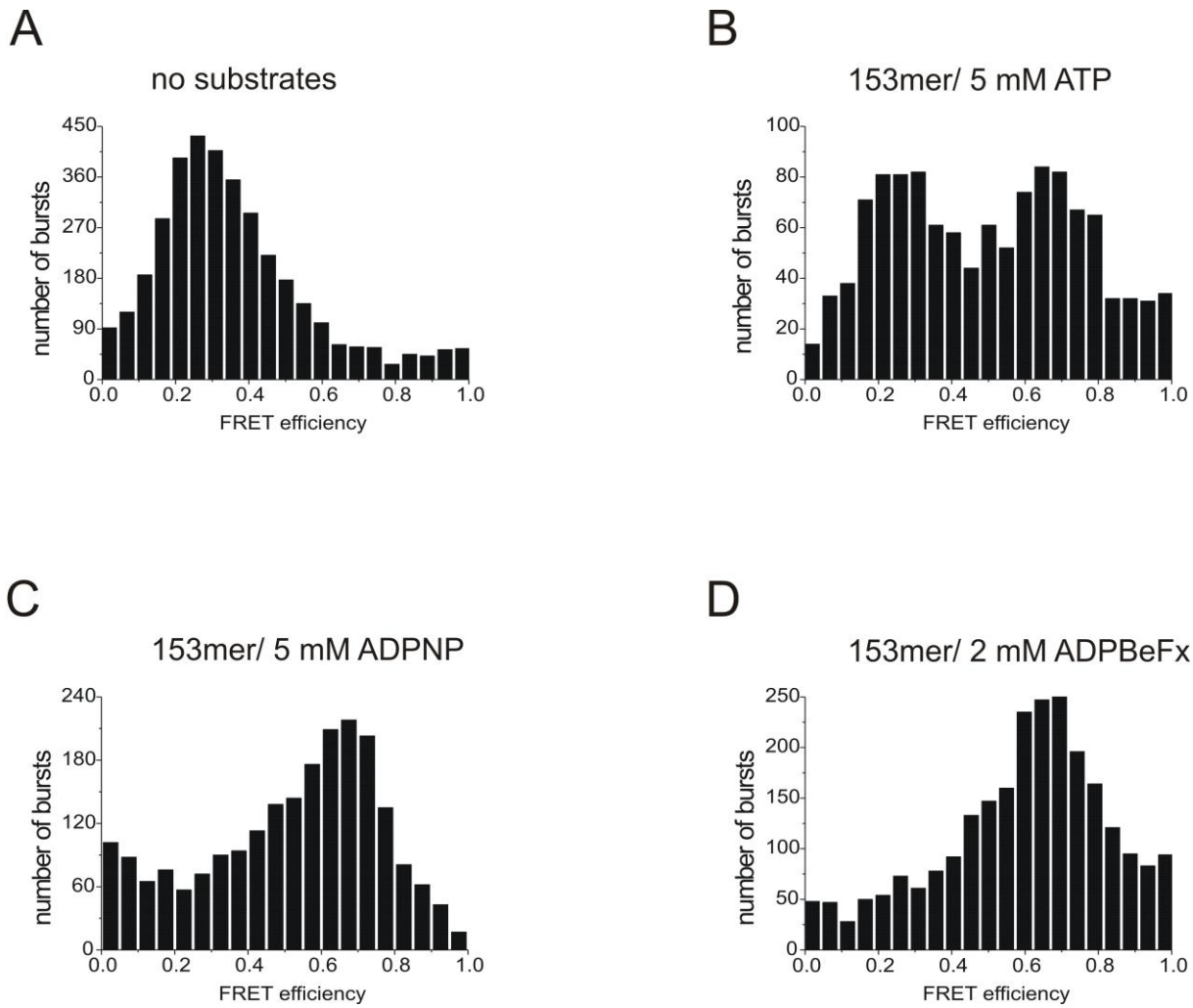

Figure 45: Conformational states of the YxiN linker mutant lk 9

Figure 45 shows the conformational states of the YxiN linker mutant lk 9 with the 153mer RNA substrate and different nucleotides as well as with no substrate. Single molecule FRET experiments were carried out as described in section 4.13.4. Panel A shows the conformational state of lk 9 in the absence of any substrate, which is an open conformation. Panel B shows the conformational state of lk 9 in the presence of ATP and 153mer RNA. There is a pronounced population at a FRET efficiency corresponding to a closed conformation, but also a pronounced population at a FRET efficiency corresponding to an open conformation. Panel C shows the conformational state of lk 9 in the presence of ADPNP and panel D shows the conformational state of lk 9 in the presence of ADP·BeF_x. In these cases, the FRET efficiency measured corresponds to a closed conformation.

Figure 46: Conformational states of the YxiN linker mutant lk 11

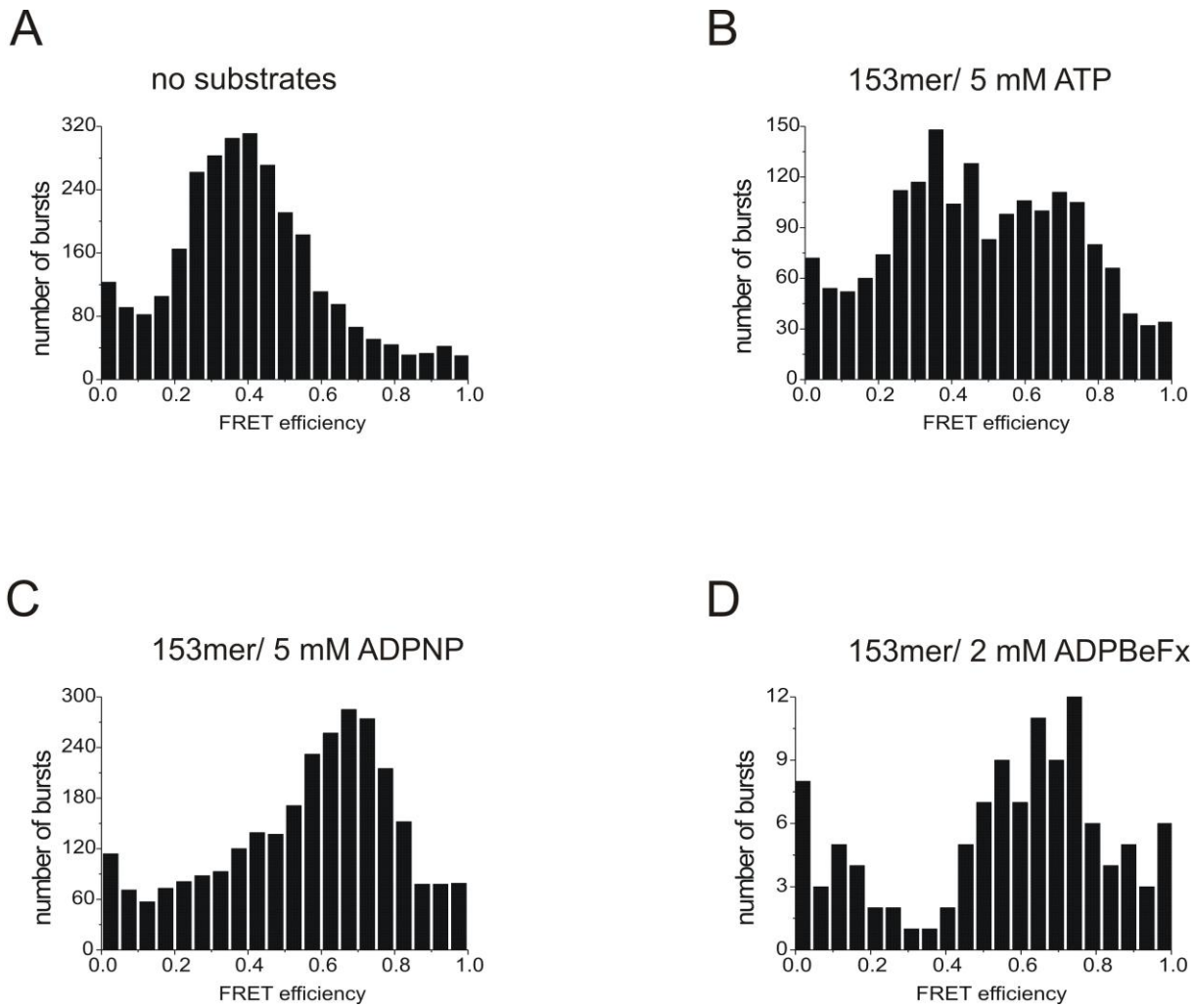

Figure 46: Conformational states of the YxiN linker mutant lk 11

Figure 46 shows the conformational states of the YxiN linker mutant lk 11 with the 153mer RNA substrate and different nucleotides as well as with no substrate. Single molecule FRET experiments were carried out as described in section 4.13.4. Panel A shows the conformational state of lk 11 in the absence of any substrate, which is an open conformation. Panel B shows the conformational state of lk 11 in the presence of ATP and 153mer RNA. There is a population at a FRET efficiency corresponding to a closed conformation, but also at a FRET efficiency corresponding to an open conformation. Panel C shows the conformational state of lk 11 in the presence of 153mer RNA and ADPNP. The measured FRET efficiency corresponds to a closed conformation. Panel D shows the conformational state in the presence of ADP·BeF_x. In this case, the FRET efficiency measured corresponds to a closed conformation.

Figure 47: Conformational states of the YxiN linker mutant lk 13

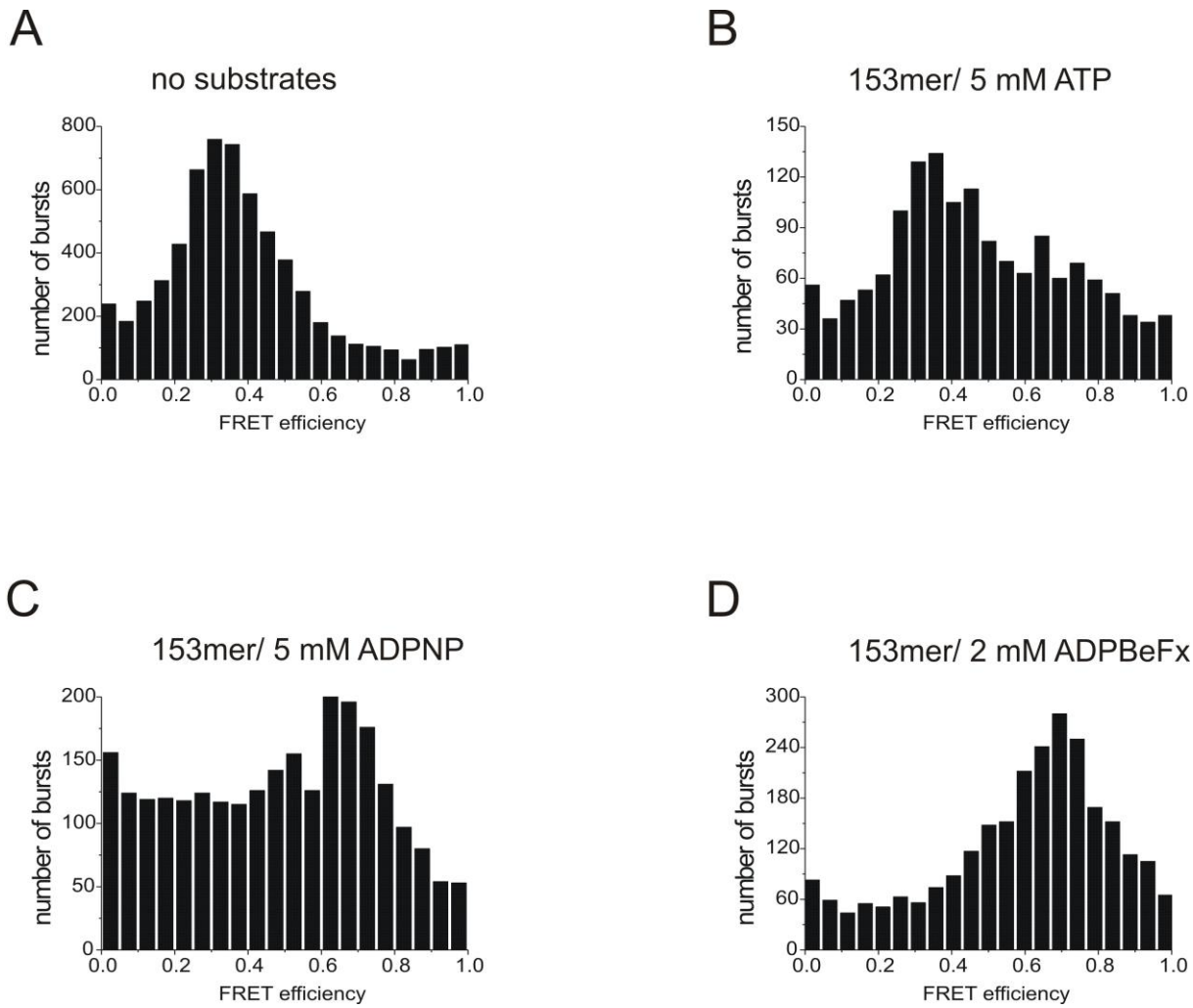

Figure 47: Conformational states of the YxiN linker mutant lk 13

Figure 47 shows the conformational states of the YxiN linker mutant lk 13 with the 153mer RNA substrate and different nucleotides as well as with no substrate. Single molecule FRET experiments were carried out as described in section 4.13.4. Panel A shows the conformational state of lk 13 in the absence of any substrate, which is an open conformation. Panel B shows the conformational state of lk 13 in the presence of ATP and 153mer RNA. There is a pronounced population at a FRET efficiency corresponding to an open conformation. Panel C shows the conformational state of lk 13 in the presence of 153mer RNA and ADPNP. The measured FRET efficiency corresponds to a closed conformation. Panel D shows the conformational state in the presence of ADP·BeF_x. In this case, the FRET efficiency measured corresponds to a closed conformation.

In contrast to the enzymatically active mutants YxiN lk 7 to YxiN lk 13, the enzymatically inactive mutants YxiN lk 4, YxiN lk 3 and YxiN lk 15 show a single peak at a FRET efficiency of 0.35 (YxiN lk 3 and YxiN lk 4) and 0.45 (YxiN lk 15) respectively that correspond to an open conformation in the presence of ATP and 153mer RNA. Although these mutants retain the capability of binding ATP and RNA as shown in Figures 27/28 and 30 they cannot adopt a closed conformation. Also in the presence of the non-hydrolysable ATP-analogue ADPNP and 153mer RNA all of these mutants cannot adopt a closed conformation as reflected by the FRET efficiencies of 0.35 (YxiN lk 3), 0.25 (YxiN lk 4) and 0.45 (YxiN lk 15). In the presence of the non-hydrolysable ATP-analogue ADP·BeF_x[65-67] they do not show they same conformation. The enzymatically active mutants, YxiN lk 4 and YxiN lk 15 adopt a closed conformation as reflected by the corresponding FRET efficiencies of 0.7 (YxiN lk 4) and 0.6 (YxiN lk 4). ADP·BeF_x, representing an activated state of the enzyme thus differs from ATP in that respect. Binding of ATP and RNA is not sufficient to close the cleft in the catalytic core in these mutants, but the ATP-analogue representing the activated state is sufficient to do so. The YxiN linker mutant YxiN lk 3 is the only construct showing an open conformation reflected by a peak at 0.3 FRET efficiency.

Figure 48: Conformational states of the YxiN linker mutant lk 3

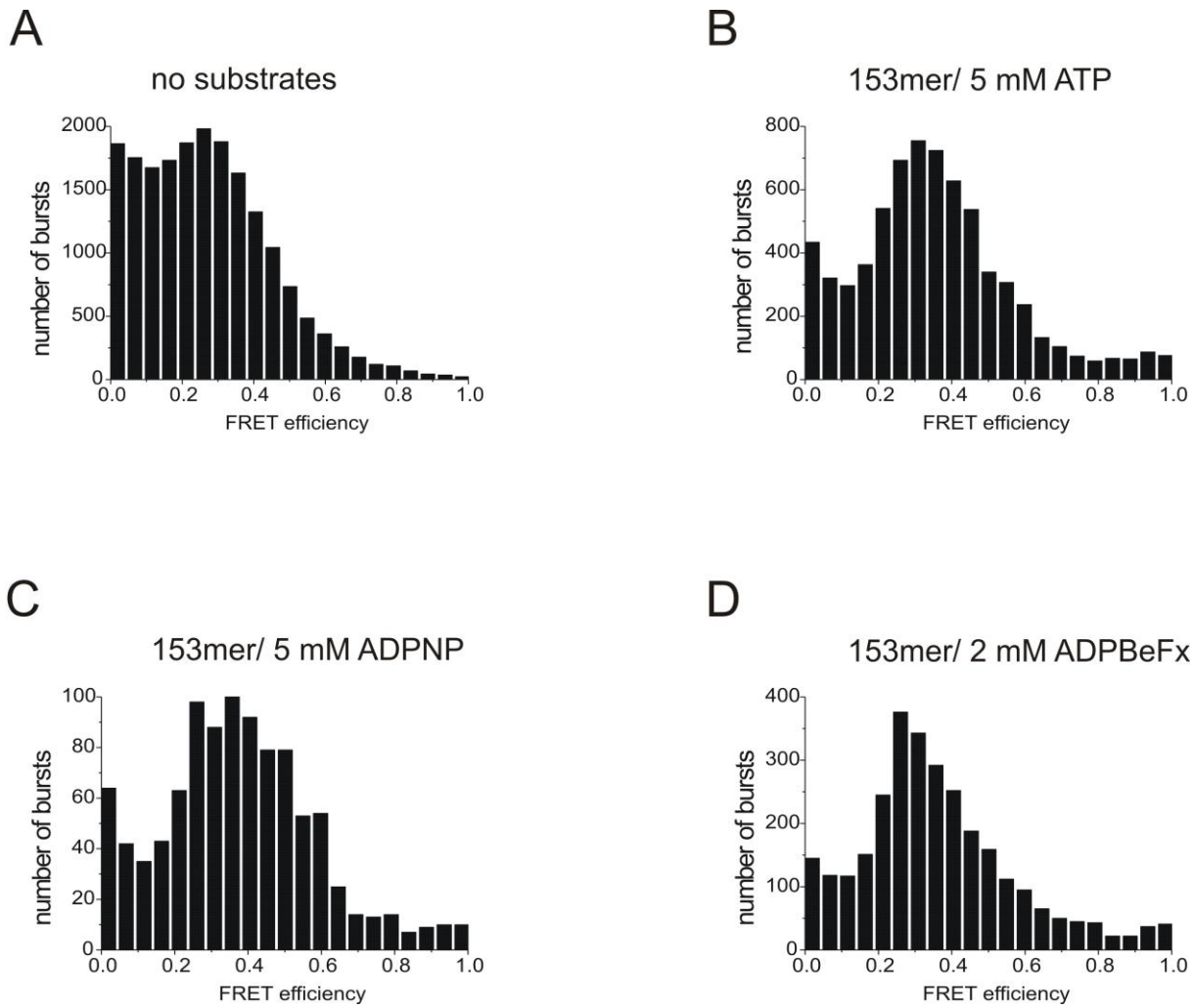

Figure 48: Conformational states of the YxiN linker mutant lk 3

Figure 48 shows the conformational states of the YxiN linker mutant lk 3 with the 153mer RNA substrate and different nucleotides as well as with no substrate. Single molecule FRET experiments were carried out as described in section 4.13.4. Panel A shows the conformational state of lk 3 in the absence of any substrate, Panel B shows the conformational state of lk 3 in the presence of 153mer RNA and ATP, Panel C in the presence of 153mer and ADPNP and Panel D in the presence of ADP·BeF_x. They all display FRET efficiencies corresponding to an open conformation.

Figure 49: Conformational states of the YxiN linker mutant lk 4

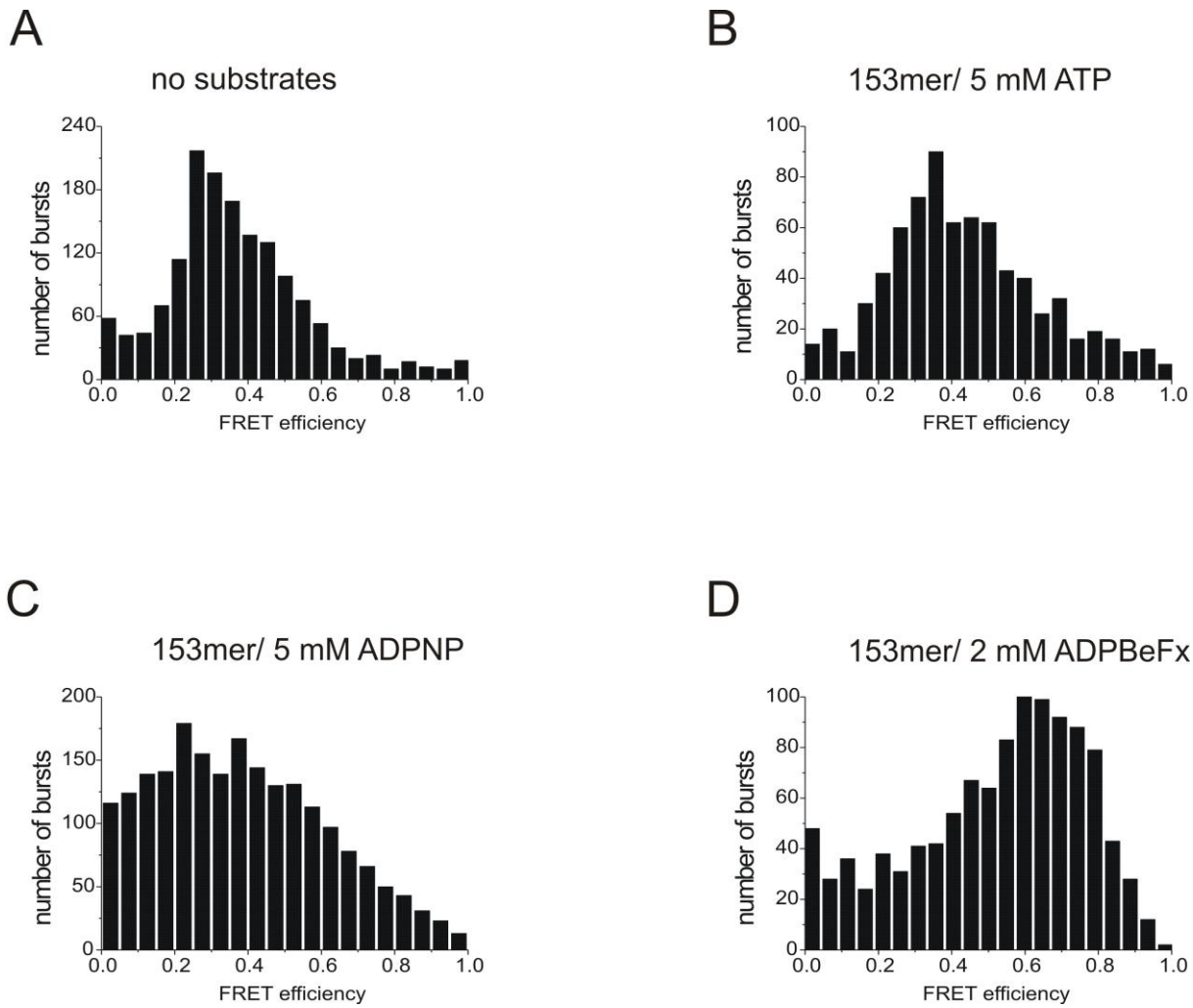

Figure 49: Conformational states of the YxiN linker mutant lk 4

Figure 49 shows the conformational states of the YxiN linker mutant lk 4 with the 153mer RNA substrate and different nucleotides as well as with no substrate. Single molecule FRET experiments were carried out as described in section 4.13.4. Panel A shows the conformational state of lk 4 in the absence of any substrate, which is an open conformation. Panel B shows the conformational state of lk 4 in the presence of 153mer RNA and ATP, Panel C in the presence of 153mer and ADPNP. They both display FRET efficiencies corresponding to an open conformation. Panel D shows the conformational state in the presence of ADP·BeF_x. In this case, the FRET efficiency measured corresponds to a closed conformation.

Figure 50: Conformational states of the YxiN linker mutant lk 15

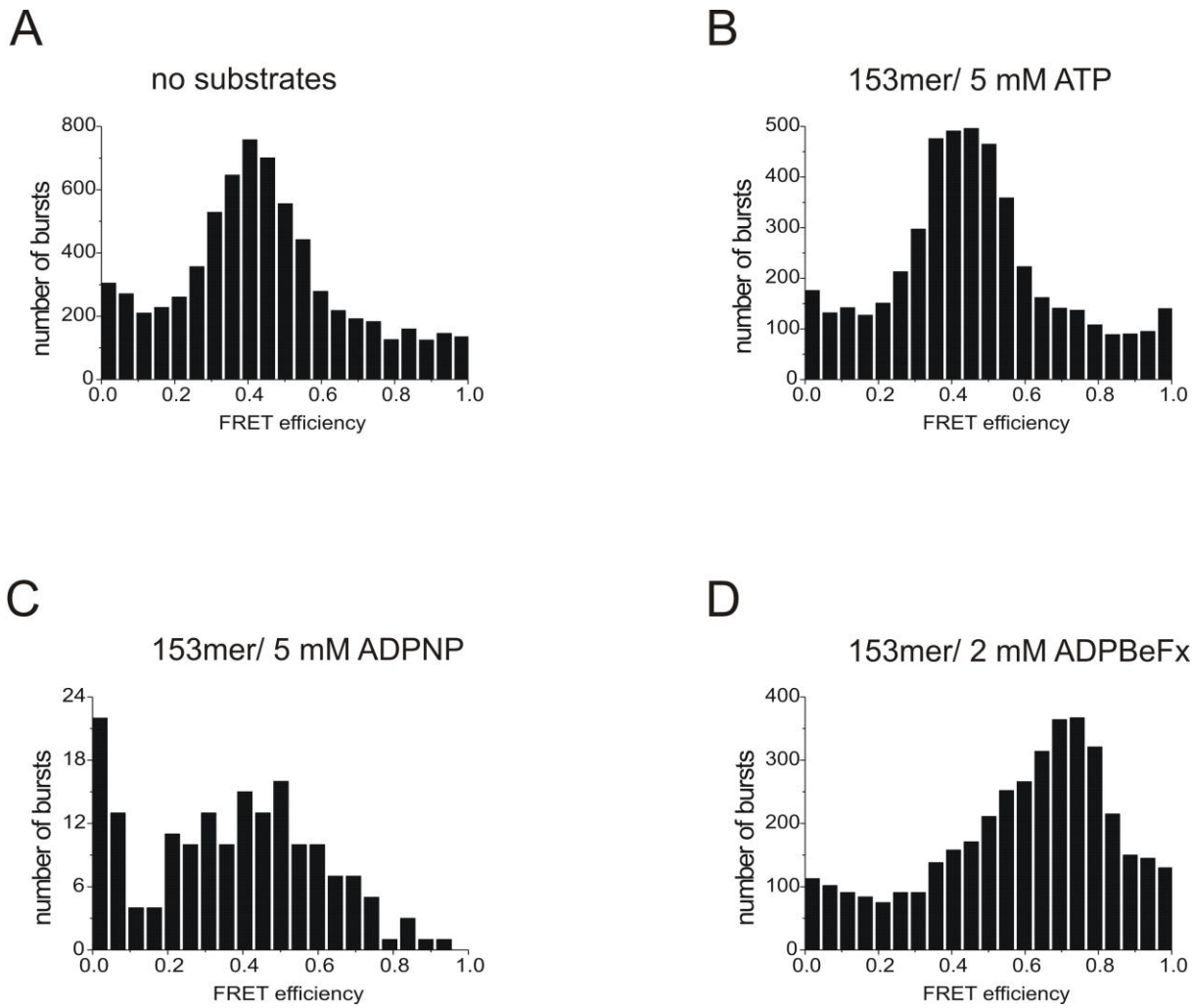

Figure 50: Conformational states of the YxiN linker mutant lk 15

Figure 50 shows the conformational states of the YxiN linker mutant lk 15 with the 153mer RNA substrate and different nucleotides as well as with no substrate. Single molecule FRET experiments were carried out as described in section 4.13.4. Panel A shows the conformational state of lk 15 in the absence of any substrate. Panel B shows the conformational state of lk 15 in the presence of ATP and 153mer RNA and Panel C shows the conformational state of lk 15 in the presence of 153mer RNA and ADPNP. They all display FRET efficiencies corresponding to an open conformation. Panel D shows the conformational state in the presence of ADP·BeF_x. In this case, the FRET efficiency measured corresponds to a closed conformation.

In the presence of ATP and 153mer RNA there is a clear difference between enzymatically active mutants and enzymatically inactive mutants in the conformational states. The active mutants adopt a closed conformation in the presence of both nucleotides and an additional open conformation in the presence of ATP, since they can finish their enzymatic cycle. In the presence of ADPNP or ADP·BeF_x there is no such discrimination between enzymatically active and inactive mutants. All mutants (YxiN lk 4 to YxiN lk 15) adopt a closed conformation with ADP·BeF_x and 153mer RNA. The YxiN linker mutant YxiN lk 3 is the only construct showing an open conformation. ADP·BeF_x thus can trap all but the shortest linker mutant in a closed conformation. YxiN lk 4, which is the shortest linker mutant still adopting a closed conformation shows a lower FRET efficiency than the other linker mutants and YxiN wildtype, indicating that the cleft in the catalytic core is partly open in the YxiN lk 4. This could originate from a restricted movement between the two RecA domains of the catalytic core, and might also explain why YxiN lk 3 does not show any closure at all. To make sure, that the closure of the catalytic cleft is not an ADP·BeF_x-dependent artefact, smFRET measurements of all the YxiN mutants in the presence of ADP·BeF_x but in the absence of 153mer RNA were performed. All mutants show a single peak at FRET efficiencies corresponding to their respective open conformation. Therefore it is the combined binding of ADP·BeF_x and 153mer RNA that induces the closure of the cleft in the catalytic core.

Figure 51: Conformational state of the YxiN linker mutants with ADP·BeF$_x$ but no RNA substrate

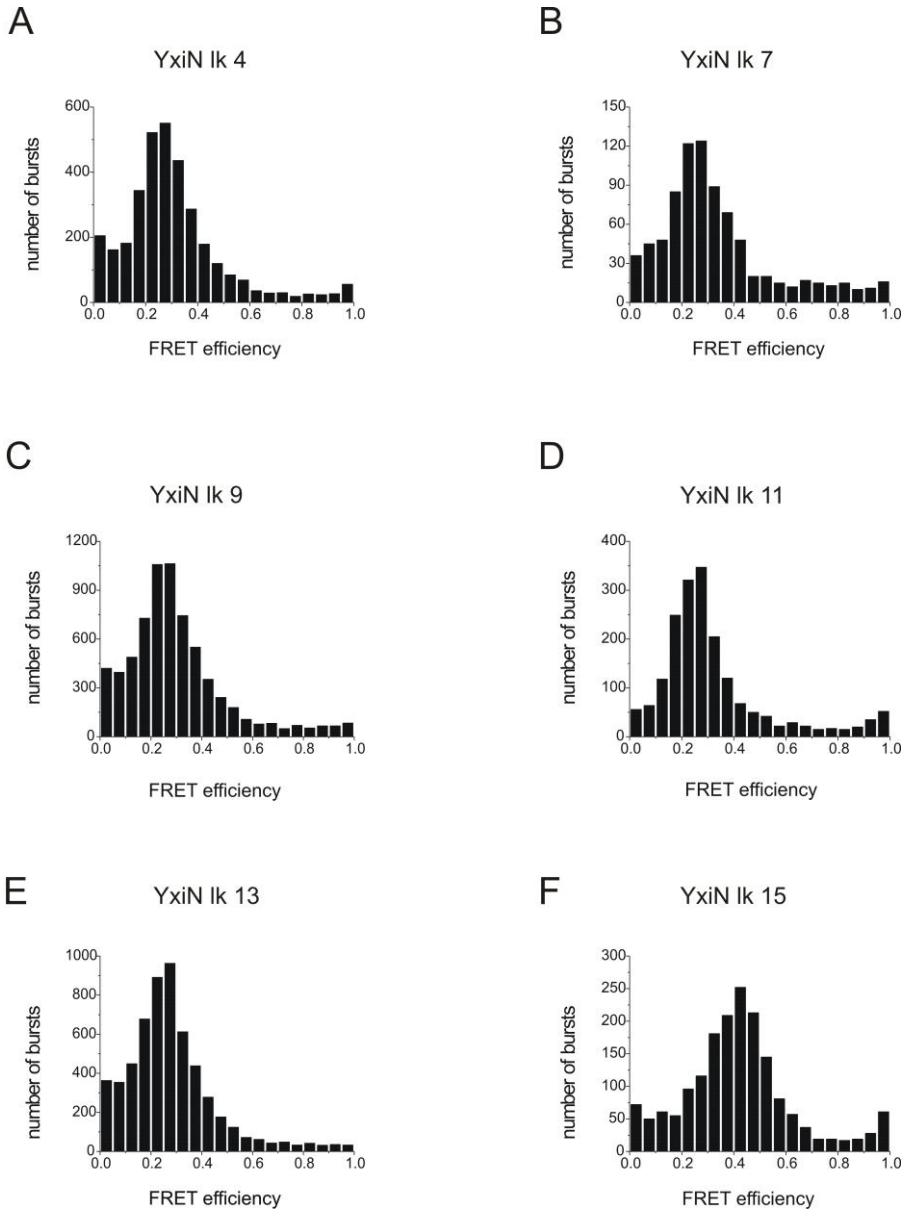

Figure 51: Conformational state of the YxiN linker mutants with ADP·BeFx but no RNA substrate

Figure 51 shows control measurements of those YxiN linker mutants, which display a closure of the cleft in the presence of 153mer RNA and ADP·BeF$_x$. All YxiN linker mutants show a distinct FRET population at FRET efficiencies corresponding to an open conformation.

6. Discussion and Outlook

YxiN from *B.subtilis* belongs to the group of DEAD-box proteins and consists of the typical building blocks of this class of enzymes with the catalytic core and an additional C-terminal domain. The catalytic RecA domains of the core of different DEAD-box proteins can be superimposed very well on one RecA subunit but not on the other in the absence of any substrate[16, 50-54, 68]. Upon binding of RNA and nucleotides a conformational change occurs that leads to a very good superimposition of both RecA subunits[38, 55, 68-69]. This structural evidence in addition to the finding that a covalent linkage between the two RecA subunits of the catalytic core is essential for helicase activity[49] gave rise to the hypothesis for the need for interdomain communication. In the work presented here a thorough investigation of the role of the linker between the two RecA subunits in inter-domain communication was performed. RNA and nucleotide binding affinities, ATP hydrolysis and double stranded RNA unwinding rates were determined and conformational states examined.

6.1 Nucleotide affinities in the absence and presence of RNA

In this part of the work a systematic investigation of the dissociation constants of YxiN wildtype and YxiN linker mutants for nucleotides representing intermediates of the nucleotide cycle and RNA were determined. In the absence of RNA, YxiN wildtype shows higher affinity for the pre-hydrolysis[65-67] ATP analogue ADP·BeF_x, the post-hydrolysis[65-67] ATP analogue ADP·MgF_x, and ADP than for ATP.

In the motif VI mutant R330A there is a switch in nucleotide preference, namely the affinity for ATP is higher than for the wildtype and the affinity for ADP·BeF_x is lower than for the wildtype. The affinity for ADP is in the same range for both enzymes. The same mutant also appears to have increased cooperative binding of RNA and the pre-hydrolysis ATP-analogue

ADP·BeF_x[65-67]. This is reflected by the fact that the affinity of YxiN wildtype for the 32mer minimal RNA substrate in the absence of any nucleotide changes 1.3-fold in the presence of ADP·BeF_x. For the motif VI mutant R330A this is different with the change in affinity for the 32mer minimal RNA substrate being roughly 11-fold in the presence of ADP·BeF_x. The change in affinity in the presence of the non-hydrolysable ATP-analogue ADPNP compared to the nucleotide-free state is 1.4-fold and thus comparable to the 1.8-fold change observed for YxiN wildtype. This mutant thus seems to be deficient in discriminating between the not activated state of the nucleotide cycle, represented by ADPNP and the activated state of the nucleotide cycle, represented by ADP·BeF_x and has a clear impact on RNA binding and nucleotide selectivity.

Mutations in the linker connecting the two RecA domains of the catalytic core resulted in higher affinities for ATP compared to YxiN wildtype. For ADP·BeF_x the same mutants show lower affinities compared to YxiN wildtype. These lower affinities reflect the fact that the preference for the activated nucleotide state, represented by ADP·BeF_x observed for the wildtype enzyme is lost in the YxiN linker mutants. All linker mutations but the shortest show no gain or loss in affinity for ADP. Therefore it appears that at the final step, at the end of the nucleotide cycle the flexibility of the core subunits does not seem to have an impact on nucleotide binding. It is worth noting that already the construct with the conserved linker length (YxiN lk 9) has a clear effect on nucleotide affinities if nucleotide affinities are normalised to the ADP affinity (ATP/ADP and ADP·BeF_x/ADP). The ratio of ATP/ADP is 5.5 for YxiN wildtype and 1.1 for YxiN lk 9, thus there is a 5-fold reduction in this ratio. A 2-fold reduction from a ratio of 2 in YxiN wildtype for ADP·BeF_x/ADP is found to a ration of 1 for YxiN lk 9. This is especially surprising taking into account that this construct is a conservative amino acid exchange from threonine to serine in the only conserved amino acid (T211A) in the linker sequence. To investigate the impact of exchanging this amino acid, a mutation from threonine to alanine was introduced. Preliminary results on nucleotide binding of this mutant indicate, that the effect on the ratio of ADP·BeF_x/ADP is lost, the ratio being wildtype-like as reflected by the ratios of 1.9 for YxiN wildtype and 1.5 for YxiN T211A. On the other hand these preliminary results suggest that effect on the ratio of ATP/ADP is still present as reflected by the ratios of 5.5 for YxiN wildtype and 1.2 for YxiN T211A. Therefore this conserved threonine could play a role in recognition and discrimination of the

nucleotide before an activation step. A more thorough investigation of the conserved threonine is therefore required.

In the presence of an RNA substrate, the affinity for ATP is higher compared to the affinity without any RNA substrate for YxiN wildtype. Furthermore, the affinity for ADP·BeF_x is virtually identical to the affinity for ATP and also similar to the affinity determined without an RNA substrate. There is a coupling of RNA and ATP binding that is not observed for RNA and ADP·BeF_x binding. Regarding the YxiN linker mutants, affinities for ATP in the presence of RNA are increased for mutants with a shorter length and decreased for mutants with a longer length compared to YxiN wildtype. There is no more loss in affinities for ADP·BeF_x in the YxiN linker mutants as seen in the absence of RNA but the affinities for ADP in the presence of RNA are decreased in all the YxiN linker mutants compared to YxiN wildtype. The desensitisation for ADP·BeF_x observed for the YxiN linker mutants in the absence of RNA is not observable anymore in the presence of RNA, they seem to lose sensitivity for the differences between ATP and ADP·BeF_x when bound to RNA. Mutations in the motif VI or in the linker of the catalytic core have an impact on nucleotide affinities, both in the absence and the presence of an RNA substrate. In addition there also is an impact on the cooperative binding of nucleotide and RNA.

6.2 RNA affinities in the absence and presence of different nucleotides

YxiN wildtype binds a 32mer minimal RNA substrate with nanomolar affinities. A minor increase in RNA affinity can be observed in the presence of ADPNP, ADP·BeF_x and ADP. In contrast, the affinity for the 32mer RNA in the presence of ADP·MgF_x shows a minimal decrease. In the context of the enzymatic activity cycle these higher affinities in the ADPNP and ADP·BeF_x states indicate a cooperativity in binding of nucleotide and RNA, which is reasonable, as stronger binding upon presence of both substrates provides a higher

population probability of functional complexes. The higher affinities found for the ADPNP and ADP·BeF_x state for RNA compared to the nucleotide-free state and the the ADP·MgF_x state found to have a lower RNA affinity are in good agreement with the finding that phosphate release results in a reset of an enzyme with a low RNA affinity state in the presence of ADP[39]. Furthermore it is described that DEAD-box proteins exhibit a low RNA affinity in the nucleotide-free and the ADP bound state[69-71]. The fact that the ADP-bound state shows a minimally higher affinity for RNA than the nucleotide-free state is not in agreement with this. RNA affinities in the ATP bound state were determined for some DEAD-box proteins and vary from low binding affinities for Dbp5 and eIF4A in the low µM range[69,72] and high binding affinities for DbpA in the high pM range[42, 73]. The RNA affinity determined for YxiN is comparable to the lower RNA affinities. In the presence of ADPNP, ADP·BeF_x or ADP·AlF_4, a high affinity RNA binding state is promoted in several DEAD-box proteins[39, 46, 69, 72, 74]. These high affinity states for ADPNP and ADP·BeF_x are observed for YxiN wildtype as well. RNA affinities in the ADP·MgF_x bound state are drastically lower than in the other nucleotide bound states. A decrease in affinity after hydrolysis of ATP could indicate that this might correlate with strand release. In the process of unwinding throughout the nucleotide cycle, the first strand gets released after ATP hydrolysis and the second strand with the release of ADP and P_i. The hypothesis that RNA affinities reflect the order of strand release might be tested by determining the affinities of a complementary 32 bp long strand, since most probably, the sequence in combination with the length is the determining factor, of which strand gets released upon ATP hydrolysis.

The motif I mutant K52Q is known to be ATPase deficient but able to close the cleft in the catalytic core[56]. This motif I mutant shows an approximately 2-fold decreased affinity for RNA in the absence of any nucleotide. The affinities in the presence of ATP, ADPNP, ADP·BeF_x and ADP are increased compared to the nucleotide-free state and in the case of ADP·BeF_x and ADP also compared to YxiN wildtype. The deficiency in ATP hydrolysis has no impact on the cooperativity of 32mer RNA and nucleotide binding as reflected by this increase in 32mer RNA affinity in the presence of nucleotides for both enzymes YxiN wildtype and YxiN K52Q.

The motif VI mutant is also found to be ATPase deficient and exhibits a clearly lower affinity for a 32mer RNA substrate in the absence of nucleotides compared to YxiN wildtype. However, the affinity increases in the presence of ADP·BeF_x and is higher than that observed for the YxiN wildtype. On the other hand affinities for the same RNA substrate are lower in the presence of ADPNP and ADP and also lower than the affinity determined for YxiN wildtype (ADPNP) or comparable to YxiN wildtype (ADP). The motif VI mutant R330A thus has an impact on RNA binding and also on nucleotide selectivity.

RNA affinities were also determined for the mutants of the linker in the catalytic core YxiN lk 3, YxiN lk 9 and YxiN lk 15. In the absence of nucleotide an approximate 1.5-fold minor increase in affinity for the 32mer RNA substrate was observed for all tested YxiN linker mutants compared to YxiN wildtype. In the presence of ADPNP there is a clear 2.5-fold decrease in affinity for the YxiN lk 3 and the YxiN lk 15 mutant. In contrast the YxiN lk 9 mutant rather shows a 2.5-fold increase in RNA affinity in the presence of ADPNP. For both the shortest and the longest linker construct amplitudes of the fluorescence anisotropy increase upon protein binding is rather small rendering an overestimation of the dissociation constant possible. The smaller amplitude of the fluorescence anisotropy increase in the shortest and the longest linker construct might originate from a loss of the RNA affinity conferred by the catalytic core. This would render the fluorescent dye attached to the RNA more flexible in these constructs, assuming that the dye is attached to the RNA end involved in core binding. This assumption is reasonable as the dye is attached on the RNA end lacking the hairpin recognised by the RBD. In presence of ADP·BeF_x there is a dramatic 8.5-fold increase in RNA affinity in the YxiN lk 15 mutant. Only minor changes compared to the drastic affinity increase for YxiN lk 15 are observed for the YxiN lk 3 mutant (2.7-fold decrease) and for the YxiN lk 9 (1.5-fold increase). At the end of the catalytic cycle, in the presence of ADP, the most striking finding is that YxiN lk 9 shows a drastic 4-fold decrease in RNA affinity compared to YxiN wildtype, while the other mutants YxiN lk 3 and YxiN lk 15 show only minor changes with a 1.5-fold and a 2-fold increased 32mer RNA affinity. Possibly, the serine to theronine mutation in the linker leads to restrictions in the RNA binding ability at the final step of the nucleotide cycle that can be circumvented by having a more flexible or a more restricted linker connecting the RecA domains in the core. In the beginning of the nucleotide cycle, on the other hand, too much or too little flexibility leads to small

fluorescent anisotropy amplitudes upon protein binding and also to 32mer RNA affinities different to YxiN wildtype. Changes in the linker thus affect binding of a rather short RNA substrate to YxiN, although the major contribution of RNA binding is provided by the RNA binding domain[41].

Binding of 32mer RNA to the catalytic core of YxiN could not be determined. RNA affinities of 32mer RNA to the YxiN RBD fused to a GST lie between 1.5 µM and 5.9 µM depending on the presence of nucleotides. There is clearly no influence of nucleotides on RNA binding to the YxiN RBD as expected since there are no nucleotide binding sites located in that domain. The RNA affinities of 376 nM for YxiN wildtype and 1.5 to 5.9 µM for the YxiN RBD determined in this study using fluorescence anisotropy are significantly lower than RNA affinities of 4.6 nM for YxiN wildtype and 5.2 nM for YxiN RBD[41] determined by gel shift assays with a 5'-P^{32} labelled 30mer minimal RNA substrate. Since the substrates are identical in sequence and highly similar in size the difference in binding affinities cannot be attributed to differences in the substrate, but might rather be due to the different methods used. Since the substrate used in this study contains a fluorescein label at the 5'-end of the RNA strand it is conceivable that the fluorophor interacts with the protein. This can be further supported by the observation that a 32mer/9mer RNA substrate with a 5'-Cy5 label on the 32mer and 3'-Cy3 label on the 9mer, results in RNA binding affinities comparable to the ones found for the fluorescein labelled substrate. All in all the mutations introduced have an impact on RNA binding throughout the nucleotide cycle.

6.3 ATP hydrolysis

In the absence of RNA substrates, YxiN wildtype exhibits an extremely low ATPase activity with a k_{cat} of 0.03 min^{-1}[33] which is increased almost 2000-fold to a higher k_{cat} value of 55 min^{-1} (0.91 s^{-1}) in the presence of a 30mer[41] and to k_{cat} values between 2.4 s^{-1}[56] and 4.1 s^{-1} [49] in the presence of an 153mer RNA substrate. YxiN thus is an RNA stimulated ATPase. The

results obtained in this study are in very good agreement with these earlier findings showing a hydrolysis rate of 5.2 s^{-1} for 153mer stimulated ATP hydrolysis. Its homolog DbpA in *E.coli* hydrolyses ATP at a rate virtually identical to YxiN (5 s^{-1} / 4.8 s^{-1})[45, 71]. Slower ATP hydrolysis is found for Hera from *T. thermophilus* with a k_{cat} of 1.8 - 2.6 s^{-1} depending on the RNA substrate chosen for stimulation[75] and for the *E.coli* enzyme SrmB with an ATP hydrolysis rate of 0.005 min^{-1}[34]. Higher ATP hydrolysis rates are observed for the *S.cervesiae* enzyme Ded1 with k_{cat} values of 2 - 10 s^{-1}[76-77]. In comparison to other DEAD-box proteins YxiN therefore exhibits a rather high ATP hydrolysis rate.

The R330A mutation in the motif VI leads to a loss in ATPase activity. This can be explained by the fact that this mutation leads to a drastically reduced binding of RNA in the absence of any nucleotide and in the presence of ADPNP. There is no loss in ATP binding but rather an increase in ATP affinity. Therefore a loss of RNA binding could possibly lead to a loss in stimulation and therefore to a loss in ATPase activities. The intrinsic ATPase activity of 0.03 min^{-1}[33] might be too low to be observed in the conditions of the spectroscopic assay performed.

The same loss in ATPase activity can be observed for the YxiN catalytic core linker mutations. YxiN lk 3, YxiN lk 4 and YxiN lk 15 are completely ATPase deficient, YxiN lk 5 and YxiN lk 13 are clearly slower in ATP hydrolysis, YxiN lk 9 and YxiN lk 11 show ATP hydrolysis rates comparable to YxiN wildtype. The gradual loss of ATPase activity in both the longer and the shorter linker constructs could be attributed to a tighter binding of ATP to the YxiN linker mutants that might hinder stepping through the hydrolysis process. Loss of cooperativity between binding of ATP and RNA could also play a role since the binding of RNA in the presence of ADPNP is impaired. The linker thus seems to play a regulatory role regarding the ATP hydrolysis activity of YxiN. This is in good agreement with the finding that stepwise conversion of the eIF4A linker to the corresponding Vasa sequence resulted in enhanced ATPase activity, which revealed the linker to be a regulatory element[78]. Regarding ATPase activity gradually changing the linker length to shorter and longer sequences leads to a gradual loss in ATPase activity as well. Again, the linker size does have an impact on regulation of an enzymatic activity.

6.3 double stranded RNA unwinding activity

YxiN wildtype supports unwinding of a double stranded RNA substrate consisting of a Cy3-labeled 9mer hybridised to a Cy5-labeled 32mer in the presence of either, ATP and ADP·BeF_x. Efficient unwinding activity of stable duplexes in the presence of ADP·BeF_x but not in the presence of ADP·AlF_4 could also be observed for other the DEAD-box proteins Ded1, Mss116 from *S.cerevisiae* and eIF4A from *H.sapiens*[39]. This suggests that the energy of ATP hydrolysis is not required for strand separation, but for fast enzyme release and multiple substrate turnovers[65]. Furthermore eIF4A has similar unwinding rates with ATP and ATPγS supporting the hypothesis, that ATP hydrolysis is not the rate limiting step for RNA unwinding[79]. Interestingly, all these enzymes and also CYT-19 from *N.crassa* can achieve complete strand separation using a single ATP[36]. These findings imply that also ADPNP should promote double stranded RNA unwinding. Unwinding activity in presence of this nucleotide could nevertheless not been shown for any of these DEAD-box proteins and also not for YxiN. ADPNP unlike ADP·BeF_x thus does not mimic ATP in eliciting or stabilising a protein conformation that promotes strand separation, although no differences in structure are observed[36].

Previous findings show that ATP promotes faster double stranded RNA unwinding then ADP·BeF_x in Ded1, Mss116 and eIF4A[39]. This was also observed for YxiN wildtype performing a polyacrylamide gel unwinding assay with 5'-labelled 32mer. However, unwinding rates determined with the FRET based fluorescent assay in the presence of ADP·BeF_x are even faster than in presence of ATP. This discrepancy might be due to limitations in the method. There is a dead time of a few seconds between the addition of enzyme and nucleotide before the fluorescent measurement can be started. If the unwinding reaction takes place rather fast, the very first part of the slope is missed, negatively influencing the calculated unwinding rates, by overestimating the later time points in the reaction. Since the unwinding rates for the catalytic core linker mutants are higher for ATP and not for ADP·BeF_x this hypothesis seems rather plausible. In these mutants all unwinding rates are in general lower in the presence of ADP·BeF_x than in the presence of ATP with a trend towards loss of unwinding activity in the longer and the shorter linker

constructs. This is in very good agreement with the finding that also ATP hydrolysis is diminished in these mutants. Nevertheless loss in ATPase activity cannot directly account for the loss of unwinding activity as binding of ATP and not hydrolysis is necessary for unwinding reactions. The loss of ATP affinity observed for the longer YxiN linker constructs could explain the loss of unwinding activity for these mutants, but not for the shorter linker constructs that have a high affinity for ATP.

Again this work clearly shows that the linker in the catalytic core has a regulatory impact on the enzymatic function of YxiN, but it is still difficult to determine the actual mechanism by which this regulation is achieved.

6.4 Conformational state of the catalytic core

In the absence of 153mer RNA and nucleotide YxiN wildtype adopts an open conformation as reflected by a FRET efficiency of 0.4[46]. A closed conformation reflected by a FRET efficiency of 0.7[46] is induced upon addition of 153mer RNA and ADPNP, ADP·BeF_x or ADP·MgF_x as well as with ATP[46]. In the presence of only one substrate or in the presence of 153mer RNA and ADP, the closure of the cleft in the catalytic core cannot be observed. As reflected by the fact, that pre-hydrolysis as well as post-hydrolysis analogues of ATP induce a closed conformation in the catalytic core, ATP hydrolysis does not lead to a reset of the enzyme to an open conformation, but release of the phosphate has to occur prior to reopening of the cleft. In the presence of ADP and 153mer a minor peak corresponding to a closed conformation can be found in high concentrations of ADP indicating, that a small subfraction of the enzymes is in a closed conformation even at the end of the enzymatic cycle.

The motif VI mutant R330A shows an open conformation in the absence of any substrate and a closed conformation in the presence of ADP·BeF_x. The loss in ATPase activity and reduced RNA binding affinities thus is not reflected in the conformational state. This is in

good agreement with the earlier findings that the motif I mutant K52Q that is ATPase and unwinding deficient still assumes the closed conformation, indicating that closure of the cleft is necessary, but not sufficient to induce enzymatic activity[56].

The mutations of the linker in the catalytic core YxiN lk 5 to YxiN lk 13 show the same conformational changes as wildtype in the presence of the different substrates, although YxiN lk 5 is ATPase deficient and barely unwinds a double stranded RNA substrate. Again, closure of the cleft is not sufficient to induce enzymatic activity. In the longest YxiN linker mutant, YxiN lk 15 ADPNP or ATP and 153mer RNA substrate do not induce a closed conformation anymore. The same is seen for the YxiN linker construct YxiN lk 4. Both mutants adopt a closed conformation in the presence of ADP·BeF_x and 153mer though. Although ADP·BeF_x mimics ATP that it can support double stranded RNA unwinding, there seems to be a substantial difference in binding of the nucleotide to the enzyme as it can force YxiN mutants in a closed conformation, that are in an open conformation in the ATP- and RNA-bound state. Interestingly the shortest linker construct, YxiN lk 3 also does not adopt a closed conformation in the presence of ADP·BeF_x and 153mer. In this case the differences in the binding geometry seem to be overcome by the most constricted movement of the catalytic core domains.

All in all, single molecule FRET studies indicate, that the length of the linker in the catalytic core is essential for the enzyme to adopt the correct conformation in the presence of different substrates. If the movement of the two RecA domains relative to each other is too restricted, adopting a closed conformation is hindered. On the other hand, if there is too little limitation of the movement of the two RecA domains relative to each other, the correct conformation can not be adopted either. The need for a limitation in flexibility of the catalytic core is also evident from the finding, that addition of the N-terminal domain of the catalytic core to the C-terminal domain of the catalytic core plus RBD does not lead to a functional enzyme[49].

6.5 The role of the linker in other two-domain proteins

The DEAD-box protein eIF4A harbours the only linker in the catalytic core of a DEAD-box protein which has a function assigned. eIF4A is part of the eIF4F initiation complex and unwinds local secondary structures in mRNA allowing the 43S rRNA to bind during the initiation of translation. The linker in the catalytic core of human eIF4A III undergoes a conformational change with ADPNP and RNA bound that ensures the close proximity of the two RecA domains needed for enzymatic activity[78]. If now an inhibitor of eIF4A, PatA, is present there is an increase in ATPase and helicase activity[80-81]. This modulation in enzyme activity is conferred by binding of the inhibitor to the linker in the presence of RNA and ATP and therefore inducing a more closed conformation[78]. Similar to YxiN there is also an influence of the linker in the catalytic core, although it is not clear, how the linker controls enzymatic function in YxiN.

Moving from RNA chaperones to protein chaperones the linker between the ATPase domain and the substrate binding domain of DnaK is found to be necessary and sufficient to stimulate the activity of the ATPase domain. Here the linker is proposed to be a switch in the enzyme. If the linker binds to a binding site in the ATPase domain it stimulates ATPase activity of this domain. Normally the linker is prevented from binding to the ATPase domain but upon substrate binding the linker gets available for binding on the ATPase domain, therefore the linker plays a role in interdomain communication[82].

The need for a certain length of the linker between two domains as seen for YxiN is also found in the eukaryotic ion transporting ATPase sarcoplasmic reticulum Ca^{2+}-ATPase (SERCA1a) that catalyses Ca^{2+} transport coupled to ATP hydrolysis[83-84]. SERCA1a consists of three cytoplasmic domains, the nucleotide binding domain, the phosphorylation domain and the actuator domain and ten transmembrane helices. Here the linker length between the actuator domain and the first transmembrane helix is critical for the correct positioning and the interactions of the actuator domain and the phosphorylation domain to cause structural changes important for Ca^{2+} release[85]. A similar dependence on the linker length is also found between the actuator domain and the transmembrane helix 3[86].

A linker between two domains of a protein could also play a role in nucleic acid binding as seen in the PaxD protein from the anthozoan cnidarian *Acropora maillepora*. Here the linker region makes minor groove DNA contacts, but the contribution of the linker to DNA binding and specificity has not been extensively studied[87]. Although in the case of YxiN, specific RNA binding of the linker was not shown, there is a clear effect seen on RNA binding with mutations in the linker with decreased affinities in the presence of ADPNP.

The study at hand shows a clear impact of the linker in the catalytic core of the DEAD-box protein YxiN from *B.subtilis* on substrate binding properties (nucleotide and RNA affinities), on enzymatic functions (ATPase and double stranded RNA unwinding activity) and on the conformational state of the enzyme with a clear dependence on the length of the linker. Too much flexibility or too much restriction in the linker sequence leads to impairments in all properties investigated. Thus the linker plays an important regulatory role. Examination of all the enzymatic properties of the mutation of the only conserved amino acid residue T211A might shed some additional light onto the role of the linker in the catalytic core of YxiN. Studies on the structural integrity of constructs consisting of either the N-terminal or the C-terminal catalytic core domain and the linker could be applied to get insight on some structural function in regulation. In addition labelling-experiments of the linker in presence of both substrates could highlight a possible involvement in substrate binding.

7. References

1. Evans, D., S.M. Marquez, and N.R. Pace, *RNase P: interface of the RNA and protein worlds.* Trends Biochem Sci, 2006. **31**(6): p. 333-41.
2. Staley, J.P. and C. Guthrie, *Mechanical devices of the spliceosome: motors, clocks, springs, and things.* Cell, 1998. **92**(3): p. 315-26.
3. Puglisi, J.D., *mRNA processing: the 3'-end justifies the means.* Nat Struct Biol, 2000. **7**(4): p. 263-4.
4. Keenan, R.J., et al., *The signal recognition particle.* Annu Rev Biochem, 2001. **70**: p. 755-75.
5. Collins, K., *The biogenesis and regulation of telomerase holoenzymes.* Nat Rev Mol Cell Biol, 2006. **7**(7): p. 484-94.
6. Sigler, P.B., *An analysis of the structure of tRNA.* Annu Rev Biophys Bioeng, 1975. **4**(00): p. 477-527.
7. Devoe, H. and I. Tinoco, Jr., *The stability of helical polynucleotides: base contributions.* J Mol Biol, 1962. **4**: p. 500-17.
8. Mathews, D.H. and D.H. Turner, *Prediction of RNA secondary structure by free energy minimization.* Curr Opin Struct Biol, 2006. **16**(3): p. 270-8.
9. Batey, R.T., *Structures of regulatory elements in mRNAs.* Curr Opin Struct Biol, 2006. **16**(3): p. 299-306.
10. Herschlag, D., *RNA chaperones and the RNA folding problem.* J Biol Chem, 1995. **270**(36): p. 20871-4.
11. Turner, D.H.S., N. and Freier, S.M., *Thermodynamics and Kinetics of Base-Pairing and of DNA and RNA Self-Assembly and Helix-Coil Transition.* Nucleic Acids Res, 1990: p. 201-227.
12. Russell, R., *RNA misfolding and the action of chaperones.* Front Biosci, 2008. **13**: p. 1-20.
13. Karpel, R.L., Swistel, D.G., Miller, N.S., Geroch, M.E., Lu, C. and Fresco, J.R., *Acceleration of RNA renaturation by nucleic acid unwinding proteins* Brookhaven Symp Biol, 1975: p. 165-174.
14. Karpel, R.L.a.B., A.C., *Physical studies of the interaction of a calf thymus helix-destabilizing protein with nucleic acids.* Biochemistry, 1980. **19**: p. 4674-4682.
15. Cordin, O., et al., *The DEAD-box protein family of RNA helicases.* Gene, 2006. **367**: p. 17-37.
16. Cheng, Z., Coller, J., Parker, R. and Song, H., *Crystal structure and functional analysis of DEAD-box protein Dhh1p.* RNA, 2005. **11**: p. 1258-1270.
17. Linder, P., *Dead-box proteins: a family affair--active and passive players in RNP-remodeling.* Nucleic Acids Res, 2006. **34**(15): p. 4168-80.
18. Fairman, M.E., et al., *Protein displacement by DExH/D "RNA helicases" without duplex unwinding.* Science, 2004. **304**(5671): p. 730-4.
19. Yang, Q., et al., *DEAD-box proteins unwind duplexes by local strand separation.* Mol Cell, 2007. **28**(2): p. 253-63.
20. Halls, C., et al., *Involvement of DEAD-box proteins in group I and group II intron splicing. Biochemical characterization of Mss116p, ATP hydrolysis-dependent and -independent mechanisms, and general RNA chaperone activity.* J Mol Biol, 2007. **365**(3): p. 835-55.
21. Rajkowitsch, L., et al., *RNA chaperones, RNA annealers and RNA helicases.* RNA Biol, 2007. **4**(3): p. 118-30.
22. Tanner, N.K. and P. Linder, *DExD/H box RNA helicases: from generic motors to specific dissociation functions.* Mol Cell, 2001. **8**(2): p. 251-62.
23. Walker, J.E., Sarste, M., Runswick, M.J., and Gay, N.J., *Distantly related sequences in the a- and b- subunits of ATP synthase, myosin, kinases and other ATP-requiring enzymes and a common nucleotide binding fold.* EMBO J, 1982. **1**: p. 945-951.
24. Fry, D.C., S.A. Kuby, and A.S. Mildvan, *ATP-binding site of adenylate kinase: mechanistic implications of its homology with ras-encoded p21, F1-ATPase, and other nucleotide-binding proteins.* Proc Natl Acad Sci U S A, 1986. **83**(4): p. 907-11.

25. Pause, A. and N. Sonenberg, *Mutational analysis of a DEAD box RNA helicase: the mammalian translation initiation factor eIF-4A.* EMBO J, 1992. **11**(7): p. 2643-54.
26. Schwer, B. and T. Meszaros, *RNA helicase dynamics in pre-mRNA splicing.* EMBO J, 2000. **19**(23): p. 6582-91.
27. Banroques, J., et al., *Motif III in superfamily 2 "helicases" helps convert the binding energy of ATP into a high-affinity RNA binding site in the yeast DEAD-box protein Ded1.* J Mol Biol, 2010. **396**(4): p. 949-66.
28. Story, R.M. and T.A. Steitz, *Structure of the recA protein-ADP complex.* Nature, 1992. **355**(6358): p. 374-6.
29. Caruthers, J.M. and D.B. McKay, *Helicase structure and mechanism.* Curr Opin Struct Biol, 2002. **12**(1): p. 123-33.
30. Jankowsky, E. and M.E. Fairman, *RNA helicases--one fold for many functions.* Curr Opin Struct Biol, 2007. **17**(3): p. 316-24.
31. Schmid, S.R. and P. Linder, *D-E-A-D protein family of putative RNA helicases.* Mol Microbiol, 1992. **6**(3): p. 283-91.
32. Nishi, K., et al., *An eIF-4A-like protein is a suppressor of an Escherichia coli mutant defective in 50S ribosomal subunit assembly.* Nature, 1988. **336**(6198): p. 496-8.
33. Kossen, K. and O.C. Uhlenbeck, *Cloning and biochemical characterization of Bacillus subtilis YxiN, a DEAD protein specifically activated by 23S rRNA: delineation of a novel sub-family of bacterial DEAD proteins.* Nucleic Acids Res, 1999. **27**(19): p. 3811-20.
34. Kossen, K., F.V. Karginov, and O.C. Uhlenbeck, *The carboxy-terminal domain of the DExDH protein YxiN is sufficient to confer specificity for 23S rRNA.* J Mol Biol, 2002. **324**(4): p. 625-36.
35. Rogers, G.W., Jr., N.J. Richter, and W.C. Merrick, *Biochemical and kinetic characterization of the RNA helicase activity of eukaryotic initiation factor 4A.* J Biol Chem, 1999. **274**(18): p. 12236-44.
36. Chen, Y., et al., *DEAD-box proteins can completely separate an RNA duplex using a single ATP.* Proc Natl Acad Sci U S A, 2008. **105**(51): p. 20203-8.
37. Del Campo, M. and A.M. Lambowitz, *Structure of the Yeast DEAD box protein Mss116p reveals two wedges that crimp RNA.* Mol Cell, 2009. **35**(5): p. 598-609.
38. Sengoku, T., et al., *Structural basis for RNA unwinding by the DEAD-box protein Drosophila Vasa.* Cell, 2006. **125**(2): p. 287-300.
39. Liu, F., A. Putnam, and E. Jankowsky, *ATP hydrolysis is required for DEAD-box protein recycling but not for duplex unwinding.* Proc Natl Acad Sci U S A, 2008. **105**(51): p. 20209-14.
40. Nicol, S.M. and F.V. Fuller-Pace, *The "DEAD box" protein DbpA interacts specifically with the peptidyltransferase center in 23S rRNA.* Proc Natl Acad Sci U S A, 1995. **92**(25): p. 11681-5.
41. Karginov, F.V., et al., *YxiN is a modular protein combining a DEx(D/H) core and a specific RNA-binding domain.* J Biol Chem, 2005. **280**(42): p. 35499-505.
42. Polach, K.J. and O.C. Uhlenbeck, *Cooperative binding of ATP and RNA substrates to the DEAD/H protein DbpA.* Biochemistry, 2002. **41**(11): p. 3693-702.
43. Tsu, C.A. and O.C. Uhlenbeck, *Kinetic analysis of the RNA-dependent adenosinetriphosphatase activity of DbpA, an Escherichia coli DEAD protein specific for 23S ribosomal RNA.* Biochemistry, 1998. **37**(48): p. 16989-96.
44. Diges, C.M. and O.C. Uhlenbeck, *Escherichia coli DbpA is an RNA helicase that requires hairpin 92 of 23S rRNA.* EMBO J, 2001. **20**(19): p. 5503-12.
45. Tsu, C.A., K. Kossen, and O.C. Uhlenbeck, *The Escherichia coli DEAD protein DbpA recognizes a small RNA hairpin in 23S rRNA.* RNA, 2001. **7**(5): p. 702-9.
46. Theissen, B., et al., *Cooperative binding of ATP and RNA induces a closed conformation in a DEAD box RNA helicase.* Proc Natl Acad Sci U S A, 2008. **105**(2): p. 548-53.
47. Wang, S., et al., *The domain of the Bacillus subtilis DEAD-box helicase YxiN that is responsible for specific binding of 23S rRNA has an RNA recognition motif fold.* RNA, 2006. **12**(6): p. 959-67.

48. Karow, A.R. and D. Klostermeier, *A structural model for the DEAD box helicase YxiN in solution: localization of the RNA binding domain.* J Mol Biol, 2010. **402**(4): p. 629-37.
49. Karow, A.R., B. Theissen, and D. Klostermeier, *Authentic interdomain communication in an RNA helicase reconstituted by expressed protein ligation of two helicase domains.* FEBS J, 2007. **274**(2): p. 463-73.
50. Caruthers, J.M., E.R. Johnson, and D.B. McKay, *Crystal structure of yeast initiation factor 4A, a DEAD-box RNA helicase.* Proc Natl Acad Sci U S A, 2000. **97**(24): p. 13080-5.
51. Story, R.M., H. Li, and J.N. Abelson, *Crystal structure of a DEAD box protein from the hyperthermophile Methanococcus jannaschii.* Proc Natl Acad Sci U S A, 2001. **98**(4): p. 1465-70.
52. Shi, H., et al., *Crystal structure of the human ATP-dependent splicing and export factor UAP56.* Proc Natl Acad Sci U S A, 2004. **101**(51): p. 17628-33.
53. Zhao, R., et al., *Crystal structure of UAP56, a DExD/H-box protein involved in pre-mRNA splicing and mRNA export.* Structure, 2004. **12**(8): p. 1373-81.
54. Yao, N., et al., *Structure of the hepatitis C virus RNA helicase domain.* Nat Struct Biol, 1997. **4**(6): p. 463-7.
55. Kim, J.L., et al., *Hepatitis C virus NS3 RNA helicase domain with a bound oligonucleotide: the crystal structure provides insights into the mode of unwinding.* Structure, 1998. **6**(1): p. 89-100.
56. Karow, A.R. and D. Klostermeier, *A conformational change in the helicase core is necessary but not sufficient for RNA unwinding by the DEAD box helicase YxiN.* Nucleic Acids Res, 2009. **37**(13): p. 4464-71.
57. Laemmli, U.K., *Cleavage of structural proteins during the assembly of the head of bacteriophage T4.* Nature, 1970. **227**: p. 680-685.
58. Aregger, R. and D. Klostermeier, *The DEAD box helicase YxiN maintains a closed conformation during ATP hydrolysis.* Biochemistry, 2009. **48**(45): p. 10679-81.
59. Theissen, B., *Conformational changes in the catalytic cycle of the RNA-helicase YxiN - fluorescence resonance energy transfer in single molecules.* Dissertation Universität Bayreuth, 2006.
60. Studier, F.W., *Protein production by auto-induction in high density shaking cultures.* Protein Expr Purif, 2005. **41**(1): p. 207-34.
61. Adam, H., *Adenosin-5' Diphosphat und Adenosin-5' Monophosphat in Methoden der Enzymatischen Analyse.* Bergmeyer HU, ed. Verlag Chemie, 1962: p. 573-577.
62. Hiratsuka, T., *New ribose-modified fluorescent analogs of adenine and guanine nucleotides available as substrates for various enzymes.* Biochemica et Biophysica Acta, 1983(742): p. 496-508.
63. Magde, D., Wong, R. and Seybold, P.G., *Fluorescence quantum yields and their relation to lifetimes of rhodamine 6G and fluorescein in nine solvents: improved absolute standards for quantum yields.* Photochem Photobiol, 2002(75): p. 327-334.
64. Spreitler, F., *Einzelmolekül-FRET an Biomolekülen.* Diplomarbeit Universtität Bayreuth, 2006.
65. Bigay, J., et al., *Fluoride complexes of aluminium or beryllium act on G-proteins as reversibly bound analogues of the gamma phosphate of GTP.* EMBO J, 1987. **6**(10): p. 2907-13.
66. Fisher, A.J., et al., *X-ray structures of the myosin motor domain of Dictyostelium discoideum complexed with MgADP.BeFx and MgADP.AlF4.* Biochemistry, 1995. **34**(28): p. 8960-72.
67. Chabre, M., *Aluminofluoride and beryllofluoride complexes: a new phosphate analogs in enzymology.* Trends Biochem Sci, 1990. **15**(1): p. 6-10.
68. Andersen, C.B., et al., *Structure of the exon junction core complex with a trapped DEAD-box ATPase bound to RNA.* Science, 2006. **313**(5795): p. 1968-72.
69. Nielsen, K.H., et al., *Mechanism of ATP turnover inhibition in the EJC.* RNA, 2009. **15**(1): p. 67-75.

70. Lorsch, J.R. and D. Herschlag, *The DEAD box protein eIF4A. 2. A cycle of nucleotide and RNA-dependent conformational changes.* Biochemistry, 1998. **37**(8): p. 2194-206.
71. Henn, A., et al., *The ATPase cycle mechanism of the DEAD-box rRNA helicase, DbpA.* J Mol Biol, 2008. **377**(1): p. 193-205.
72. Rozovsky, N., A.C. Butterworth, and M.J. Moore, *Interactions between eIF4AI and its accessory factors eIF4B and eIF4H.* RNA, 2008. **14**(10): p. 2136-48.
73. Elles, L.M. and O.C. Uhlenbeck, *Mutation of the arginine finger in the active site of Escherichia coli DbpA abolishes ATPase and helicase activity and confers a dominant slow growth phenotype.* Nucleic Acids Res, 2008. **36**(1): p. 41-50.
74. Ballut, L., et al., *The exon junction core complex is locked onto RNA by inhibition of eIF4AIII ATPase activity.* Nat Struct Mol Biol, 2005. **12**(10): p. 861-9.
75. Linden, M.H., R.K. Hartmann, and D. Klostermeier, *The putative RNase P motif in the DEAD box helicase Hera is dispensable for efficient interaction with RNA and helicase activity.* Nucleic Acids Res, 2008. **36**(18): p. 5800-11.
76. Iost, I., M. Dreyfus, and P. Linder, *Ded1p, a DEAD-box protein required for translation initiation in Saccharomyces cerevisiae, is an RNA helicase.* J Biol Chem, 1999. **274**(25): p. 17677-83.
77. Cordin, O., et al., *The newly discovered Q motif of DEAD-box RNA helicases regulates RNA-binding and helicase activity.* EMBO J, 2004. **23**(13): p. 2478-87.
78. Low, W.K., et al., *Substrate-dependent targeting of eukaryotic translation initiation factor 4A by pateamine A: negation of domain-linker regulation of activity.* Chem Biol, 2007. **14**(6): p. 715-27.
79. Peck, M.L. and D. Herschlag, *Adenosine 5'-O-(3-thio)triphosphate (ATPgammaS) is a substrate for the nucleotide hydrolysis and RNA unwinding activities of eukaryotic translation initiation factor eIF4A.* RNA, 2003. **9**(10): p. 1180-7.
80. Low, W.K., et al., *Inhibition of eukaryotic translation initiation by the marine natural product pateamine A.* Mol Cell, 2005. **20**(5): p. 709-22.
81. Bordeleau, M.E., et al., *Stimulation of mammalian translation initiation factor eIF4A activity by a small molecule inhibitor of eukaryotic translation.* Proc Natl Acad Sci U S A, 2005. **102**(30): p. 10460-5.
82. Swain, J.F., et al., *Hsp70 chaperone ligands control domain association via an allosteric mechanism mediated by the interdomain linker.* Mol Cell, 2007. **26**(1): p. 27-39.
83. Hasselbach, W. and M. Makinose, *[The calcium pump of the "relaxing granules" of muscle and its dependence on ATP-splitting].* Biochem Z, 1961. **333**: p. 518-28.
84. Ebashi, S. and F. Lipmann, *Adenosine Triphosphate-Linked Concentration of Calcium Ions in a Particulate Fraction of Rabbit Muscle.* J Cell Biol, 1962. **14**(3): p. 389-400.
85. Daiho, T., et al., *Critical role of Glu40-Ser48 loop linking actuator domain and first transmembrane helix of Ca2+-ATPase in Ca2+ deocclusion and release from ADP-insensitive phosphoenzyme.* J Biol Chem, 2007. **282**(47): p. 34429-47.
86. Holdensen, A.N. and J.P. Andersen, *The length of the A-M3 linker is a crucial determinant of the rate of the Ca2+ transport cycle of sarcoplasmic reticulum Ca2+-ATPase.* J Biol Chem, 2009. **284**(18): p. 12258-65.
87. Nordstrom, K., et al., *Mutational analysis of the Acropora millepora PaxD paired domain highlights the importance of the linker region for DNA binding.* Gene, 2003. **320**: p. 81-7.

8. Acknowledgments

My first and sincere thank goes to Prof. Dagmar Klostermeier. Thank you for your faith in me, for giving me a second chance to graduate, for all the input and support on this very interesting project.

Many thanks go to the whole Klostermeier crowd. Thanks Anne Karow, for your great support and collaboration on our shared “baby” YxiN. You made my work very agreeable from the very beginning. Thanks Tobias Heck, Martin Lanz, Manuel Hilbert and Airat Gubaev for all the scientific discussions and thoughts we shared. Thank you very much Stefan Jungblut, Lenz Steimer, Alexandra Andreou and Agneyo Ganguly. You were not only great labmates during all the time we shared, but also great friends. Thank you guys suffering for me when proof-reading my very first drafts of this thesis. Thank you Ines Hertel, for always being patient with the chaotic bunch of people we were, for the calmness you emanate, in short, for being the person you are.

Not to forget all the members of the 6th floor that make scientific life possible. Thanks to Beatrice Lang and Fatima Reis for cleaning up our mess with always a smile in the face and ready for a short chat. Thanks Leo Faletti and Simon Saner for all the help you provided with any technical issue we could think of. Many thanks Corinne Salvisberg and Susanna Notz. Whenever there was anything administrative to be done, you were there for me.

All members of the Seelig groups, thank you all for the great atmosphere we shared on “our” floor, for all the nice coffee-breaks, lunches and Teestunde seminars. I enjoyed being around you.

Thanks also go to Jessica Guddorf, Daniela Bremann and the Schönhoff group members in Münster. After our move you helped me with every issue one can think of. You made feeling comfortable in the new lab easy.

Thanks from the bottom of my heart to my family. My parents Franz and Helen for the life-long support in any decision I made, my siblings Andreas and Manuela for being themselves,

giving all the support they could give their “bigger” sister. There are no words to describe how grateful I am, to be part of this family.

Christina Ursprung, Patrick Franke, Andrea Stauffer, Céline Gerber and Raphael Urbani I would like to thank your for your friendship. You know what you guys mean to me. Thank you very much for being there for me in any situation. Marc Mertes, Christian Bürger and Tobina Schubert, you made my private move to Münster a success. Thank you.